Technical Report

TR-10-38

Large scale gas injection test (Lasgit) performed at the Äspö Hard Rock Laboratory

Summary report 2008

R J Cuss, J F Harrington, D J Noy
British Geological Survey

February 2010

Svensk Kärnbränslehantering AB
Swedish Nuclear Fuel
and Waste Management Co

Box 250, SE-101 24 Stockholm
Phone +46 8 459 84 00

SKB

Large scale gas injection test (Lasgit) performed at the Äspö Hard Rock Laboratory

Summary report 2008

R J Cuss, J F Harrington, D J Noy
British Geological Survey

February 2010

Keywords: Lasgit, Gas injection, Bentonite, Modelling, Hydration, Hydraulic, Storage, Gas entry pressure.

Acknowledgements

This study was undertaken by staff from the British Geological Survey (Radioactive Waste Team). Funding for the study was provided by SKB (Stockholm), the British Geological Survey and the European Commission through the NF-PRO project (Understanding and physical and numerical modelling of the key processes in the near-field, and their coupling, for different host rocks and repository strategies) undertaken within the auspices of the EURATOM 6th framework programme.

The authors would like to thank Patrik Sellin for his support of the research area, SKB colleagues at the Äspö Hard Rock Laboratory for their help in the set-up, maintenance and operation of the Lasgit experiment, and colleagues at Clay Technology AB who were responsible for the original installation of the Geokon instrumentation and buffer clay.

Abstract

This report describes the set-up, operation and observations from the first 1,385 days (3.8 years) of the large scale gas injection test (Lasgit) experiment conducted at the Äspö Hard Rock Laboratory. During this time the bentonite buffer has been artificially hydrated and has given new insight into the evolution of the buffer.

After 2 years (849 days) of artificial hydration a canister filter was identified to perform a series of hydraulic and gas tests, a period that lasted 268 days. The results from the gas test showed that the full-scale bentonite buffer behaved in a similar way to previous laboratory experiments. This confirms the up-scaling of laboratory observations with the addition of considerable information on the stress responses throughout the deposition hole.

During the gas testing stage, the buffer was continued to artificially hydrate. Hydraulic results, from controlled and uncontrolled events, show that the buffer continues to mature and has yet to reach full maturation.

Lasgit has yielded high quality data relating to the hydration of the bentonite and the evolution in hydrogeological properties adjacent to the deposition hole. The initial hydraulic and gas injection tests confirm the correct working of all control and data acquisition systems. Lasgit has been in successful operation for in excess of 1,385 days.

Sammanfattning

Denna rapport beskriver utformningen, driften och observationerna från de första 1 385 dagarna (3,8 år) med det storskaliga gasinjekteringstestet (Lasgit) som utförs vid Äspölaboratoriet. Under denna tid har bentonitbufferten blivit artificiellt återmättad och data därifrån har gett ny insikt om utvecklingen av en högkompakterad bentonitbuffert under isotermala förhållanden.

Efter 2 år (849 dagar) av artificiell vattentillförsel utfördes en serie av hydrauliska och gasinjekteringstester i ett filter i den nedersta uppsättningen, närmast basen av kapseln. Denna testfas varade i 268 dagar. Även om bentoniten inte var i full hydraulisk jämvikt, så visade resultaten från den första gastesten att gas genombrott i full skala genom bentonitbufferten uppträder på ett kvalitativt liknande sätt som tidigare små experiment i laboratorieskala. Detta tyder på att det är giltigt att skala upp observationer från laboratorieförsök för denna fas i utvecklingen, men ytterligare arbete krävs för att fullständigt förklara resultaten och undersöka hur om det blir förändringar allteftersom bufferten fortsätter att mättas och mogna.

Under gasinjekteringsförsöket vattenmättades bufferten artificiellt genom de övriga filtren. De hydrauliska resultaten från testerna med konstant gradient och tryckfallstester visar att bufferten fortsätter att mogna, men har ännu inte uppnått full mognad.

Lasgit har producerat högkvalitativa data om vattenupptag i bentonit under isoterma förhållanden, utvecklingen i de hydrogeologiska egenskaperna i närheten av deponeringshålet och unika uppgifter om hur gas vandrar genom kompakt bentonit i verklig förvarsskala. De inledande hydrauliska och gasinjekteringstesterna bekräftar funktionen hos alla kontroll- och datainsamlingssystem. Lasgit har nu varit i framgångsrik drift i över 1 385 dagar.

Executive summary

This report describes the set-up, operation and observations from the first 1,385 days (3.8 years) of the large scale gas injection test (Lasgit) experiment conducted at the Äspö Hard Rock Laboratory.

Hydration Stage 1 (day 106–day 849)

The deposition hole was closed on the 1st February 2005 signifying the start of the hydration phase. Groundwater inflow through a number of highly-conductive discrete fractures quickly resulted in elevated porewater pressures throughout large sections of the borehole. This lead to the formation of conductive channels (piping), the extrusion of bentonite from the deposition hole and the discharge of groundwater to the gallery floor. This problem was addressed by drilling two pressure relief holes in the surrounding rock mass to lower the porewater pressure in the vicinity of the deposition hole.

Artificial hydration began on the 18th May 2005 after 106 days of testing. In general, from this time onwards, the pressures in all of the canister filters and hydration mats (excluding the FCT and FR901) were used to hydrate the clay. Initial attempts to raise porewater pressure in the artificial hydration arrays occasionally resulted in the formation of preferential pathways, even at relatively modest excess water pressures, resulting in localized increases in porewater pressure and total stress. These pressure dependent features were not focused in one location within the bentonite but occurred at multiple sites at different times in the test history. These pathways were relatively short lived, closing when water pressure was reduced. Packers were installed into the pressure relief holes on 23rd March 2006 and sections in them closed over the period to 5th July 2006. These operations caused clear effects throughout the deposition hole in both the measured porewater pressures and, to a lesser extent, the total stresses. However, there was no repeat of the formation of piping through discrete channels so, on 20th November 2006, pressures to the artificial hydration filters on the canister were increased to 2,350 kPa.

Hydraulic and gas injection tests Stage 1 (day 843–day 1,110)

A preliminary set of baseline hydraulic measurements were started on the 25th May 2007 (day 843) with the isolation of the lower canister filters FL901 to FL904 while artificial hydration continued through all other canister filters and filter mats. Preliminary modelling of the initial hydraulic test was performed using a 2D axisymmetric variably saturated finite element porewater flow model. Hydraulic conductivity was found to range from 9×10^{-14} to 1.6×10^{-13} ms^{-1} and specific storage values were from 5.5×10^{-5} to 4.4×10^{-4} m^{-1}; filter FL903 was modelled with a hydraulic conductivity of 7.5×10^{-14} ms^{-1} and a specific storage of 2.5×10^{5} m^{1}. The design specifications of the KBS-3V concept states that hydraulic conductivity should not exceed 10^{-12} $m.s^{-1}$ (SKB TR-09-22) and /Harrington and Horseman 2003/ report the hydraulic conductivity of MX-80 as between 3.9×10^{-15} and 9.28×10^{-14} $m.s^{-1}$.

Gas injection to FL903 began on day 917. Analysis of the data indicates gas starts to flow into the buffer at a pressure of about 775 kPa, which is much lower than the expected gas entry pressure for intact bentonite. When initial gas pressurisation stopped and the pressure was held constant at around 1.85 MPa, flow into the clay spontaneously reduced, indicating that propagation of the gas pathway(s) practically ceased when the pressure stopped increasing.

Upon restarting gas injection, the observed pressure begins to deviate from the predicted value, indicating pathway propagation continues at the onset of testing. Gas flux into the clay gradually increases as the pressure in the system rises. At a gas pressure marginally greater than the local total stress measured on the rock wall (but a little smaller than the radial and axial stresses measured on and near the canister surface respectively which are between 1,049 and 2,149 mm from the gas injection point), flux into the clay rapidly increases. Gas pressure continues to rise reaching a peak pressure marginally greater than the axial stress measured at PB902. This is followed by a small spontaneous negative transient leading to a quasi steady state. The post peak gas flux exhibits dynamic behaviour (over and undershooting flux into the system) suggestive of unstable gas pathways, which are linked to a strong couple between pore pressure and gas flow as indicated by changes in porewater pressure during and after gas breakthrough.

Following the cessation of pumping, the injection flux through the bentonite declines rapidly before entering an extended period of very small flows. This is reflected in the pressure response which initially drops rapidly but then decays very slowly towards an asymptotic capillary threshold pressure, which is estimated to be around 4,900 kPa, equating to the average radial stress (PC902 and PC903) measured on the canister surface.

Following peak gas pressure a well pronounced increase in radial stress occurs around the entire base of the deposition hole, with the highest increase noted in the vertical plane below the point of injection. This strongly suggests gas preferentially moved downwards, probably along the interface between the canister and buffer. It is notable that the radial stress immediately adjacent to FL903 actually decreases during this time.

Analysis of the porewater pressure sensors located within the buffer show no obvious sensitivity to the injection of gas. In contrast, axial stress sensors located beneath and above the canister appear to register the passage of gas.

A small inflection in the rate of increase in axial stress at the base of the canister occurs shortly after the peak in gas pressure. Such a reduction in stress can only be caused by the removal of load, suggesting some form of displacement has occurred as a result of gas injection.

While it is difficult to make definitive statements regarding the exact direction and number of gas flow paths, it seems highly probably that the gas moved generally downwards away from the injection filter and then along the interface between blocks C1 and R1 and/or R1 and R2.

The observed general coupling between gas, stress and porewater pressure at the repository scale is extremely important and can be readily explained through concepts of pathway dilatancy. These observations are qualitatively similar to those reported by /Horseman et al. 2004/.

Hydration Stage 2 (day 1,110–day 1,385)

The second stage of artificial hydration began on day 1,110. This was interrupted by the failure of the Spiralair KS1/T compressor on day 1,289. The following decrease in filter pressures were modelled to provide additional data on the hydraulic evolution of the clay. Good model fits were achieved for most of the filters, which suggests that the transient behaviour can be captured in terms of a single hydraulic transport coefficient and a single hydraulic storage coefficient. The upper filters generally indicate higher values for permeability and specific storage than elsewhere in the system, ranging from 9×10^{-21} m^2 to 50×10^{-21} m^2. Values obtained for filters FL901 and FL904 (8×10^{-21} m^2 and 13.5×10^{-21} m^2 respectively) were quite similar to those from the previous hydraulic test, indicating little change in the hydraulic baseline properties between the two test stages.

Monitored porewater pressures within the bentonite have significantly increased during the test, but remain relatively low ranging from 250 kPa to 685 kPa. This is in contrast to the water pressure measured at the face of the deposition hole which ranges from 1,025 kPa to 2,555 kPa. However, three sensors in the clay show a slow decrease in pressure initiated at approximately day 1,240.

Suction has decreased throughout the experiment confirming ongoing hydration of the clay, though the rate of hydration has slowed significantly. Greatest progress in hydration of the clay has been made near to the large filter mats above the canister, whilst the least progress has occurred just below the canister.

Pore pressure monitored at the rock wall greatly increased in response to the commissioning of the packers. Since this time, pore pressure has slowly decayed, ranging between 1,025 kPa and 2,555 kPa. During 2008 four pressure "break-throughs"[1] were observed in three of the sensors. The presence of mapped or extrapolated fractures close to these events suggest the fractures play a significant role in the observed behaviour.

The total pressure sensors mounted on the rock wall have significantly increased during the experiment and now range between 1,890 kPa and 5,850 kPa. The spatial and temporal evolution in radial stress measured at the rock wall has remained fairly constant, with only small variations noted,

[1] Rapid increases or decreases in monitored porewater pressure.

primarily due to the hydraulic break-through events. Effective stress generally changes around the circumference of the depositional hole but does not exhibit any significant correlation to depth. High radial stresses are concentrated along part of the deposition hole wall at about 300º and that stress varies mainly with angular position rather than with depth.

Axial stress monitored within the clay has increased steadily to range from 4,770 kPa to 6,480 kPa. The data clearly shows a non-uniform distribution of axial stress across the major axis of the emplacement hole. The effect of the compressor failure is complex with two sensors having no change, whilst all other sensors exhibit either an absolute decrease in total stress or a reduction in the rate of stress increase. The most prominent stress drop occurred at the interface between the bentonite buffer and the concrete plug, with a near 350 kPa reduction from 6,565 kPa to 6,215 kPa.

Stress measurements on the canister surface indicate that radial and axial stress varies between 5,055 kPa and 5,385 kPa, which is comparable with the average value of radial stress monitored at the rock face. The increase in canister radial stresses have mirrored one another, while axial stress has increased at a much greater rate, such that it now represents the intermediate principal stress acting on the canister.

The axial force acting on the steel lid is now greater than the initial pre-stressing value applied during the installation phase. Since the installation and closure of packers in the pressure relief holes there has been a marked rise in the axial force acting on the lid. There is also strong evidence in later data for the stick slip movement of the conical concrete plug.

Displacement sensors mounted on the steel lid indicate a fairly uniform drop in lid height relative to the gallery floor during the early part of the test history, mirroring the relaxation in the initial pre-stressing applied to the lid. During the early stages of hydration the canister moved away from the lid due to preferential swelling of the clay near the large filter mats located above the canister. Following closure of the packers in both pressure relief holes, pore water pressures in the base of the deposition hole increased and the canister changed direction of movement and returned to a position similar (~0.5 mm) to that at the start of the test.

Complete test history (day 1–day 1,385)

Clear seasonal variation has been observed in many of the instrument outputs recorded within Lasgit when data are viewed over the entire 1,385 day (3.7 year) history. The largest variation is seen in the HRL temperature, with variation between 10 and 16°C. The canister shows similar variation, but with a 90 day lag from the HRL temperature and a range of only ±0.5°C from 13.3°C.

The temperature within the HRL closely correlates with the variation seen in axial force on the lid, the position of the lid and the stick-slip behaviour. This correlation is not perfect and an offset between displacement and temperature can on occasion be observed.

Other observations of seasonal variation appear to more closely correlate with the canister temperature, including pore pressure within the bentonite (UB), pore pressure at the wall rock (UR), radial stress (PR) and the radial & axial stresses (PC). With most of these instruments there is also some variation in the oscillation, many showing variation in lag with depth down the deposition hole.

As well as seasonal variation, it has been seen that pore pressure within Lasgit and the HRL around the 420 m level displays a long term gradual decay. The underlying cause for this behaviour remains unclear.

Lasgit has yielded high quality data relating to the hydration of the bentonite and the evolution in hydrogeological properties adjacent to the deposition hole. The initial hydraulic and gas injection tests confirm the correct working of all control and data acquisition systems. Lasgit has been in successful operation for in excess of 1,385 days.

Contents

1 Introduction

In the Swedish KBS-3 repository concept for spent nuclear fuel, copper/steel canisters containing spent fuel will be placed in large diameter (~1.8 m) boreholes drilled into the floor of the repository tunnels. The space around each canister will be filled with pre-compacted bentonite blocks, which over time, will draw in the surrounding groundwater and swell, closing up any remaining construction gaps. While the copper/steel canisters are expected to have a very substantial life, from a performance assessment perspective, it is important to consider the possible impact of groundwater penetrating a canister. Under certain conditions corrosion of the steel insert of each canister will lead to the formation of hydrogen. Radioactive decay of the waste and the radiolysis of water will produce some additional gas. Depending on the gas production rate and the rate of diffusion of gas molecules in the pores of the bentonite, it is possible that gas will accumulate in the void-space of each canister.

Current knowledge pertaining to the movement of gas in initially saturated buffer bentonite is based on small-scale laboratory studies /Donohew et al. 2000, Harrington and Horseman 1999, Horseman et al. 1999, 1997, Hume 1999, Pusch et al. 1987, 1985, Tanai et al. 1997/. Recent laboratory tests have demonstrated the importance of the boundary condition on gas migration /Harrington and Horseman 2003, Horseman et al. 2004/. Gas penetration and subsequent flow is accompanied by local dilation of the buffer clay. Porewater pressure and total stress acting within the clay are strongly affected by the passage of gas. The maximum gas pressure attainable during a discharge event, in part, relates to the geometry and spatial distribution of both the gas pathways within the buffer and the characteristics of the fractures distributed along the walls of the emplacement borehole. The transmissivity and hydrostatic pressure of these features will affect the maximum gas pressure that can be generated within the buffer.

While significant improvements in our understanding of the gas-buffer system have taken place /Harrington and Horseman 2003/, recent laboratory work has highlighted a number of uncertainties, notably the sensitivity of the gas migration process to experimental boundary conditions and possible scale-dependency of the measured responses. These issues were best addressed by undertaking a large-scale gas injection test or “Lasgit”.

Lasgit is a full-scale demonstration experiment operated by SKB at the Äspö Hard Rock Laboratory at a depth of 420 m. The objective of Lasgit is to provide quantitative data to improve process understanding and test/validate modelling approaches which might be used in performance assessment.

This report is the second in a series published on the status of the Lasgit experiment. /Harrington et al. 2007/ covered the initial stage of artificial hydration and the first stage of gas testing. This report mainly covers the activities of 2008 (artificial hydration), but also re-examines all data to date with particular emphasis placed on the impact of seasonal variations on experimental parameters and the evolution of the system over the last 3.7 years of testing.

2 Characterisation of deposition hole

This section is a review of a number of SKB International Progress Reports (IPR). These include IPR-03-28 Geological mapping of the assembly hall and deposition hole /Hardenby and Lundin 2003/, IPR-04-52 The Lasgit hole DA3147G01 hydrogeology /Hardenby 2004/ and IPR-07-14 Hydraulic tests with surface packer systems /Nowak et al. 2007/. Additional information is also introduced that has been presented at various Lasgit project meetings.

The Lasgit experiment has been commissioned in deposition hole number DA3147G01; the first emplacement borehole to be drilled at the Äspö Hard Rock Laboratory (HRL). The experiment is located within the Tunnel Boring Machine (TBM) assembly hall which is situated on the 420 m-level of the tunnel system. The tunnel system is comprised of an underground access ramp (TASA) approximately 3,600 m long. It is initially straight but between sections 1,600–3,100 m turns into a spiral.

The deposition hole has a length of 8.5 m and a diameter of around 1.75 m. A full scale KBS-3 canister has been modified for the Lasgit experiment with twelve circular filters of varying dimensions located on its surface to provide point sources for gas injection, mimicking potential canister defects (Section 3.2.2). These filters are used to inject water during the hydration stage and gas during gas testing.

2.1 Geological mapping (IPR-03-28)

The area around the Lasgit experiment has been comprehensively mapped by Carljohan Hardenby and Jan Lundin. These studies can be divided into 1) the TBM assembly hall and trial pit, and 2) the deposition hole DA3147G01.

2.1.1 Geological mapping of the TBM assembly hall

The assembly hall constitutes an enlarged section of the TASA main tunnel. It is higher and wider than the connecting tunnels for about 30 m of its length. It was excavated using conventional drilling and blasting techniques in 1994 and was created for the assembly of the tunnel boring machine that was used later in 1994 to bore the final part of the TASA (408.5 m, Section 3,191.2–3,599.7).

As a part of the general geological characterization of the tunnels at Äspö HRL the geological mapping of the walls and roof of the TBM assembly hall was completed shortly after the excavation was completed in 1994. Currently, the majority of the exposed surface of the walls and roof in the assembly hall are covered with shotcrete and the floor is paved.

The TBM assembly hall was previously used for the SKB-project “Demonstration of the Deposition Technology”. The purpose of that project was to develop and test methodology and equipment for deposition of canisters for spent fuel in full-scale and in a realistic environment. The assembly hall was intended to serve as a reloading station for canisters. During the reloading process a temporary deposition hole for a canister was needed. The reloading station was, however, never constructed.

As a part of the characterisation work in 1998 a pit was excavated to expose the rock in the TBM assembly hall floor in an area suitable for the reloading station. The pit floor was mapped and the results were used to decide where to drill two short core bore holes, KA3147G01 and KA3153G01. The results from all of these studies were used to decide where DA3147G01 was to be completed. Basic information for these holes is contained in Table 2-1.

Table 2-1. Co-ordinates of the pilot and the deposition holes in the TBM assembly hall. Notes: Negative dip indicates downwards; * = centre of the top of the hole, natural tunnel rock floor; # = centre of the top of the hole, top of tunnel concrete floor at the time of the drilling; @ = centre of the hole bottom.

Borehole category	ID – Codes	X coordinate	Y coordinate	Z coordinate	Dip°	Length (m)
Deposition hole	DA3147G01	7312.491	2313.562	–418.450#	–90	8.830@
Pilot hole	KA3147G01	7312.490	2313.554	–419.561*	–90	8.0
Pilot hole	KA3153G01	7311.511	2308.194	–419.053*	–90	8.0

The results of the various geological mappings of the TBM assembly hall are shown in Figure 2-1. There are basically four rock types present (Table 2-2 summarises the relative proportions of the three main rock types):

- Grey, medium-grained Äspö diorite (with or without feldspar megacrysts) is the dominant rock type.
- Reddish or sometimes grey, fine to medium-grained "fine-grained granite" occurs in minor amounts as veins, dykes or irregular bodies.
- A dark-blackish green, fine- to medium-grained greenstone is less common than the reddish fine-grained granite and occurs mainly as xenoliths within the Äspö diorite.
- Pinkish to reddish pegmatite is the least common rock type in the TBM assembly hall. Fine-grained granite sometimes forms hybrids with Äspö diorite.

The rock is regarded as "fresh" (i.e. no alteration aside from some minor oxidation of the rock normally in connection with fractures). The contacts between the rock types are mostly tight and sharp. More diffuse contacts are commonly found where a distinct rock type grades into a hybrid one.

All recorded fracture orientations have been plotted in Schmidt net and joint rosette diagrams, as shown in Figure 2-2. Three major fracture sets have been distinguished having the following mean orientations: 120º/80º, 180º/15º and 20º/80º (strike/dip right hand rule). The 120º/80º fracture set is the most prominent. However, /Hardenby and Lundin 2003/ showed that in certain locations the major fracture sets may be divided into two sets with mean orientations of 120º/80º and 140º/90º.

Only a few fractures showed evidence of displacements along the fracture surfaces. The apparent dislocations varied between 0.05–0.2 m. All fractures except one are steeply dipping. Three of them strike WNW–NW or ESE–SE and two of them, found in the deposition hole, lack record of strike. Lineations on the fracture planes have not been recorded, neither on dislocated planes or non-dislocated ones.

Most fractures contained more than one type of filling. Chlorite is by far the most common fracture filling and is found in 60–80% of all fractures, as shown in Table 2-3. Calcite, epidote and oxidation rims along fractures also appear frequently. Quartz, fine-grained granite and pegmatite appear in a few of the fractures. The latter two fillings are veins that are too thin to be recorded as rock types. Clay and grout was observed in a few fractures in the walls of the TBM assembly hall. Fe-precipitation/gel was found in a few fractures in the deposition hole.

The fracture surfaces are mostly planar and rough. Planar and smooth fracture surfaces are rather common too in the walls, roof and pit floor of the TBM assembly hall. A few fractures are undulating or arched; they may be smooth or rough. Since healed and tight fractures commonly were regarded to be rough, this "roughness-class" is believed to be over-represented. It is often impossible to judge how rough fracture planes of tight, healed fractures are.

When the mapping of the walls and roof of the TBM assembly hall took place all fractures were regarded as tight and healed. If all the water bearing fractures in the walls and roof are considered as open they will constitute 13% of the fractures recorded there, which is similar to the deposition hole (Section 2.1.2).

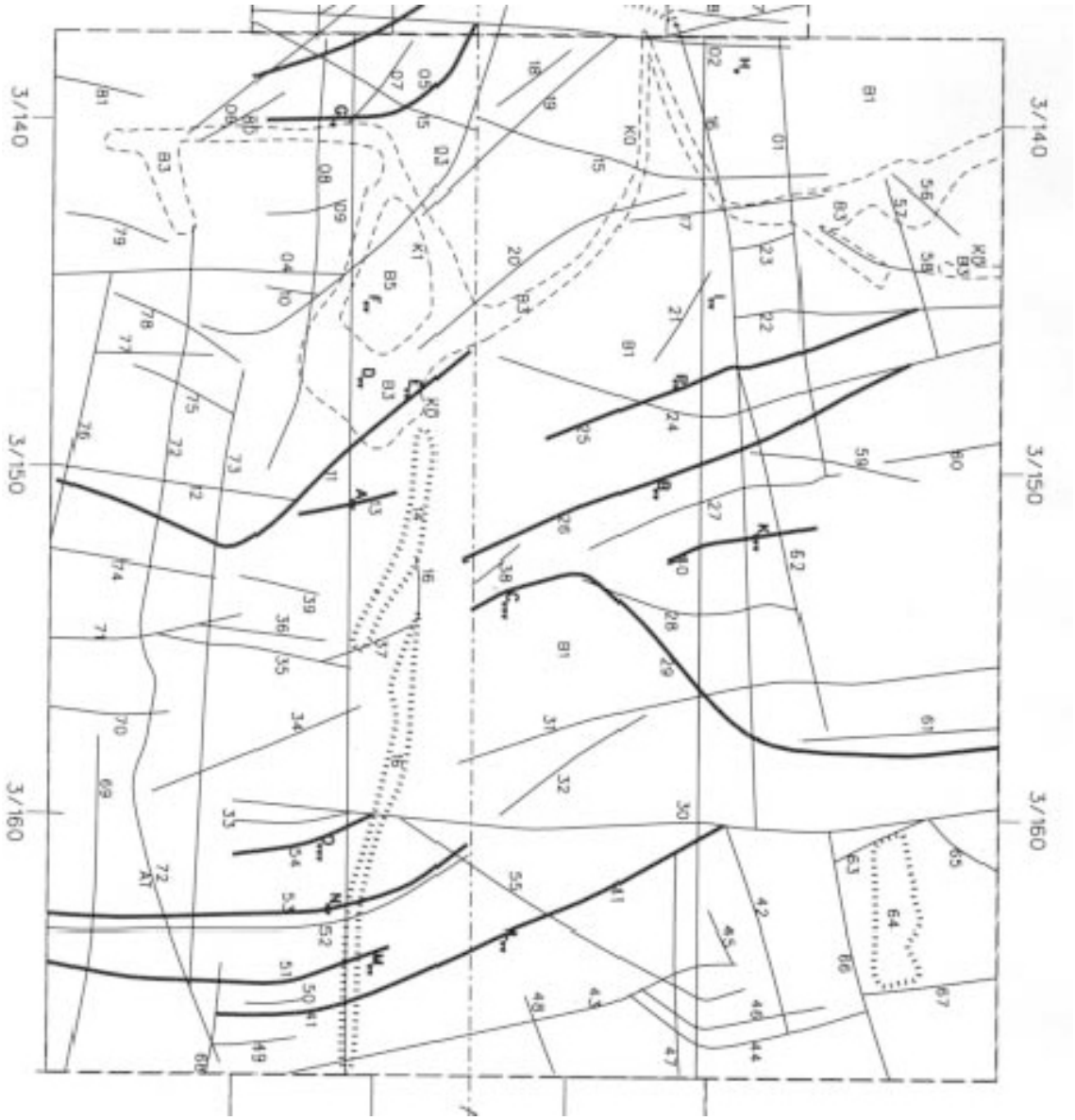

Figure 2-1. *Geological mapping of the TBM assembly hall, roof and side walls.* ***Legend:*** Rock types: *B1 = Äspö diorite, greyish and medium-grained with feldspar megacrysts. B3 = fine-grained granite, reddish brown. B5 = Greenstone, dark and fine-grained.* Contacts: *K0–K1 and dashed line. K0 = contact between B1 and B3. K1 = contact between B3 and B5.* Fractures: *01–81 and continuous line (thick lines represent water bearing fractures).* Water: *A–I and K–P and v = damp-minor seepage, occasional drops, vv = wet-seepage, drops or minor flow or vvv = flow.*

Table 2-2. Rock type distribution for the TBM assembly hall, walls and roof.

Rock type	Area m²	Percentage of mapped area (side walls, and roof, 809 m²)
Äspö diorite	752.37	93
Fine-grained granite	40.45	5
Greenstone	16.18	2
Total	809	100

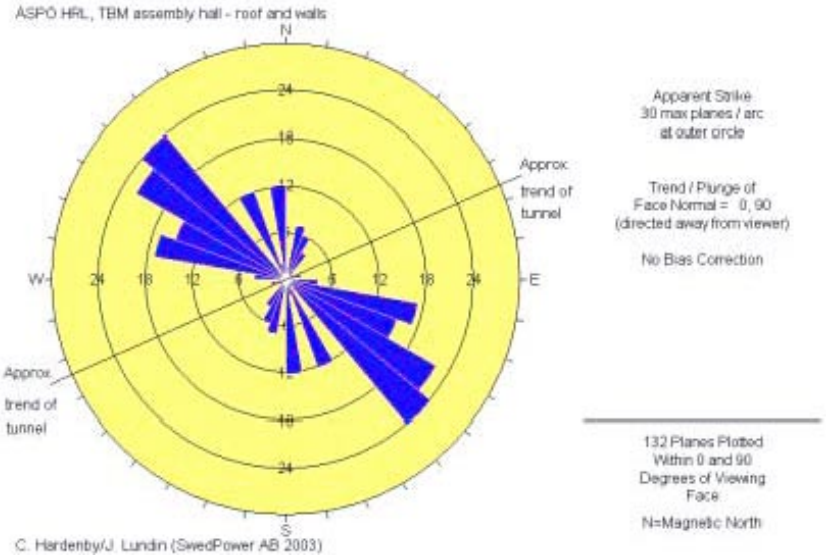

Figure 2-2. *Fracture orientations from the roof and side walls of the TBM assembly hall presented in Schmidt net and joint rosette diagrams.*

Table 2-3. Distribution of fracture fillings in the TBM assemble hall, walls and roof.

Filling	No of observations	% of all observations (total 132 fractures)
Chlorite	104	79
Calcite	47	36
Oxidation rim	38	29
Epidote	4	3
Clay	8	6
Grout	9	7
Fine-grained granite	1	1
Pegmatite	1	1
No filling or not observed	2	2

With a few exceptions, the fracture widths were not recorded while the geological mapping of the TBM assembly hall took place. Most fractures are, however, rather narrow, <1–2 mm. The standard mapping of the assembly hall (walls and roof) and the pit-floor, using a cut-off of about 1 m, shows that only 7% and about 45% respectively of the fractures are shorter than 2 m. With the same cut-off, about 70% of the fractures measured in the deposition hole are less than 2 m in length. The longest fracture observed in the deposition hole was just under 6 m, in the pit-floor 7 m and in the walls and roof of the assembly hall 20–25 m.

The Rock Mass Rating (RMR)-values (approximately 70–75) indicate that the rock mass of the TBM assembly hall and the deposition hole can be classified as being of good quality.

2.1.2 Mapping of deposition hole DA3147G01

Deposition hole DA3147G01 was constructed in 1999 using a specially made vertically drilling Robbins TBM. Soon after completion the hole was geologically mapped in detail from a cage hooked up to a lift. The result of the detailed mapping of the deposition hole is shown in Figure 2-3.

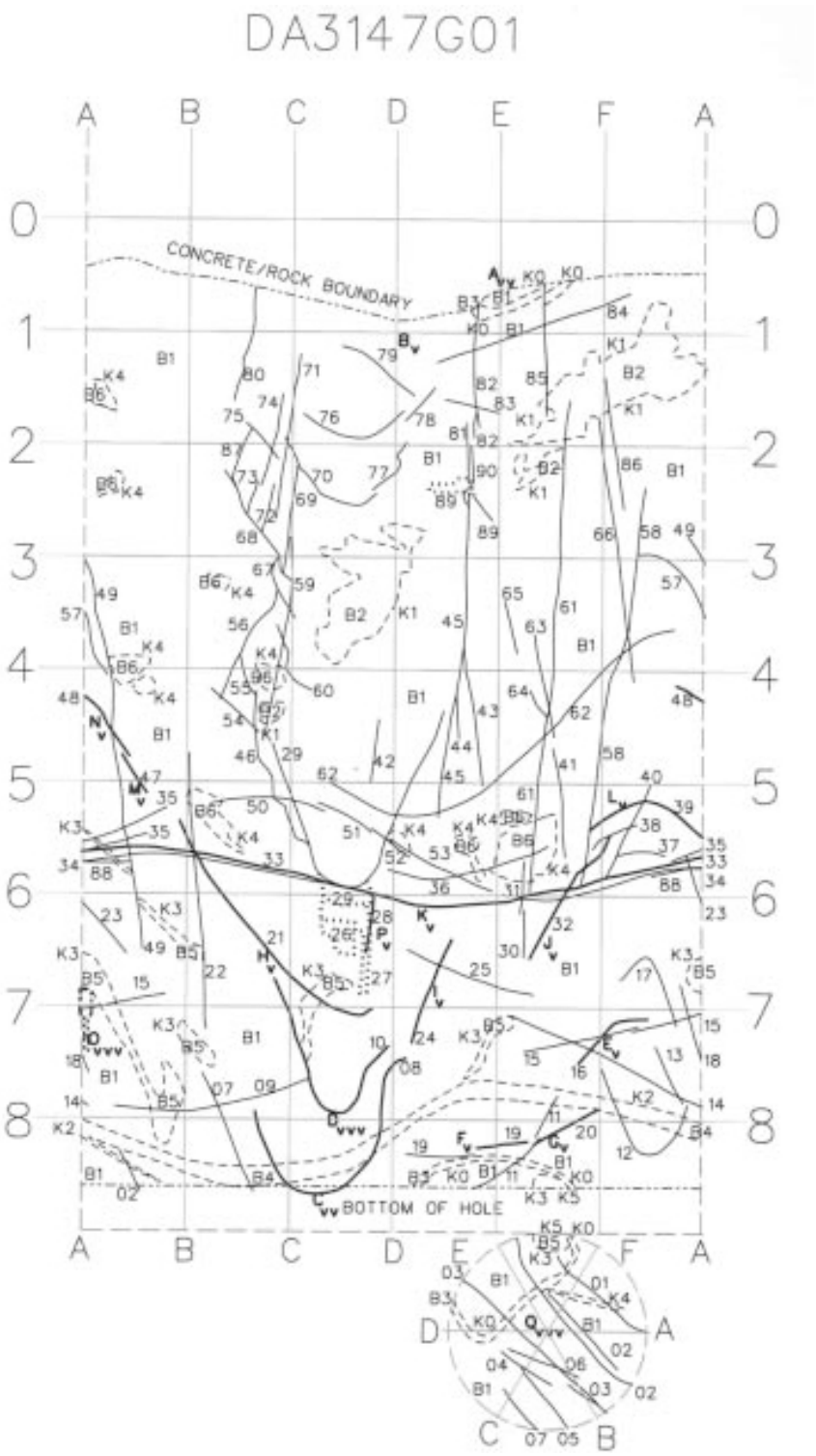

Figure 2-3. *Geological mapping of the deposition hole DA3147G01.* ***Legend:*** Rock types: *B1 = Äspö diorite, greyish and medium-grained with feldspar megacrysts; B2 = greenstone xenolith, black and fine-grained, includes some B1 and B4; B3 = "fine-grained" granite, greyish red and medium-grained; B4 = pegmatite, red and coarse-grained; B5 = "fine-grained" granite – hybrid of B1 and B3, greyish red and medium grained; B6 = greenstone xenolith, black and fine-grained.* Contacts: *K0–K5 and dashed line; K0 = contact between B1 and B3; K1 = contact between B1 and B2; K2 = contact between B1 and B4; K3 = contact between B1 and B5; K4 = contact between B1 and B6; K5 = contact between B5 and B3.* Fractures: *01–90 and continuous line (thick lines represent water bearing fractures).* Water: *A–Q and v = damp-minor seepage, occasional drops; vv = wet-seepage, drops or minor flow; vvv = flow.*

Similar to the geological mapping of the TBM assembly hall, four major rock types have been distinguished in the deposition hole; Äspö diorite, greenstone, fine-grained granite, and pegmatite. Besides some specific features (listed below) the rock types resemble those that have been described for the walls and roof of the assembly hall:

- **Äspö diorite.** In the deposition hole the Äspö diorite is mainly of the feldspar megacryst bearing type. The colour is grey-dark grey sometimes slightly reddish grey. It constitutes about 85% of the hole-surfaces (wall and bottom) and is spread throughout the hole.
- **Greenstone.** The "greenstone" that was found in the deposition hole is fine-grained and black. It occurs as xenoliths scattered in the Äspö diorite. The patches of "greenstone" (7% of the hole-surfaces) may sometimes include minor amounts of the Äspö diorite itself and pegmatite.
- **Fine-grained granite.** Two greyish red to pinkish red rock varieties assembled under the generic name fine-grained granite constitute 5% of the hole-surfaces. They appear in approximately equal amounts mainly in the lower part of the hole. One type is medium grained and may be regarded as a hybrid between fine-grained granite and Äspö diorite and occurs often as small "lenses" in the Äspö diorite proper. The other, fine- to medium-grained type and a more typical representative of the fine-grained grained granite forms 0.05–0.1 m wide veins. It occurs also as fracture filling.
- **Pegmatite.** It constitutes only 3% of the mapped surfaces. It appears as a light red approximately 0.1 m wide vein in the lower part of the hole.

Table 2-4 summarises the occurrence of the rock types. It is shown as the estimated area of rock type exposure and in percentage of total mapped area. About 50% of the contacts are tight and sharp. These are the ones between Äspö diorite and pegmatite, Äspö diorite and the fine-grained granite (in its "pure" state) and Äspö diorite and greenstone xenoliths (without any admixture of Äspö diorite or pegmatite). The boundaries between Äspö diorite and the impure greenstone xenolites, the Äspö diorite and the hybrid variety of fine-grained granite as well as the boundaries between the latter and the "pure" variety are on the other hand diffuse.

The distribution of fractures on the deposition hole wall and bottom is shown in Figure 2-3. The fracture orientations are presented in Schmidt net and joint rosette diagrams in Figure 2-4, which shows two major fracture sets. One of them is rather steeply dipping and has a mean orientation of approximately 120°/75° (strike/dip right). The other is gently dipping with a mean orientation of 195°/20°.

Most of the fractures (57%) in the deposition hole were found to be natural, most probably formerly healed and tight fractures, that now are more or less re-opened due to the drilling of the hole. Twenty-nine percent were healed and tight fractures and 14% were truly open natural fractures.

Six types of fracture filling material (oxidation included) have been observed (Table 2-5). The most common material is chlorite that is found in 72% of the 92 recorded fractures. Epidote and calcite are noted in 13% and 12% respectively of the observations. Fine-grained granite and quartz is found in 5% and 2% respectively of the fractures. Reddish oxidation of the rock is found along some of the fractures proper or occasionally as separate thin reddish streaks, recorded as fractures. Twenty-eight percent of the fractures show some oxidation. Some Fe-precipitate, often as a gel, has been found along a few (8%) of the fractures of which about half are water bearing.

All mapped fractures have a rough surface, mostly planar (80% of all fractures) but also undulating (19%) and arched (1%), see Table 2-6. Since many fractures are tight and healed it is often difficult to determine the surface roughness. For these cases, the surface structure term "undefined" was introduced by /Hardenby and Lundin 2003/. When all fractures that are tight and healed are considered having surface roughness "undefined" and those that are open are "rough" as originally indicated in the database, then the distribution will be as "alternative 2" in Table 2-6.

The size of the canister deposition hole will limit the fracture trace lengths. In Table 2-7 the fracture lengths have been grouped into intervals of 1 m. The table shows that 45% of the fractures are shorter than 1 m while 38% are found within the interval 1–2 m. Therefore most of the fractures (about 85%) in the deposition hole are shorter than 2 m. Only 2% of the fractures exceed 4.0 m in length. The table also shows what the distribution of fracture lengths would be if a cut off of 1 m is used instead of 0.5 m. When making a comparison with the fracture length distribution obtained from mapping of the walls, roof and floor of the assembly hall it has to be remembered that fracture length cut off was about 1 m when that mapping took place.

Table 2-4. Rock type distribution in deposition hole DA3147G01.

Rock type	Area (m²)	% of mapped area (hole wall and bottom 48 m²)
Äspö diorite	40.8	85
Greenstone	3.36	7
Fine grained granite	2.4	5
Pegmatite	1.44	3
Total	48	100

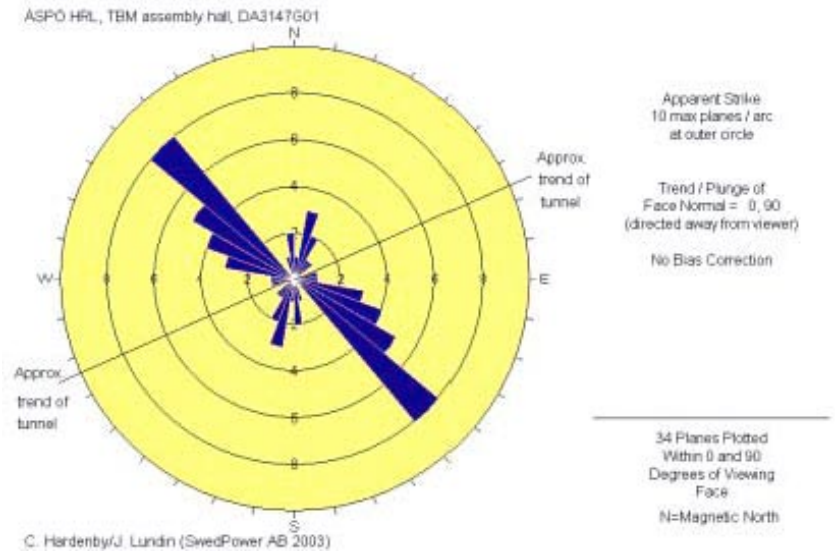

Figure 2-4. *Fracture orientations (partly compass readings and partly graphical interpretation) from DA3147G01 presented in Schmidt net and joint rosette diagrams.*

Table 2-5. Distribution of fracture fillings in deposition hole DA3147G01.

Filling	No of observations	% of all observations (total 92 fractures)
Chlorite	66	72
Oxidation rim/streak	26	28
Epidote	12	13
Calcite	11	12
Fine-grained granite	5	5
Quartz	2	2
Fe-precipitate/gel	7	8
No filling or not observed	6	7

Table 2-6. Distribution of fracture surface categories in deposition hole DA3147G01.

Surface category	No of fractures (alternative 1)	% of all fractures (total 92)	No of fractures (alternative 2)	% of all fractures (total 92)
Planar and rough	74	80	49	54
Planar and undefined			25	27
Undulating and rough	17	19	14	15
Undulating and undefined			3	3
Arched and rough	1	1	1	1
Totally	92	100	92	100

Table 2-7. Distribution of fracture lengths in deposition hole DA3147G01.

Length interval in meters	Detailed mapping of canister deposition hole			
	Cut off of 0.5 m			Cut off of 1 m
	No of fractures		% of all the 92 fractures	% of all the 51 fractures
<1	41	(–)	45	–
1–2	35	(35)	38	68
2–3	9	(9)	10	18
3–4	5	(5)	5	10
4–5	1	(1)	1	2
5–6	1	(1)	1	2
Total	92	(51)	100	100

2.2 Hydrogeology (IPR-04-52)

Several observations of water occurrence were made during the geological mapping. Additionally, as a part of the Lasgit project some hydrogeological tests have been performed in the large deposition hole DA3147G01. These include pressure build up and pressure drop tests and gas leakage tests.

2.2.1 Water observations in the TBM assembly hall

Leakage of water was recorded at a number of locations of which some were patches on the rock surface and some were fractures. In the Äspö tunnel system as a whole the water-bearing fractures commonly are steeply dipping, striking NW or SE.

Where the quantity of the water leakage, originating from micro-cracks in the rock mass or from distinct fractures in the walls and roof of the assembly hall, was measured it was normally < 0.3 litres/minute. However, three fractures discharged as much as 2–4 litres/minute. Observations of water leakage are lacking from the pit-floor due to constant inflow from the side-walls of the pit.

The measured inflow of water in the two pilot holes KA3147G01 and KA3153G01 was about 1.15 and 0.1 litres/minute respectively during the pressure build up test with water pressures about 9 and 13 bars.

The TBM assembly hall is no wetter than the rest of the Äspö tunnel system. However, the walls and roof both discharge some water though this is from discrete locations which are unevenly distributed.

2.2.2 Water observations in the large deposition hole DA3147G01

The water-bearing fractures in the deposition hole are, besides a few sub-horizontal-gently dipping ones, rather steeply dipping towards SW whereas those in the walls and roof of the assembly hall are steeply dipping towards the SW or NE. Occurrences of water are summarised in Table 2-8.

The leakage of water in the deposition hole was of minor seepage or occasional drops. It was, however, not measured. Leakage between concrete and rock at the top of the hole and a drill hole ending close to the bottom of the deposition hole gave each about 0.5 litres of water per minute.

2.2.3 Hydrogeological tests in the deposition hole

The inflow of water into the Lasgit hole was measured using the setup shown in Figure 2-5. Water originating from the surrounding tunnel floor (termed “external water”) was prevented from entering the deposition hole and was measured separately. Ingress of water to the Lasgit hole, entering through the fractures and the rock mass of the hole wall and bottom (“internal water”), was measured by using a level indicator to study the rise of the water level over time.

During the period the measurements took place, the inflow of “external water” varied between 10–20 litres/day or 0.007–0.013 litres/minute, as shown in Figure 2-6.

Table 2-8. Occurrences of water in deposition hole DA3147G01.

Origin of water	Number of observations	Character of water leakage	Flow (l/min)	Remarks
Rock	1	(1) Damp, minor seepage or occasional drops	"0"	The whole hole wall is damp to wet.
Rock	2	(3) Wet – flow	0.1–0.5	Quantity estimated from leakage between concrete and rock. The whole bottom is very wet due to leakage above
Fracture	11	(1) Damp, minor seepage or occasional drops	"0"	Quantity has not been estimated or measured
Fracture	1	(2) Wet, seepage, minor flow or drops	"0"	Quantity has not been estimated or measured
Fracture	1	(3) Wet – Flow	"0"	Quantity has not been estimated or measured. Most leakage from lower part of fracture
Drill hole	1	(3) Wet – Flow	0.5	

Figure 2-5. *Deposition hole DA3147G01 with the circular drain and small plastic container (greyish).*

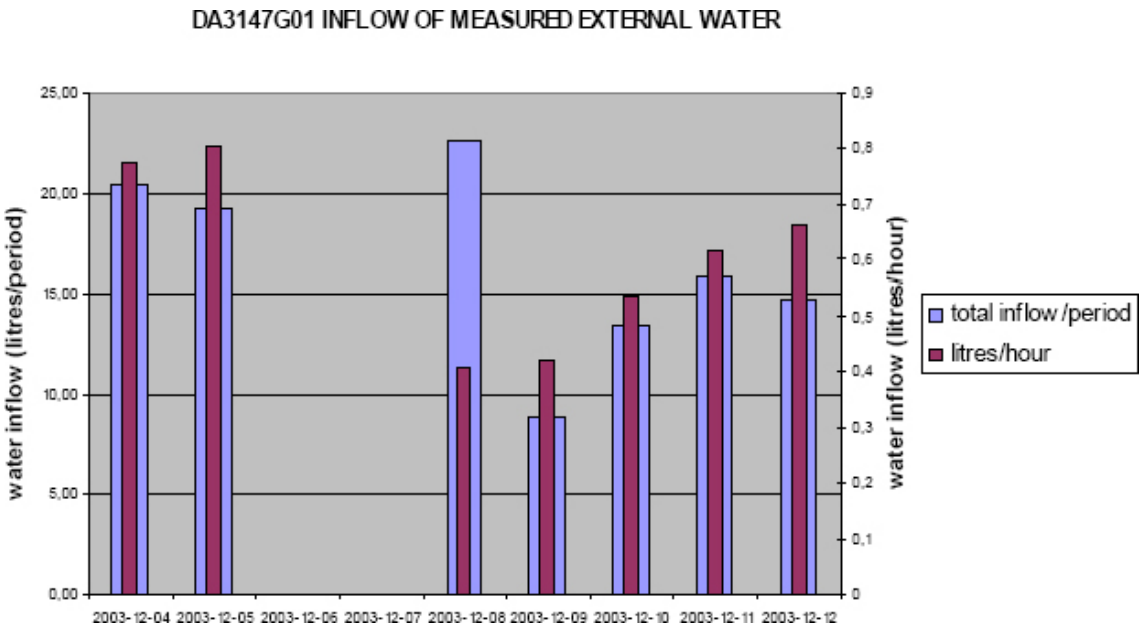

Figure 2-6. *Inflow of measured external water, total inflow and inflow rate (litres/hour) per measuring interval in deposition hole DA3147G01.*

The inflow of "internal water" was about 240 litres/day or 0.17 litres/minute if the theoretical evaporation was not considered and 266 litres/day or 0.2 litres/minute if it was, as summarised in Table 2-9.

To get an estimate of the evaporation in the TBM assembly hall an *in situ* test was performed in March 2004. It showed that the evaporation from a 1 metre square free water surface was 0.67 litres/day. This means that the evaporation from the free, circular water surface down in the deposition hole is 1.6 litres/day (possible evaporation from the hole wall not included). This corresponds to 0.7% of the "internal" inflow which is much less than the accuracy of the method used to measure the inflow (± 2.5–3%). Thus, the evaporation from the free water surface down in the hole may be neglected.

At the time when the measurements of "internal water" inflow took place the theoretical evaporation from the hole wall could have been as much as about 24 litres/day. This is under the condition that the entire hole wall acts as a free water surface which is not the case since large parts of the wall were dry-damp. As such the evaporation from the hole wall is of minor importance for this study and the measured inflow of "internal water" can be regarded as the real inflow.

Table 2-9. Inflow of internal water into deposition hole DA3147G01 in December 2003 (water level refers to recorded level relative to a reference level at the upper part of the hole at the end date of an interval).

Interval		No of hours	Water level (m)	Change in water level (m)	Quantity of water (litres)	Inflow rate		
Start	End					(litres /day)	(litres /hr)	(litres/min)
Day Time	Day Time							
	12 13:50		8.203					
12 13:50	15 16:07	74.3	7.915	0.315	757.7	244.8	10.2	0.17
15 16:07	17 10:30	42.4	7.745	0.170	408.9	231.5	9.6	0.16
Total		116.7		0.485	1,166.6			
Mean						239.9	10.0	0.17

2.2.4 Pressure build up and pressure drop tests

Pressure build up tests have been made not only in the anchor holes but also in pilot holes drilled in the planned centres of all the large deposition holes on the 420 m level prior to the drilling of the deposition hole. These tests show a water pressure varying between 3–20 bars in the anchor holes and 0–27 bars in the pilot holes.

The pressure drop tests or pulse tests performed in the anchor holes gave varying results too. While none of the curves reach a well defined asymptote, the pressure decays are sufficiently well defined to provide an estimate of the hydraulic properties. The calculated hydraulic conductivities and transmissivities varied between 1×10^{-12}–7×10^{-10} m.s^{-1} and 9×10^{-12}–3×10^{-9} m^2.s^{-1} respectively. Figure 2-7 shows an example of a pressure drop test.

2.2.5 Gas leakage test

A gas leakage test was performed in six of the ten anchor holes in order to investigate whether there were any connections between the anchor holes and the water filled Lasgit hole. Anchor holes were incrementally pressurised. Gas leakage was seen as bubbles on the water surface in the Lasgit hole, as shown in Figure 2-8, and in the neighbouring anchor holes. With the help of a video camera the gas leakage was located on the wall of the Lasgit hole and registered on drawings; one example is shown in Figure 2-9. Results from these tests clearly demonstrate that a number of fractures intersect both the neighbouring anchor holes and the Lasgit deposition hole. Table 2-10 summarises the observations during the gas leakage tests.

It can also be seen that pressurising rock anchors on one side of the deposition hole often resulted in gas leakage on the opposite side of the hole. This shows that the fracture network is complex and that gas does not always flow to the nearest fracture in the deposition hole, but follows a path of least resistance. The varying results of the respective pressure tests are likely to be due to variations in fracture geometry and transmissivity as well as the geospatial distribution of boreholes along the various features. Leakage between packer and hole walls is, however, another possibility and cannot be ruled out.

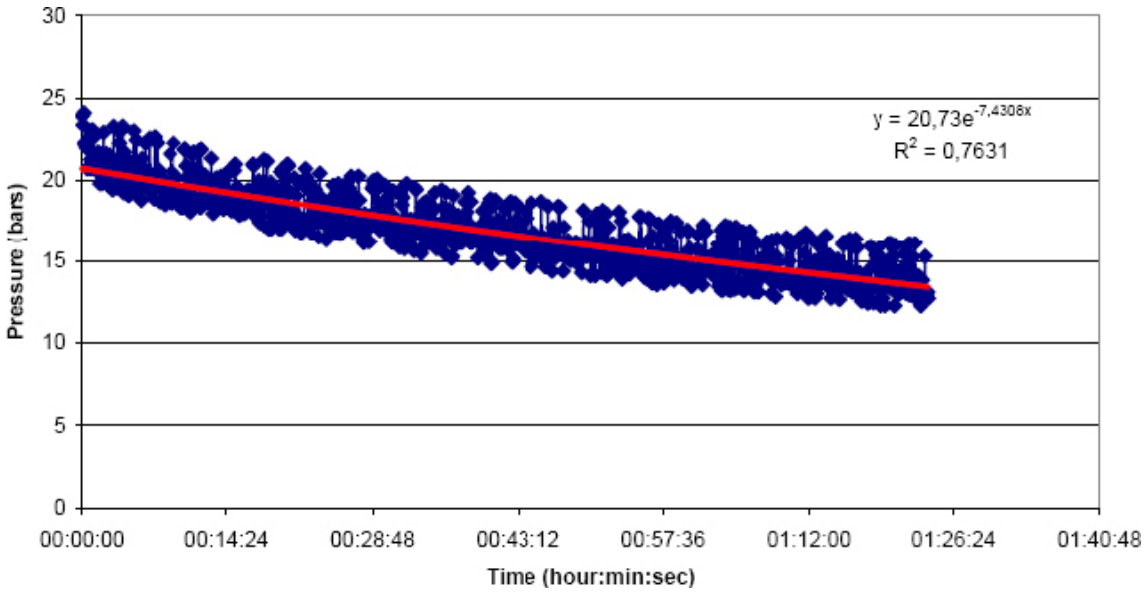

Figure 2-7. *Pressure drop test in HA3147G01 (individual readings and trend line).*

Figure 2-8. Gas bubbles on the water surface in the Lasgit hole.

Table 2-10. Notes from the gas leakage test in the Lasgit hole DA3147G01 and some of the anchor holes.

Pressurized Anchor Hole No	Start April 2004 Day/time (d/h:min)	Max pressure Time (h:min)	Max pressure Pressure (bars)	End April 2004 Day/time (d/h:min)	End pressure (bars)	Notes G01–G10 refer to the anchor holes.
HA3147G01	21/13:37	13:41	20	21/15:26	16.5	G01: some bubbles observed above the packer, G10: bubbles, G02 and G09: a few bubbles.
HA3147G02	20/13:22	13:32	20	20/15:24	16	G02: lots of bubbles observed above the packer, G03: lots of bubbles, G01 and G10: bubbles and G05: a few bubbles
HA3147G04	20/10:26	10:35	20	20/11:45	16	G04: bubbles observed above the packer and G05: bubbles
HA3147G06	–/10:39	10:55	20	–/11:21	20	G06: some bubbles above the packer
HA3147G08	21/10:59	11:11	20	21/12:11	19.5	G08: a few bubbles above the packer
HA3147G10	21/08:48	09:00	20	21/09:40	19	G10: a few bubbles above the packer, G01 and G09: a few bubbles

2.2.6 EDZ in the deposition hole (IPR-07-14)

An Excavation Disturbed/Damaged Zone (EDZ) is formed around circular openings (boreholes, tunnels etc) when they are constructed. During construction, supporting rock material is removed. However, the stress in the system is not reduced, so the rock around the perimeter of a tunnel has to support the load that was previously carried by the removed mass from within the tunnel. This leads to stress concentrations round the circumference of the tunnel wall.

The geological mapping of the deposition hole did not describe any of the “classic” features observed around tunnels with significant EDZ’s. However, the damage can often be microscopic and not obvious to the naked eye, so the lack of spalling material is not symptomatic of an absent EDZ and further tests were performed in order to establish (or not) the existence of an EDZ.

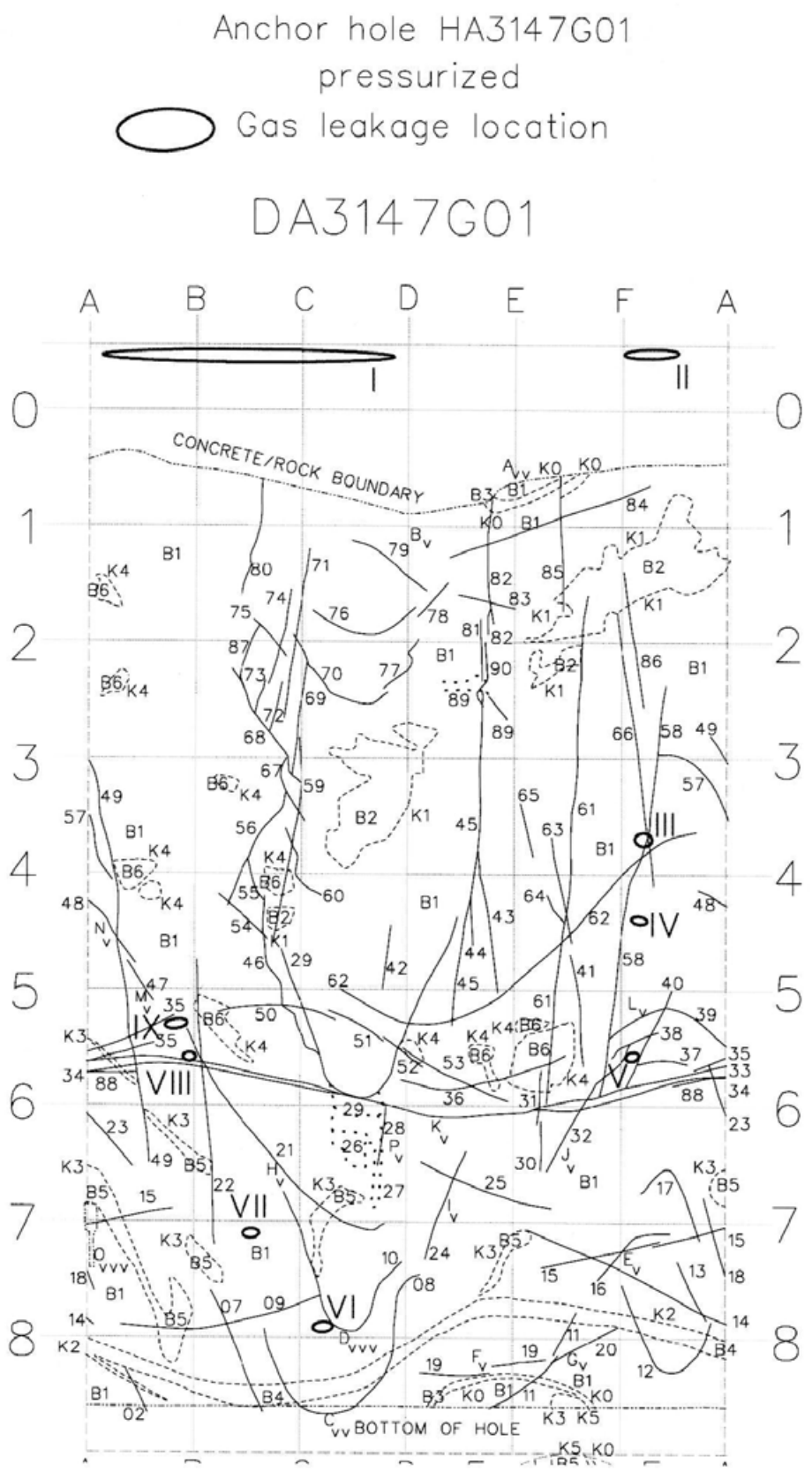

Figure 2-9. *Gas leakage locations in DA3147G01 when anchor hole HA3147G01 was pressurized.* ***Legend:*** *I. Bubbles on the surface; II. Some bubbles on the surface; III–V. Bubbles from one spot; VI. Bubbles; VII. Some bubbles, one spot; VIII. Bubbles, one spot, top of slot; IX. Bubbles from three spots in a row.*

Bundesanstalt für Geowissenschaften und Rohstoffe (BGR) developed a surface packer system designed to test for the presence of an EDZ at the Äspö site. This type of packer is fixed directly on the gallery wall and is therefore able to characterize the surface area most damaged during excavation of the deposition hole. This surface packer system was used at a number of locations in the HRL at Äspö including galleries (excavated by drill and blast), the TBM and deposition holes; including DA3147G01 **(**the Lasgit deposition hole).

A photograph of the surface packer system is shown in Figure 2-10 and as a schematic in Figure 2-11. The packer comprises a circular metal unit sealed to the rock surface using bentonite which is held in place by fixing bolts attached within the rock. Water or gas is introduced and pressure decay is monitored. For the measurements within the Lasgit deposition hole only local water was used as an injection fluid.

Tests were planned at two positions with water-bearing fractures in the deposition hole and on one position without visible fractures. The tests on the fractured positions failed. Instead of swelling, the bentonite was washed out of the furrow during the hydration stage by the inflowing water from the fracture. A similar response was noted during the initial hydration stage of the main Lasgit experiment (Section 4). The asperities on the wall of the deposition hole on these positions turned out to be too rough.

On the position without visible fractures a test sequence of two pulses (160 kPa and 220 kPa) was conducted. An axially symmetric model was used for the test analysis. Figure 2-12 shows a comparison of the measured pressure evolution in the surface packer (grey line) and calculated pressure evolutions for several permeability values. The calculated pressure evolution for a permeability of the rock of 10^{-19} m² agrees well with the measured data. However, one limitation of this method is the potential for water leakage through the bentonite packer assembly rather than within the diorite rock mass. Assuming this effect is negligible, /Nowak et al. 2007/ conclude there is no evidence of an EDZ in the Lasgit deposition hole and as such quote a permeability value for the “intact” granite of 10^{-19} m^2.

Figure 2-10. *The surface packer system of BGR shown in situ ready for the start of a test.*

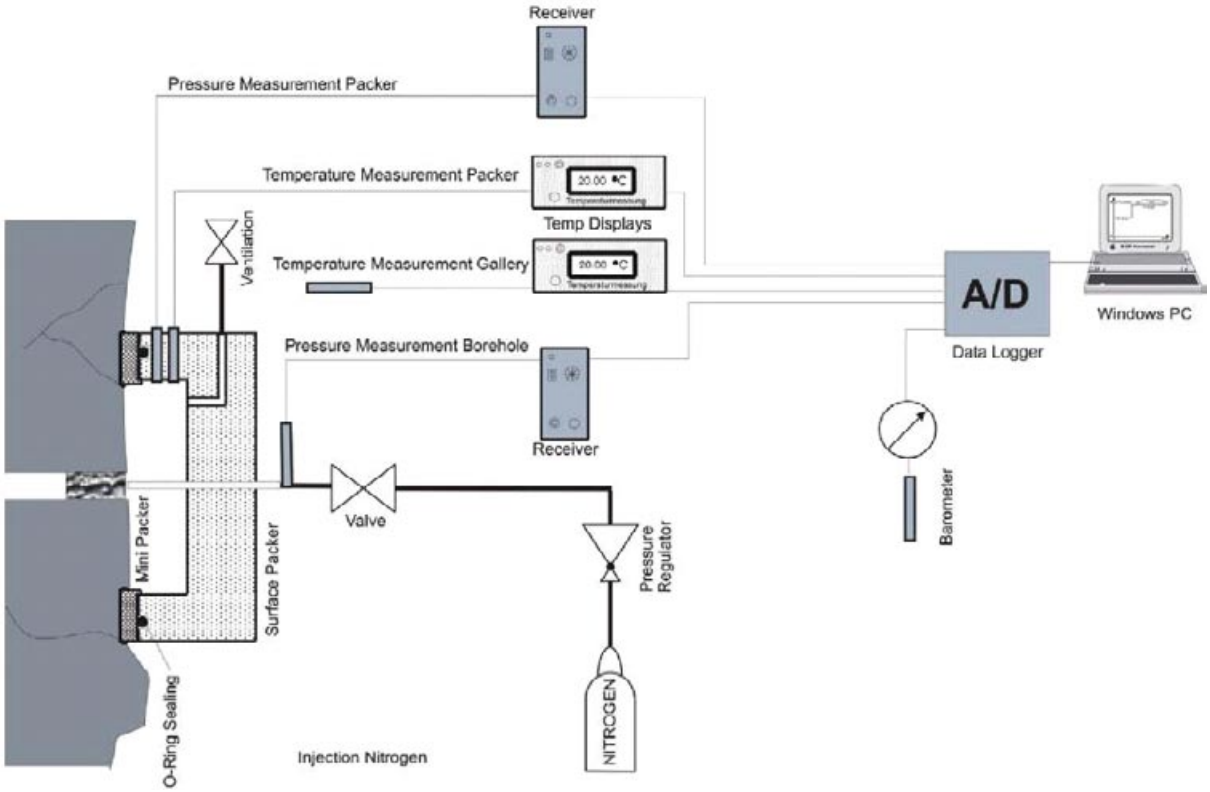

Figure 2-11. *The surface packer and mini packer system shown as a schematic.*

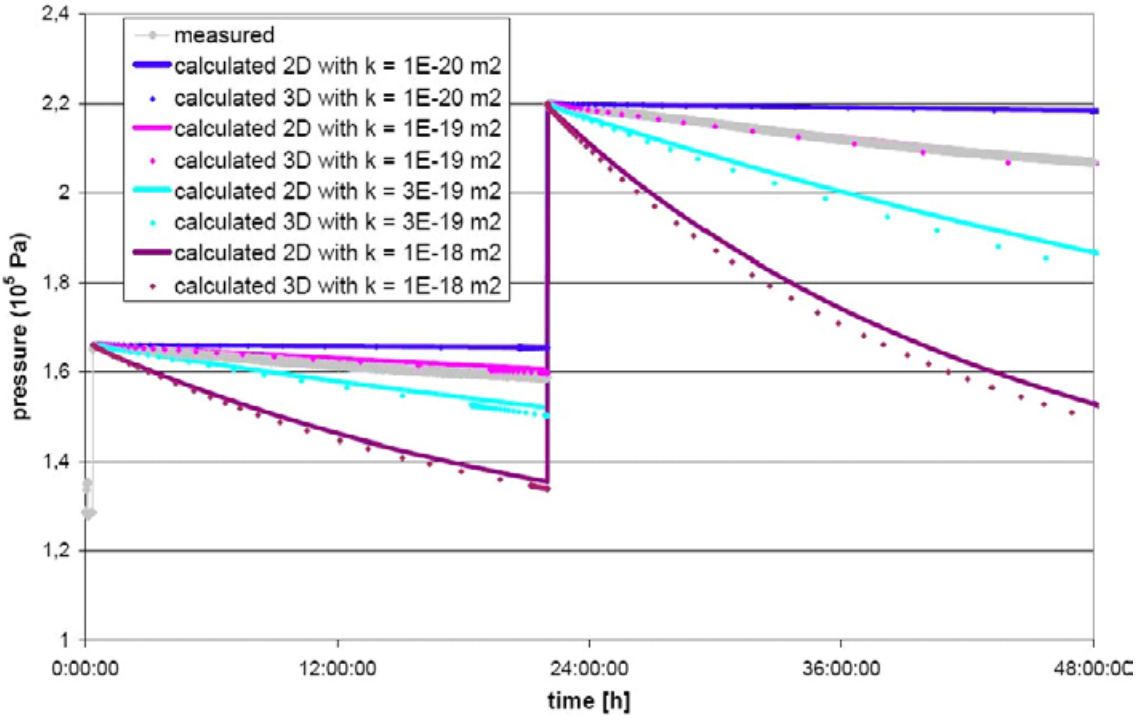

Figure 2-12. *Result from surface packer test in deposition hole DA3147G01 (Lasgit).*

3 Experimental geometry and data reduction

The Lasgit experiment has been commissioned in deposition hole No. DA3147G01 – the first emplacement borehole to be drilled at the Äspö URL. The deposition hole has a length of 8.5 m and a diameter of around 1.75 m. A full scale KBS-3 canister has been modified for the Lasgit experiment with twelve circular filters of varying dimensions located on its surface to provide point sources for gas injection, mimicking potential canister defects. These filters can also be used to inject water during the hydration stage.

The deposition hole, buffer and canister are equipped with instrumentation to measure the total stress, porewater pressure and relative humidity in 32, 26 and 7 positions respectively. Additional instrumentation continually monitors variations in temperature, relative displacement of the lid and the restraining forces on the rock anchors. The emplacement hole has been capped by a conical concrete plug retained by a reinforced steel lid capable of withstanding over 5,000 tonnes of force. Figure 3-1 shows a photograph of the test site following the installation stage.

The state-of-the-art experimental monitoring and control systems for Lasgit are housed in the "Gas Laboratory" which is a self-contained unit designed and assembled by BGS within a modified shipping container. A customised graphical interface based on National Instruments LabVIEW™ software enables remote control and monitoring to be undertaken by project staff from any Internet connected PC around the world.

3.1 Gas laboratory

The Gas Laboratory is housed in a fully insulated pre-fabricated shipping container. This facility houses all experimental circuits (hydration, hydraulic and gas injection) as well as data acquisition and telemetry systems.

The shipping container housing the Gas Laboratory has been partitioned into two sections. The first comprises the office area and contains the workstation plus general office furniture, telemetry system and main electrical consumer unit. The second area contains all of the experimental apparatus, test circuits and data acquisition systems. Figure 3-2 shows a full 360º panorama inside the gas laboratory.

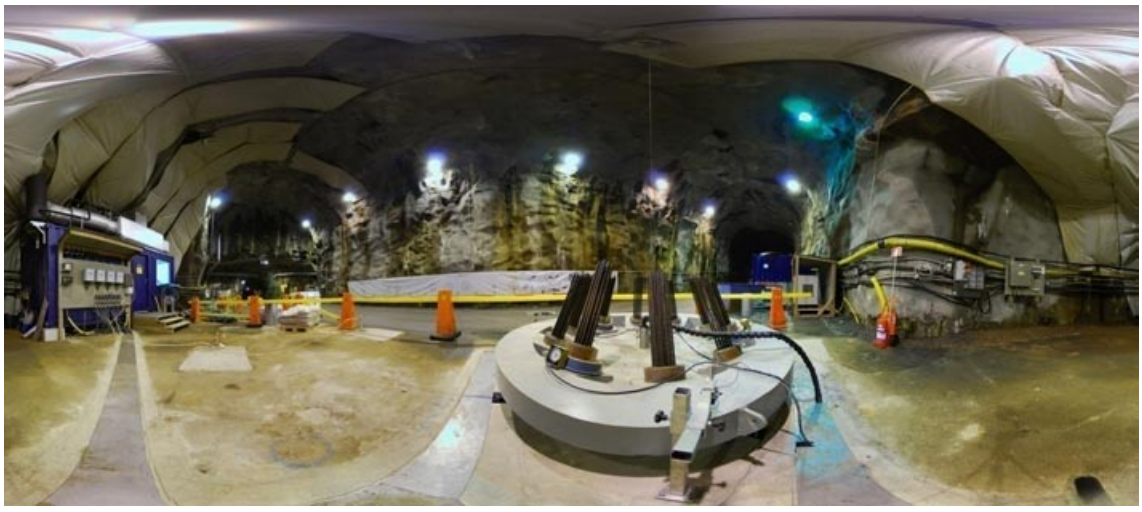

Figure 3-1. *A panoramic view of the Large-scale gas injection test (Lasgit) 420 m below ground at the Äspö Hard Rock Laboratory in Sweden.*

Figure 3-2. *A panoramic view of the Lasgit gas laboratory.*

Temperature in both the office and laboratory sections is controlled by two independent air conditioning systems. The temperature set point in the Laboratory section was set at 14°C, similar to the ambient conditions within the Lasgit deposition hole; the air-conditioning achieved a mean temperature of 15.8°C. To prevent overloading of the air-conditioning system the temperature in the office compartment was reduced at day 750 and although temperature oscillated on an annual basis the mean temperature reduced to 15.0°C. To maintain a flow-through of air and help to minimise condensation, the air is continuously replaced and its humidity controlled to prevent damage to test systems. Temperature sensors located in both compartments of the Gas Laboratory are continuously monitored by the data acquisition software and by the Alpha Alarm system, the latter providing 24hr support in the event of a system failure.

3.2 Apparatus and instrumentation

The following sections describe the key components of the Lasgit system.

3.2.1 The lid and retaining setup

The pressure that would be exerted by the backfill as the tunnel gallery was closed is generated using a heavy 2,600 mm diameter SS2172 carbon steel lid; this also prevents an uncontrolled expansion of the bentonite. At the top of the buffer a waterproof and sealed rubber mat is placed, upon which a conical shaped concrete plug was poured using K 40 quality concrete /Bäck 2003/ to close the deposition hole, the top of which was level with the TBM assemble floor. On top of this plug, the steel lid was anchored to the rock by 10 anchor cables. The lid and rock anchors can be seen in Figure 3-1.

The retaining system (i.e. concrete plug, steel lid and anchoring cables) is designed for a maximum operating pressure of 20 MPa. The rationale in using a conically shaped concrete plug is to (a) ensure that the plug can move upwards when subject to high axial pressures and (b) can be readily dismantled at the end of testing.

The anchor system comprises cables of type VSL 19-15, which are secured using a low-pH cementitious injection grout within ten holes of 162 mm diameter, 11 m length, and angled at 21.8° from the deposition hole. Each cable is grouted for 8 m length of the cable to ensure the anchors can accommodate the forces which will be generated during testing. The retaining system is also design to allow small vertical deformations of the concrete plug and steel lid when subject to high axial forces.

The anchor cables holding the lid were pre-tensioned to 1,300 kN using two hydraulic jacks in parallel. Three of the anchors include Glötzel load cells of type kN 5,000 A160 M/DKV6, with a maximum load 5,500 kN. These are used to log load on the rock anchors, and thus the load exerted by the buffer, during the operation of the test.

3.2.2 The canister and filter array

The canister used in Lasgit is a standard KBS-3 design, with additional filters. This design consists of a 50 mm thick outer copper skin, which acts as a corrosion barrier in the oxygen-poor groundwater of the crystalline rock selected for disposal, and a nodular iron insert to provide strength and rigidity (see Figure 3-4a). Each canister weighs up to 27 tonnes (including the fuel rod assemblies), is 4.835 metres long and has a diameter of 1.05 metre.

Figure 3-3 shows a sketch cross-section through the deposition hole, giving dimensions of the individual elements of the KBS-3V concept. The space around the canister is filled with pre-compacted bentonite blocks, which, once hydrated, acts as a low permeability diffusional barrier. The unique physicochemical properties of the bentonite depend on its colloidal behaviour and enormous specific surface. These include high sorption capacity, very high plasticity and excellent fracture self-sealing characteristics, severely limiting the migration of any radionuclides released from a canister after closure of the repository. The bentonite used is MX-80 /Johannesson 2003/ with a water content of 22% (for the ring-shaped blocks) and 26% (for the cylindrical blocks).

The space between the bentonite rings and wall-rock was in-filled using bentonite pellets, manufactured by Saut-Conreursin in France. Each pellet is pressed from bentonite and has dimensions of 16.3 × 16.3 × 8.3 mm, a water content of about 17% and an expected density of a single pellet of about 2,050 kg·m^{-3}. The expected bulk density of the fillings is approximately 1,230 kg·m^{-3}.

Table 3-1 shows the dimensions and starting physical properties of the pre-compacted bentonite rings. As shown, a high degree of saturation (between 95.1% and 99.7%) was achieved, with bulk densities ranging between 2,018 kg·m^{-3} and 2,061 kg·m^{-3}. Table 3-2 shows the expected density and swelling pressure after saturation at different sections of the deposition hole. This predicts a swelling pressure of between 3,970 kPa and 4,368 kPa within the Lasgit depositional hole, with greater pressure achieved above and below the canister.

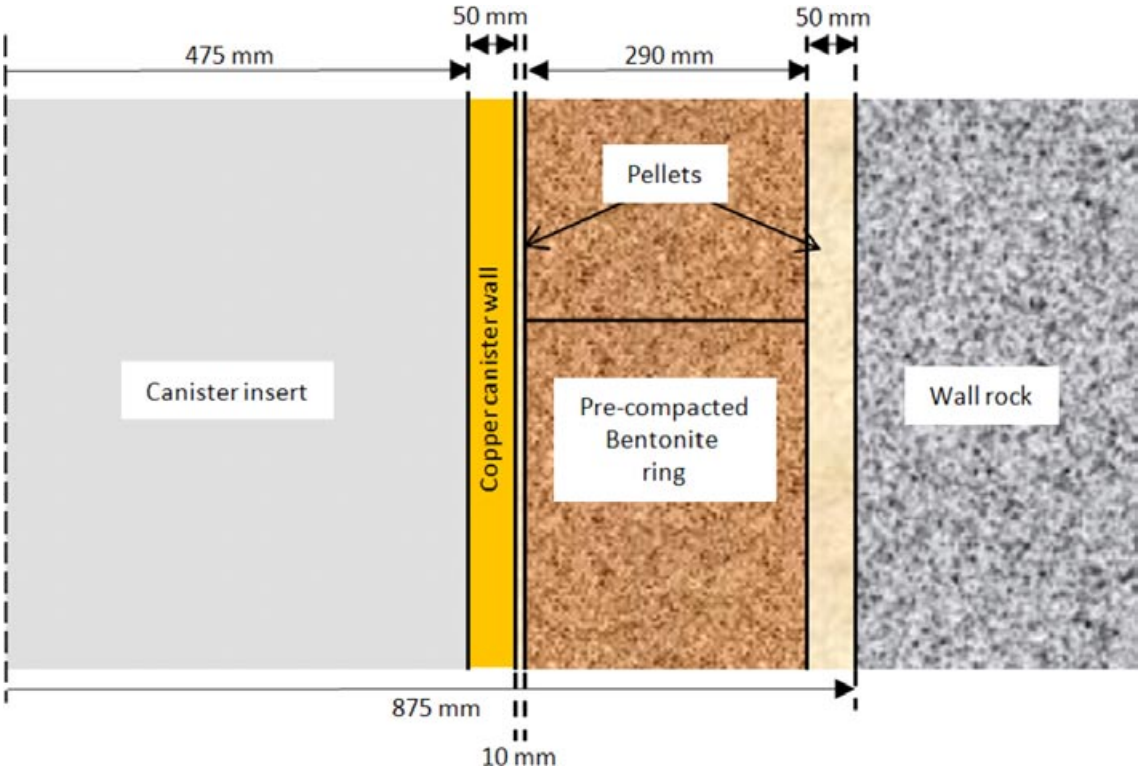

Figure 3-3. *Cross-section sketch through the Lasgit deposition hole. Surrounding the copper canister is a 290 mm thick annulus of pre-compacted bentonite. This leaves a 10 mm gap on the inside between the bentonite and canister and a 50 mm gap between the bentonite and the wallrock, which is filled with bentonite pellets.*

Table 3-1. Properties and dimensions of the bentonite buffer.

Block No.	Date at Comp.	Block No In deposition hole	Moisture content	Bulk density (kg/m3)	Degree of Saturation	Void ratio	Dry density (kg/m3)	Dens at sat (kg/m3)	Weight (kg)	Height (mm)	Diam. D1 (mm)	Diam. D2 (mm)	Diam. D3 (mm)
LASC1	16/09/2003	Extra block	0.265	2018.1	0.993	0.743	1594.9	2021.2	2140.0	507.4	1623.3	1639.3	0
LASC2	17/09/2003	C1	0.264	2015.2	0.986	0.743	1594.8	2021.2	2112.0	501.4	1623.5	1639.35	0
LASC3	17/09/2003	C2	0.262	2020.4	0.989	0.736	1601.2	2025.2	2116.0	501.0	1623.45	1639.4	0
LASC4	18/09/2003	C3	0.261	2017.4	0.984	0.738	1599.9	2024.4	2096.0	496.9	1623.75	1639.45	0
LASC5	18/09/2003	C4	0.268	2017.9	0.997	0.746	1592.0	2019.3	2116.0	501.6	1623.7	1639.45	0
LASC6	19/09/2003	C5	0.260	2020.9	0.986	0.733	1604.0	2027.0	2114.0	500.5	1623.45	1639.3	0
LASR1	23/09/2003	Extra block	0.225	2055.5	0.951	0.656	1678.6	2074.8	1268.0	516.7	1625.25	1639.65	1070
LASR2	25/09/2003	R1	0.230	2050.2	0.958	0.668	1666.6	2067.1	1248.0	509.4	1625.6	1639.65	1069.6
LASR3	25/09/2003	R2	0.226	2054.1	0.953	0.659	1675.2	2072.6	1236.0	504.3	1624.8	1639.7	1070
LASR4	25/09/2003	R3	0.227	2059.6	0.962	0.656	1678.6	2074.8	1234.0	501.9	1624.75	1639.65	1069.7
LASR5	26/09/2003	R4	0.232	2057.0	0.970	0.665	1669.8	2069.2	1234.0	502.5	1624.95	1639.4	1069.5
LASR6	26/09/2003	R5	0.228	2059.7	0.964	0.657	1677.6	2074.2	1236.0	502.6	1624.9	1639.6	1069.6
LASR7	29/09/2003	R6	0.233	2058.4	0.974	0.665	1669.3	2068.9	1236.0	502.6	1625	1639.5	1069.2
LASR8	29/09/2003	R7	0.228	2050.8	0.953	0.664	1670.3	2069.5	1224.0	499.8	1625	1639.6	1069.5
LASR9	29/09/2003	Extra block	0.224	2060.6	0.956	0.651	1683.4	2077.9	1246.0	506.1	1624.75	1639.6	1069
LASR10	30/09/2003	R8	0.228	2054.1	0.957	0.661	1673.4	2071.4	1228.0	500.3	1624.85	1639.7	1069
LASR11	30/09/2003	R9	0.227	2061.4	0.964	0.655	1679.9	2075.6	1238.0	502.7	1625.25	1639.45	1069.3
LASR12	30/09/2003	R10	0.227	2061.1	0.964	0.655	1679.5	2075.3	1236.0	502.3	1625	1639.5	1069.2
Average LASC			0.263	2018.3					2115.7	501.4	1623.5	1639.4	0.0
Average LASR			0.228	2056.9					1238.7	504.3	1625.0	1639.6	1069.5

Table 3-2. Expected density and swelling pressure after saturation at different sections of the deposition hole.

Section	Density at saturation (kg·m^{-3})	Void ratio	Dry density (kg·m^{-3})	Expected swelling pressure (kPa)
C – above and below canister	1,972	0.831	1,518	4,368
R – at canister	1,964	0.846	1,506	3,970

A series of filters were added to the canister surface in order to simulate a point defect perforation of the canister. A filter was also added to the bottom of the canister to look at the impact of the energy stored within a large volume of gas and its impact on the mechanisms of gas entry and movement. The design of the filter assemblies (Figure 3-4b) had to accommodate a number of engineering and experimental considerations. To help maintain structural integrity and strength of the canister, the diameter of the filter assemblies were minimised, in order to retain as much of the original canister material as possible (Figure 3-4c). The rigidity of the canister was enhanced by securing each filter assembly with 8 Monel cap-screws, tensioned uniformly to apply an even load.

Figure 3-4. *The canister as used in the Lasgit test. The canister comprises a standard KBS-3 canister, made up of a copper canister and cast iron insert (a). Twelve filters (b) are placed at three levels along the length of the canister in recesses (c). The complete Lasgit canister is shown in (d) with the filters in place and the associated pipework coming through the canister lid.*

To minimise leakage of test fluids around each filter assembly into the main body of the canister, a dual O-ring sealing mechanism was developed. All pressure connections were made using standard 1/8" BSP stainless steel male connectors. An advantage of using this type of fitting was that it ensured engaged thread lengths are constant for each pressure connection, allowing each fitting to be tightened to a similar torque, reducing the chance of leakage and accidental shearing of the copper threads.

Each filter array has been designed with dual ports to facilitate the removal of test permeants and "sweeping" of the sintered filter. The size of the filter discs installed in each housing have been varied to examine the effect of gas pressure gradient on the gas entry pressure (Table 3-3). The filter housings were also profiled with respect to the major axis of the cylinder to help reduce the potential for voids or "bridging", caused by the flat face of the housing protruding from the curved surface of the canister.

The maximum fluid pressure generated within each filter assembly is continuously monitored and controlled by reciprocating ISCO syringe pumps (Section 3.2.3). Alarm functions embedded in each pump controller provide a facility for controlling the maximum fluid pressure generated by the pump system. Force gauges, mounted on a number of the rock anchors holding the lid in position, continually monitor the pressure applied to the lid by the bentonite so that pumping can be stopped if the force exceeds a pre-determined value.

To minimise corrosion and galvanic responses between the porous filter and the main body of the filter assembly (manufactured from C103 copper), a number of alternative sinter materials were examined. After consultation with SKB, it was decided to use sintered bronze as the filter material. This copper-alloy is mechanically robust, can be readily machined, and because of its copper content, should exhibit low corrosion and galvanic responses when in communication with the canister infra-structure and test permeants. To prevent intrusion of bentonite during the testing, a relatively small mean pore size distribution for the sintered bronze discs was selected (i.e. 4 to 8 microns). This range in pore size equates to an air entry pressure of between 0.02 and 0.04 MPa, assuming circular pores and an interfacial tension coefficient between the gas and porewater of 7.275×10^{-2} Nm^{-1} at 20°C. This air-entry value is well below the excepted gas entry pressure for saturated buffer bentonite.

Given the relatively low cost of manufacture it was decided to place 13 filter assemblies at specific locations on the canister surface. In order to provide adequate contingency and provide additional points of porewater pressure measurement, a decision was made to place four filter assemblies at 90º intervals around the circumference of the canister at each selected elevation (Figure 3-5). To improve the spatial coverage of porewater pressure measurements, the upper and lower filter arrays were rotated 45º with respect to the mid-plane array. This results in a triangular mesh of porewater pressure measurements. An additional filter assembly was also placed in the base of the canister (Figure 3-6) in communication through a gas-actuated valve with the internal void space of the canister.

Table 3-3. Dimensions of hydration mats and canister filters.

Device name	Location	Units	Description	Dimensions (mm)		
				Height	Width	Radius
AXG0FR901	Rock wall	kPa	Pressure in filter mat 1	350	5,500	
AXG0FR902	Rock wall	kPa	Pressure in filter mat 2	750	5,500	
AXG0FB903	Bentonite	kPa	Pressure in filter mat 3	–	–	400
AXG0FB904	Bentonite	kPa	Pressure in filter mat 4	–	–	400
PXG0FL901	Cannister	kPa	Pressure in injection filter	–	–	50
PXG0FL902	Cannister	kPa	Pressure in injection filter	–	–	5
PXG0FL903	Cannister	kPa	Pressure in injection filter	–	–	50
PXG0FL904	Cannister	kPa	Pressure in injection filter	–	–	25
PXG0FM905	Cannister	kPa	Pressure in injection filter	–	–	50
PXG0FM906	Cannister	kPa	Pressure in injection filter	–	–	50
PXG0FM907	Cannister	kPa	Pressure in injection filter	–	–	50
PXG0FM908	Cannister	kPa	Pressure in injection filter	–	–	50
PXG0FU909	Cannister	kPa	Pressure in injection filter	–	–	50
PXG0FU910	Cannister	kPa	Pressure in injection filter	–	–	25
PXG0FU911	Cannister	kPa	Pressure in injection filter	–	–	50
PXG0FU912	Cannister	kPa	Pressure in injection filter	–	–	5
PXG0FC901	Cannister	kPa	Pressure in injection filter	–	–	–

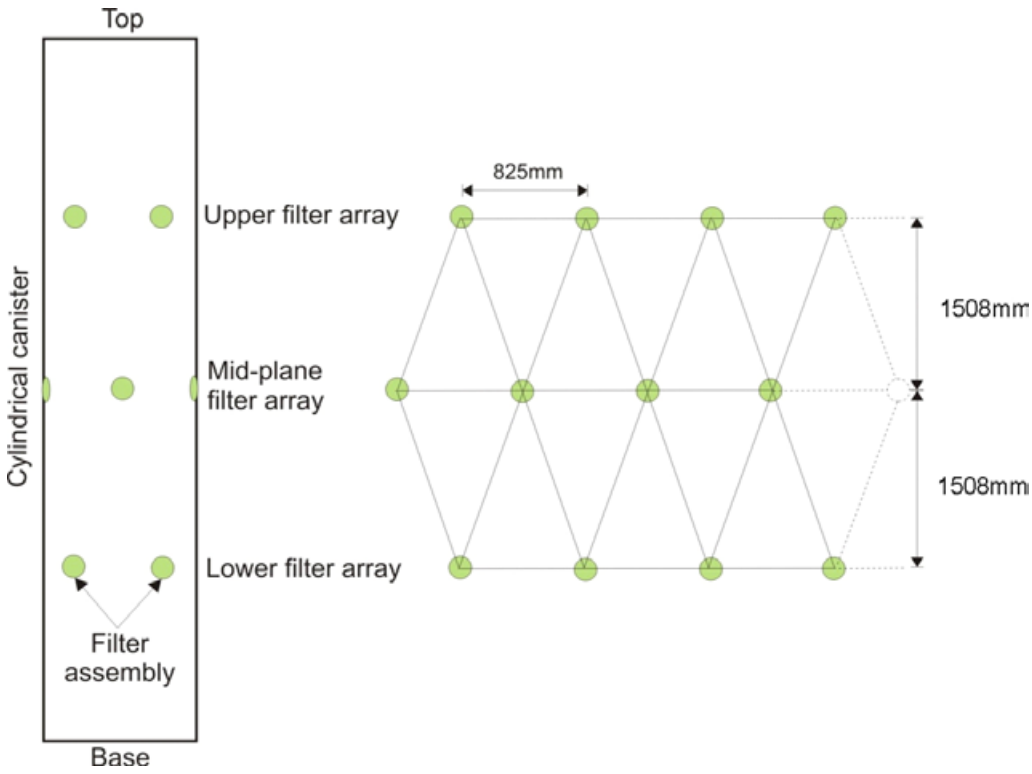

Figure 3-5. *Schematic side view of canister and visible filters (shown in green). The second graphic is a 2D representation showing the relative positions of the 12 radial injection filters.*

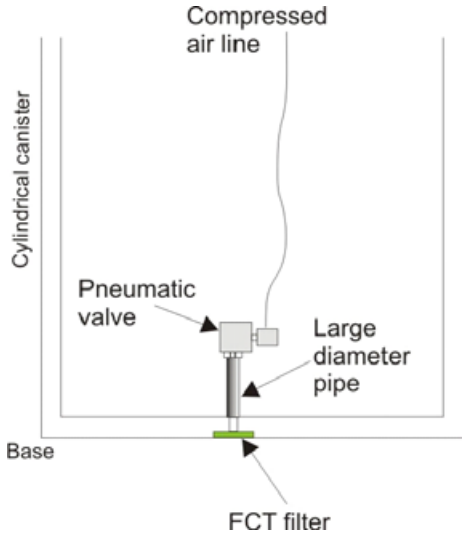

Figure 3-6. *Schematic showing the filter assembly located in the base of the canister.*

3.2.3 Reciprocating syringe pumps

Volumetric flow rates are controlled or monitored using a pair of ISCO-500, Series D, syringe pumps operated from a single digital control unit. The position of each pump piston is determined by an optically encoded disc graduated in segments equivalent to a change in volume of 31.71 ml. Movement of the pump piston is controlled by a micro-processor which continuously monitors and adjusts the rate of rotation of the encoded disc using a DC-motor connected to the piston assembly via a geared worm drive. This allows each pump to operate in either constant pressure or constant flow modes. A programme written in LabVIEW™ elicits data from the pump at pre-set time intervals. Testing is performed in an air-conditioned laboratory. Table 3-4 gives a list of the parameters logged from both ISCO pump controllers.

Table 3-4. List of logged parameters from the ISCO 500 Series D syringe pumps.

Device	Location	Units	Description
PXG0PP901	Gas Laboratory	kPa	Pressure in pump A1
PXG0PP902	Gas Laboratory	kPa	Pressure in Pump A2
PXG0PP903	Gas Laboratory	kPa	Pressure in pump B1
PXG0PP904	Gas Laboratory	kPa	Pressure in pump B2
PXG0QP901	Gas Laboratory	variable	Flowrate of pump A1
PXG0QP902	Gas Laboratory	variable	Flowrate of pump A2
PXG0QP903	Gas Laboratory	variable	Flowrate of pump B1
PXG0QP904	Gas Laboratory	variable	Flowrate of pump B2
PXG0VP901	Gas Laboratory	ml	Volume in pump A1
PXG0VP902	Gas Laboratory	ml	Volume in pump A2
PXG0VP903	Gas Laboratory	ml	Volume in pump B1
PXG0VP904	Gas Laboratory	ml	Volume in pump B2
PXG0VD901	Gas Laboratory	litres	Total cumulative volume pumped by pumps A1 and A2
PXG0VD902	Gas Laboratory	litres	Total cumulative volume pumped by pumps B1 and B2

3.2.4 Pressure transducers

Individual pressure transducers connected to each canister filter and hydration mat provide a continuous measure of up-hole pressure for each system component (Table 3-5). Each transducer is rated to 25 MPa and is accurate to 0.25% full scale. Output signals from the pressure transducers (4–20 mA) are logged by the data acquisition system. Prior to the commencement of testing each transducer was calibrated on site to a known pressure standard (Section 3.4).

3.2.5 Total stress sensors

Total stress in the Lasgit deposition hole is monitored at 32 separate locations (Table 3-6). Of these devices, 20 Geokon sensors are mounted on the rock wall (Figure 3-7), 9 Geokon sensors are located within the buffer material itself and 3 Sensotec sensors are positioned at specific locations on the can-

Table 3-5. List of pressure transducers attached to the canister filters and large hydration mats showing sensor name, location, unit of measurement and a description of the monitored parameter.

Device	Location	Units	Description
AXG0FR901	Rock wall	kPa	Pressure in filter mat 1
AXG0FR902	Rock wall	kPa	Pressure in filter mat 2
AXG0FB903	Bentonite	kPa	Pressure in filter mat 3
AXG0FB904	Bentonite	kPa	Pressure in filter mat 4
PXG0FL901	Cannister	kPa	Pressure in injection filter
PXG0FL902	Cannister	kPa	Pressure in injection filter
PXG0FL903	Cannister	kPa	Pressure in injection filter
PXG0FL904	Cannister	kPa	Pressure in injection filter
PXG0FM905	Cannister	kPa	Pressure in injection filter
PXG0FM906	Cannister	kPa	Pressure in injection filter
PXG0FM907	Cannister	kPa	Pressure in injection filter
PXG0FM908	Cannister	kPa	Pressure in injection filter
PXG0FU909	Cannister	kPa	Pressure in injection filter
PXG0FU910	Cannister	kPa	Pressure in injection filter
PXG0FU911	Cannister	kPa	Pressure in injection filter
PXG0FU912	Cannister	kPa	Pressure in injection filter
PXG0FC901	Cannister	kPa	Pressure in injection filter

Table 3-6. List of total stress sensors showing name, location, unit of measurement and a description of the monitored parameter.

Device/name	Location	Units	Description
PXG0PC901	Cannister	kPa	Pressure on outside of cannister
PXG0PC902	Cannister	kPa	Pressure on outside of cannister
PXG0PC903	Cannister	kPa	Pressure on outside of cannister
PXG0PB901	Bentonite	kPa	Pressure in bentonite
PXG0PB902	Bentonite	kPa	Pressure in bentonite
PXG0PR903	Rockwall	kPa	Pressure at bentonite/rock interface
PXG0PR904	Rockwall	kPa	Pressure at bentonite/rock interface
PXG0PR905	Rockwall	kPa	Pressure at bentonite/rock interface
PXG0PR906	Rockwall	kPa	Pressure at bentonite/rock interface
PXG0PR907	Rockwall	kPa	Pressure at bentonite/rock interface
PXG0PR908	Rockwall	kPa	Pressure at bentonite/rock interface
PXG0PR909	Rockwall	kPa	Pressure at bentonite/rock interface
PXG0PR910	Rockwall	kPa	Pressure at bentonite/rock interface
PXG0PR911	Rockwall	kPa	Pressure at bentonite/rock interface
PXG0PR912	Rockwall	kPa	Pressure at bentonite/rock interface
PXG0PR913	Rockwall	kPa	Pressure at bentonite/rock interface
PXG0PR914	Rockwall	kPa	Pressure at bentonite/rock interface
PXG0PR915	Rockwall	kPa	Pressure at bentonite/rock interface
PXG0PR916	Rockwall	kPa	Pressure at bentonite/rock interface
PXG0PR917	Rockwall	kPa	Pressure at bentonite/rock interface
PXG0PR918	Rockwall	kPa	Pressure at bentonite/rock interface
PXG0PR919	Rockwall	kPa	Pressure at bentonite/rock interface
PXG0PR920	Rockwall	kPa	Pressure at bentonite/rock interface
PXG0PR921	Rockwall	kPa	Pressure at bentonite/rock interface
PXG0PR922	Rockwall	kPa	Pressure at bentonite/rock interface
PXG0PB923	Bentonite	kPa	Pressure in bentonite
PXG0PB924	Bentonite	kPa	Pressure in bentonite
PXG0PB925	Bentonite	kPa	Pressure in bentonite
PXG0PB926	Bentonite	kPa	Pressure in bentonite
PXG0PB927	Bentonite	kPa	Pressure in bentonite
PXG0PB928	Bentonite	kPa	Pressure in bentonite
PXG0PB929	Bentonite	kPa	Pressure in bentonite

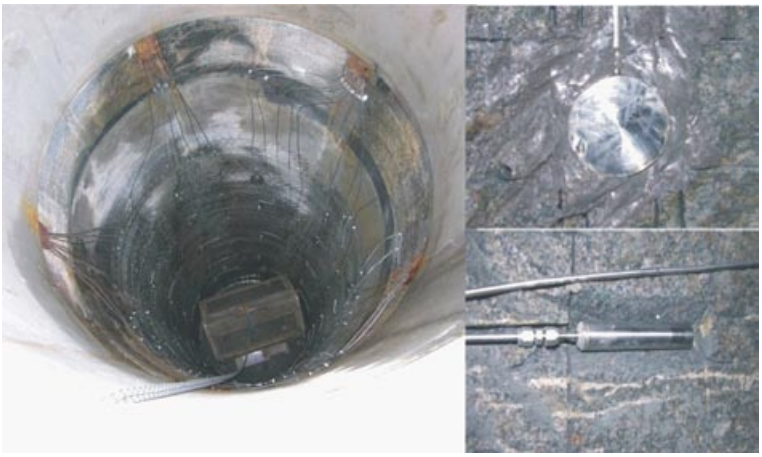

Figure 3-7. *The photograph on the left-hand side shows a view looking into the Lasgit deposition hole showing tube work containing the electrical connections from total stress and porewater pressure sensors mounted on rock face. The photographs on the upper and lower right-hand show a total stress and a porewater pressure sensor respectively.*

ister surface. Each Geokon sensor incorporates an integrated thermocouple which is used to correct the output signal from each device for fluctuations in background temperature. Factory calibrations are used to process the Geokon data into a stress value. An additional offset is then applied to the data to compensate for "drift" during the installation process. Each device outputs a resistance measurement which is collected by a custom built multilogger and then relayed to the data acquisition and control system (DAC) within the laboratory. The three stress sensors located on the canister output a current directly into the data acquisition system. These devices were calibrated prior to installation.

3.2.6 Porewater pressure sensors

The Lasgit experiment also uses Geokon porewater pressure sensors to monitor water pressure inside the buffer material and at the bentonite/diorite interface (Figure 3-7). A total of 26 sensors are used in the Lasgit hole, of which 20 are located on the rock face at the bentonite/diorite interface and 6 are positioned inside the buffer mass (Table 3-7). As with the total stress instruments described in Section 3.2.5, each device uses an integrated thermocouple to correct the output signal for thermal fluctuations in background temperature. This data is logged through the multilogger, which in turn passes on the raw outputs to the Lasgit DAC system for scaling into calibrated figures.

3.2.7 Psychrometers

To monitor the state of suction within the bentonite seven Wescor psychometric microvolt meters have been installed at various locations within the buffer mass (Table 3-8). These devices give an output between 10 and 300 microvolts and are factory calibrated with an effective operating range of 95 to 100% relative humidity. The outputs from these devices are recorded by a Campbell multilogger and downloaded to a separate stand alone PC attached to another experiment.

Table 3-7. List of porewater pressure sensors showing name, location, unit of measurement and a description of the monitored parameter.

Device	Units	Description
PXG0UB901	kPa	Porewater pressure in bentonite
PXG0UB902	kPa	Porewater pressure in bentonite
PXG0UR903	kPa	Porewater pressure at bentonite/rock interface
PXG0UR904	kPa	Porewater pressure at bentonite/rock interface
PXG0UR905	kPa	Porewater pressure at bentonite/rock interface
PXG0UR906	kPa	Porewater pressure at bentonite/rock interface
PXG0UR907	kPa	Porewater pressure at bentonite/rock interface
PXG0UR908	kPa	Porewater pressure at bentonite/rock interface
PXG0UR909	kPa	Porewater pressure at bentonite/rock interface
PXG0UR910	kPa	Porewater pressure at bentonite/rock interface
PXG0UR911	kPa	Porewater pressure at bentonite/rock interface
PXG0UR912	kPa	Porewater pressure at bentonite/rock interface
PXG0UR913	kPa	Porewater pressure at bentonite/rock interface
PXG0UR914	kPa	Porewater pressure at bentonite/rock interface
PXG0UR915	kPa	Porewater pressure at bentonite/rock interface
PXG0UR916	kPa	Porewater pressure at bentonite/rock interface
PXG0UR917	kPa	Porewater pressure at bentonite/rock interface
PXG0UR918	kPa	Porewater pressure at bentonite/rock interface
PXG0UR919	kPa	Porewater pressure at bentonite/rock interface
PXG0UR920	kPa	Porewater pressure at bentonite/rock interface
PXG0UR921	kPa	Porewater pressure at bentonite/rock interface
PXG0UR922	kPa	Porewater pressure at bentonite/rock interface
PXG0UB923	kPa	Porewater pressure in bentonite
PXG0UB924	kPa	Porewater pressure in bentonite
PXG0UB925	kPa	Porewater pressure in bentonite
PXG0UB926	kPa	Porewater pressure in bentonite

Table 3-8. List of psychrometers sensors showing name, location, unit of measurement and a description of the monitored parameter.

Device	Units	Description
WB001	%	RH in Section 2
WB002	%	RH in Section 2
WB003	%	RH in Section 11
WB004	%	RH in Section 11
WB005	%	RH in Section 14
WB006	%	RH in Section 14
WB007	%	RH in Section 16

3.2.8 Linear displacement sensors

Four linear displacement sensors (LDS) are used to continuously monitor the movement of the lid in relation to both the gallery floor and ceiling (Table 3-9). A fifth sensor is used to monitor the movement of the canister in relation to the lid. Each LDS is fixed into position by a retaining clamp bolted to either the gallery floor, lid or monel pipe (connected to the canister), with the measuring armature resting against the lid providing a continuous measure of linear displacement.

To monitor the movement of the lid with respect to the gallery ceiling, an invar wire has been run from the roof to an LDS mounted on the lid. This provides a mechanism for monitoring the true vertical displacement of the steel retaining lid. The output from each device (–3.6 to +3.6 mm) is logged directly by the DAC system.

In late 2008, two additional LDSs were installed to monitor the lateral movement of the lid to give a full three-dimensional description of the position of the lid. These two sensors are separated by 90º around the lid. During the installation of the new LDSs, the three existing LDSs were replaced with higher precision instruments.

3.2.9 Load sensors

Axial movement of the lid is limited by 10 rock anchors equally spaced around the circumference of the hole – initially pre-tensioned to 1,300 kN. Glotzl load cells (Figure 3-8) have been positioned on three of the anchor cables at approximately 120° to each other (Table 3-10). These devices provide a continuous measure of the force acting on the lid. Output signals (0–10 volts) from these devices are logged by the DAC system. To prevent possible damage to either the rock anchors or the retaining systems during gas testing, the output from each device is alarmed (Section 2.5).

Table 3-9. List of linear displacement sensors showing name, location, unit of measurement and a description of the monitored parameter.

Device	Location	Units	Description
PXG0DP901	Monel to Lid	mm	Movement of monel pipe to lid
PXG0DP902	Lid to Floor	mm	Movement of lid to gallery floor
PXG0DP903	Lid to Floor	mm	Movement of lid to gallery floor
PXG0DP904	Lid to Floor	mm	Movement of lid to gallery floor
PXG0DP905	Lid to Ceiling	mm	Movement of lid to gallery ceiling
PXG0DP906	Lateral lid	mm	Lateral movement of the lid
PXG0DP907	Lateral lid	mm	Lateral movement of the lid

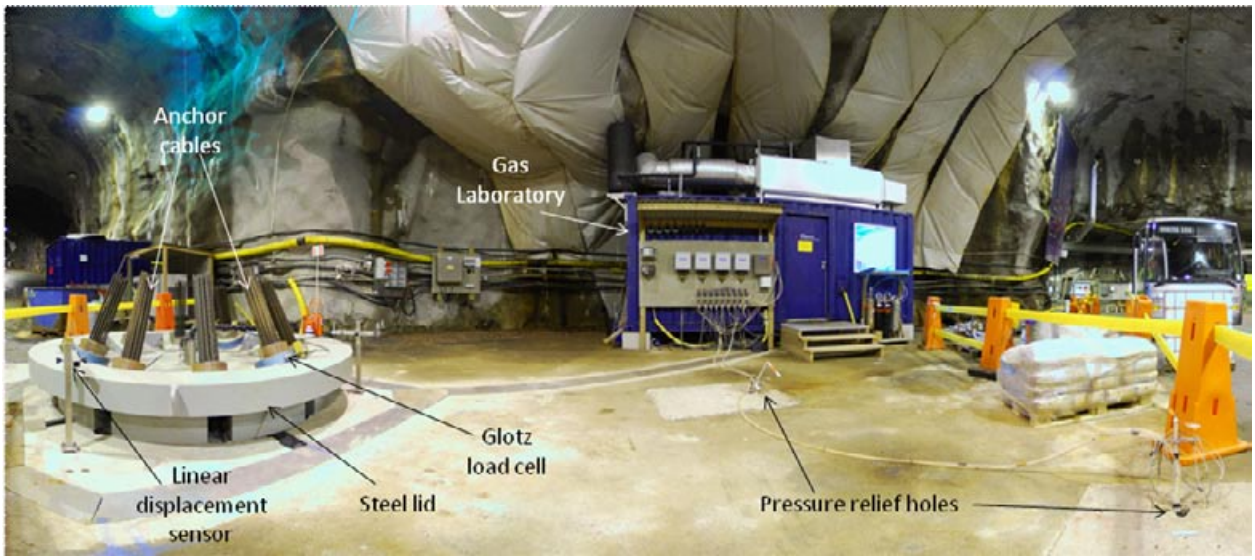

Figure 3-8. Photograph showing the lid (coloured grey), the anchor cables and linear displacement sensors. The Gas Laboratory (coloured blue) with its air-conditioning system mounted on the roof can be seen in the background.

Table 3-10. List of Glotzl load cells showing name, location, unit of measurement and a description of the monitored parameter.

Device	Location	Units	Description
PXG0LP901	Lid	kN	Force on anchor cables
PXG0LP902	Lid	kN	Force on anchor cables
PXG0LP903	Lid	kN	Force on anchor cables

3.2.10 Pressure relief holes

Following closure of the deposition hole on 1st February 2005 porewater pressure increased rapidly within the hole resulting in the extrusion of bentonite through the instrumentation ducts. In order to reduce the hydraulic gradients around the hole, and therefore the inflow rates, two pressure relief holes (PRH1 and PRH2) were drilled. Submersible pumps were initially placed in each borehole to further reduce the local porewater pressure. Once the bentonite had swelled sufficiently to close these flow pathways, packers were installed into each borehole (day 413) and sections within them closed off over the following 100 days (day 519). The position of the packers were determined from the geological mapping of the two boreholes in order to isolate key fracture zones. Figure 3-9 and Table 3-11 shows the names and position of the packered intervals for each pressure relief hole.

3.2.11 Ancillary systems

A number of ancillary systems are routinely monitored by the DAC (Table 3-12). These include: water pressure from a nearby borehole piped into the Gas Laboratory; gas pressure in the supply lines running around the laboratory section; compressed air pressure in the receiver (used to actuate servo-controlled valvework) and Geokon battery voltage (used to initiate the logging sequence).

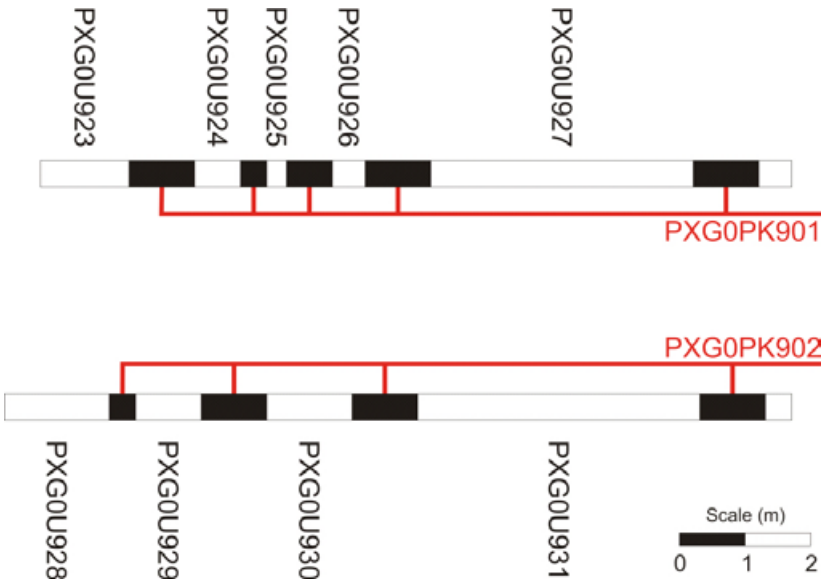

Figure 3-9. *Schematic showing the position and sizes of the packered intervals in the two pressure relief holes.*

Table 3-11. List of pressure sensors within the two pressure relief holes.

Device	Location	Units	Description	
PRH1-1	PXG0U923	PRH hole 1	kPa	Pressure relief hole
PRH1-2	PXG0U924	PRH hole 1	kPa	Pressure relief hole
PRH1-3	PXG0U925	PRH hole 1	kPa	Pressure relief hole
PRH1-4	PXG0U926	PRH hole 1	kPa	Pressure relief hole
PRH1-5	PXG0U927	PRH hole 1	kPa	Pressure relief hole
PRH2-1	PXG0U928	PRH hole 2	kPa	Pressure relief hole
PRH2-2	PXG0U929	PRH hole 2	kPa	Pressure relief hole
PRH2-3	PXG0U930	PRH hole 2	kPa	Pressure relief hole
PRH2-4	PXG0U931	PRH hole 2	kPa	Pressure relief hole

Table 3-12. List of ancillary systems contained in or connected to the Gas Laboratory.

Device	Location	Units	Description
PXG0TC901	Cannister	°C	Temperature inside the cannister
PXG0TL902	Lab	°C	Temperature near the ceiling in the lab
PXG0TL903	Lab	°C	Temperature near the floor in the lab
PXG0TO904	Office	°C	Temperature in the office
PXG0TA905	HRL	°C	Temperature outside the lab
PXG0FC901	Cannister	kPa	Pressure in injection filter
PXG0RW901	Lab	kPa	Pressure of water used to refill pumps A1, A2, B1, B2
PXG0RH902	Lab	kPa	Pressure of Helium Gas inside lab
PXG0RA903	Lab	kPa	Pressure of Compressed air in lab
PXG0VG901	Geokon	Volts	Geokon Battery level

3.3 Data acquisition and control system (DAC)

In total, over 150 instrument outputs are monitored and recorded by a customised data acquisition (DAC) graphical interface based on National Instruments LabVIEW™ software. The data acquisition system, located in the office area of the Gas Laboratory, operates on a personal computer that is connected to the SKB local area network (LAN) providing real-time data acquisition and control. Key experimental circuits and down-hole instrumentation are represented by a schematic display spread across a number of screens (Figure 3-10) located in the office section of the Gas Laboratory.

The LabVIEW software performs two primary functions. The first is to log all device outputs from both the depositional hole and the experimental apparatus (excluding the RH sensors which are monitored by existing equipment attached to another experiment at the HRL). Data is written to a hierarchical file structure that can be accessed through a secure user interface. Project participants can download experimental data from a members website. The second function of the system is to provide remote control of key experimental systems such as the ISCO syringe pumps and automated servo-controlled valve work. Proximity sensors mounted on each valve provide continuous feedback to the control system identifying the current status of a particular valve. This facility enables staff at BGS Headquarters in Keyworth to change pump settings and/or open/close any of the 68 actuated valves housed within the gas laboratory, remotely in real-time in order to initiate test sequences.

Automated alarm systems embedded in the Lasgit software (Section 3.5) can be configured to provide both e-mail notification and, under certain circumstances shutdown the ISCO pump systems if required.

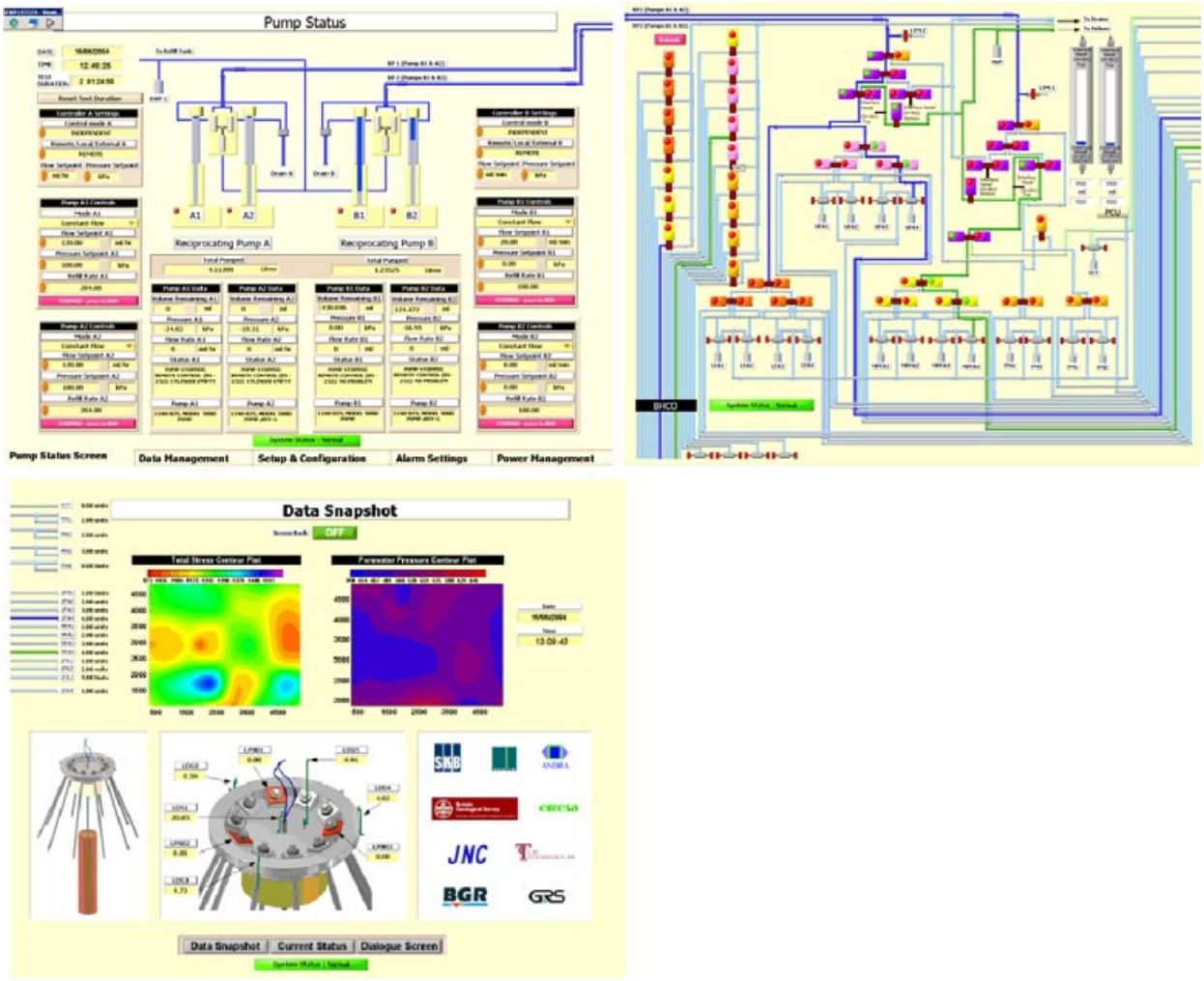

Figure 3-10. *Screen shots taken from the data acquisition software.*

3.4 Calibration

All measurement devices used in the Lasgit experiment which record pressure or displacement outputs are calibrated against known standards to ensure accurate and comparable outputs during the course of the experimental programme. This is achieved through factory calibration settings (e.g. Geokon, displacement and Glotzl instruments) or by manual calibration using a Fluke calibration unit (all transducers, thermocouples and pumps). Where calibration has been undertaken in the field, least-squares linear regression of the data is used to provide the slopes and intercepts necessary for data processing.

Data reduction during gas testing also requires an accurate determination of the total system volume during any particular test stage. Where possible the total volume of each test circuit from the syringe pump to injection filter was measured prior to the start of testing.

To minimise possible errors introduced into the data from instrumentation drift caused by the extended test duration of the Lasgit project, recalibration of laboratory pressure transducers and thermocouples is performed every 6 months, the exact date of which, is based on convenience to the test programme. As such, Lasgit data are processed in six monthly blocks as described in Section 3.6

3.5 Alarm systems

Instrumentation outputs are monitored by an alarm system incorporated into the data acquisition software. This allows the end-user to preset minimum and maximum values for each device output. If any instrument over or under ranges then an e-mail message is sent to a predefined list of project staff alerting them to the problem. When safety critical instruments such as the Glotzl cells or pumps over-range, the alarm system also automatically stops all of the ISCO pumps, preventing any risk of over pressurising the experiment or downhole infrastructure.

3.6 Error checking of Lasgit data

To date, nearly 1,400 days of logging have occurred, resulting in over 47,500 data records. This means that over 17 million cells of data exist, all of which require error checking, synchronisation, analysis and distribution to partners.

Data are generally transferred on a daily basis from Äspö Hard Rock Laboratory to BGS Keyworth using the remote Citrix server link. Once the data has been transferred to the UK, it is opened using a text editor program to ensure that the data are not corrupt. A check is made that data are not missing by comparing the time stamp of the new data with that from the previous data transfer. Once these initial checks have been conducted the data is copied to an Excel spreadsheet that contains all of the unprocessed (raw) legacy data.

All data are processed in a second spreadsheet, which is linked to the raw data sheet. Here, data are converted from raw to scaled units ready for graphing and interpretation. Graphs of all parameters of interest are available for viewing and allow on-going quality control (QC) of the data.

During 2008, the daily QC procedure was modified with every sensor being checked in individual graphs displaying the last 10 days worth of data. This improved method allows events that create only subtle changes in values to be observed. Events can be identified by their elapsed time and are plotted on all other graphs, this allows cross-correlations of sensors to be identified much easier and has already offered new insight into the hydro-mechanical response of the Lasgit system.

3.6.1 Data processing and traceability

There are a number of issues that arise in the recorded data. These include data synchronisation, erroneous values, loss of data during servicing or interruptions to logging system and transducer drift. However, a number of QC methodologies are routinely employed to ensure both the quality

and traceability of the Lasgit data. On a three-monthly basis, all data are thoroughly QC checked. This is performed using a series of conditional formatted Excel spreadsheets. Data are thoroughly checked for erroneous values or “outliers”, with every anomaly examined and a decision made whether to or not to remove, edit or retain the data point in question. To ensure a coherent and traceable process a log is made of each change to the data sheet. No changes are ever made to the raw data files.

For such a long-term experiment it is necessary to re-calibrate certain devices on a regular basis; for Lasgit this occurs bi-annually. The change in calibration alters data values in the Excel spreadsheet, which can manifest themselves as an instantaneous jump in value. In order to minimise for this, a time dependent correction is applied to the calibration coefficients. Linear drift of each instrument is assumed between the two calibrations, resulting in a steady variation over a six month period; this provides a clean, smooth data set.

4 Hydration Stage 1: Experimental results (day 106–day 849)

The first stage of hydration (day 106 – day 849) of the bentonite buffer was comprehensively reported in /Harrington et al. 2007/. No changes have been made to the data or observations since that time. However, in Section 6 of this report, we continue our observations for the second stage of hydration (day 1,110 to day 1,385) and report observations based on the full history of hydration (day 106 to day 1,385) in Section 7.

Main conclusions from the 2007 Status Report /Harrington et al. 2007/ included:

- Artificial hydration began on the 18th May 2005 after 106 days of testing. Initial attempts to raise porewater pressure in the artificial hydration arrays often resulted in the formation of preferential pathways. These pressure dependent features were not focused in one location but occurred at multiple sites at different times in the test history. These pathways appear to be relatively short lived, closing when water pressure was reduced.
- It was determined that both pressure relief holes (Section 3.2.10) should remain open until the bentonite had generated sufficient swelling pressure in order to withstand the high water pressures within the deposition hole. Packers were installed into the pressure relief holes on 23rd March 2006 (day 415) and sections in them closed off over the period to 5th July 2006 (day 519). There was no repeat of the formation of piping through discrete channels so, on 20th November 2006 (day 657); pressures to the artificial hydration filters within the deposition hole were increased to 2,350 kPa.
- Pressure data from a number of sensors including FR901, RW901 and most of the porewater pressure sensors mounted on the borehole surface, seem to suggest some form of time dependent (temporal) evolution in the hydraulic characteristics of the rock mass adjacent to the Lasgit deposition hole (as seen in Figure 4-1 and discussed later in Sections 7.2.1 and 7.2.5). Prior to closure of the packers, monitored discharge rates from the pressure relief holes show a slow progressive reduction in value with time.
- Monitored porewater pressures within the bentonite (as seen in Figure 4-2) remain low by the end of the first hydration stage, ranging from 230 kPa to 635 kPa. This is in contrast to the water pressure measured on the wall of the deposition hole which ranges from 1,055 kPa to 2,510 kPa, as seen in Figure 4-3. Suction pressures recorded at psychrometers embedded within the bentonite show that suction is declining (see Figure 7-17), confirming that resaturation is progressing, although the rate of hydration appears to be slowing.
- Throughout the stage, monitored radial stresses around the clay continued to increase steadily ranging in value from 1,685 kPa to 5,515 kPa, with an average value of 4,230 kPa (Figure 4-4). In the absence of hydraulic piping the rate at which radial stress increases appears insensitive to the absolute value of porewater pressure applied to the filter assemblies, confirming earlier modelling work by BGS /Harrington et al. 2007/. Analysis of the distribution in radial stress shows a narrow expanding zone of elevated stress propagating vertically upwards to around 3.5 m.
- Stress measurements (Figure 4-5) on the canister surface indicate radial stresses in the range 4,800 kPa and 5,030 kPa, which is comparable with the average value of radial stress monitored on the rock face. Axial stress is significantly lower at 4,380 kPa.
- Axial stress within the clay ranges from 4,910 kPa to 6,230 kPa (excluding sensor PB901 which was approximately 3,350 kPa by the end of the stage); as seen in Figure 4-6. Axial stress is non-uniformly distributed across the major axis of the emplacement hole and during this stage of the test generally exhibits only minor sensitivity to changes in porewater pressure.
- The axial force acting on the steel lid initially reduced after the deposition hole was closed but then increased following the closure of the pressure relief holes, Figure 4-7. By the end of the stage, the continuum axial swelling pressure within the bentonite is now greater than the initial pre-stress applied by the lid. The slight reduction in force prior to the closure of the pressure relief hole packers can be explained by convex deformation of the steel lid in response to the uneven distribution in axial stress.

- Displacement sensors (Figure 4-8) indicate a fairly uniform drop in lid height relative to the gallery floor during the early part of the test history, mirroring the relaxation in the initial pre-stressing applied to the lid. Analysis of the subsequent displacement data suggests a slight distortion of the lid may have occurred as it deforms to accommodate the uneven distribution in axial stress. Since the installation and closure of packers into the pressure relief holes the lid has moved significantly upwards with an increasing disparity in displacements at different locations, indicating an increased distortion, again probably linked to the uneven distribution of the axial force across the deposition hole.
- Analysis of the volumetric flow rate data indicates a disproportionably large flux into the bentonite from the canister filters, indicating a higher permeability zone in this region of the system. Volumetric flow rate through the artificial hydration filters is not particularly sensitive to the modest pressures applied to the hydration filters.
- The resaturation stage of the Lasgit experiment has been examined using numerical models developed with the TOUGH2 code and the EOS3 equation of state module. Model runs found that the impact of a single flowing fracture on the overall resaturation process was likely to be limited. In contrast, flow through the general rock mass and associated minor fractures could have a significant effect on the resaturation process depending on the permeability value selected, though this is strongly dependent on the model assumptions and parameters.
- A second group of models incorporating explicit representation of the individual bentonite rings and cylinders found that the rings around the canister were the most difficult to resaturate fully within the timescale of the experiment. In particular, if the gap between canister and bentonite rings seals quickly and effectively then full resaturation could take many years.
- The effectiveness of the seal between canister and bentonite appears to be a critical parameter in determining the overall time taken to resaturate the facility.

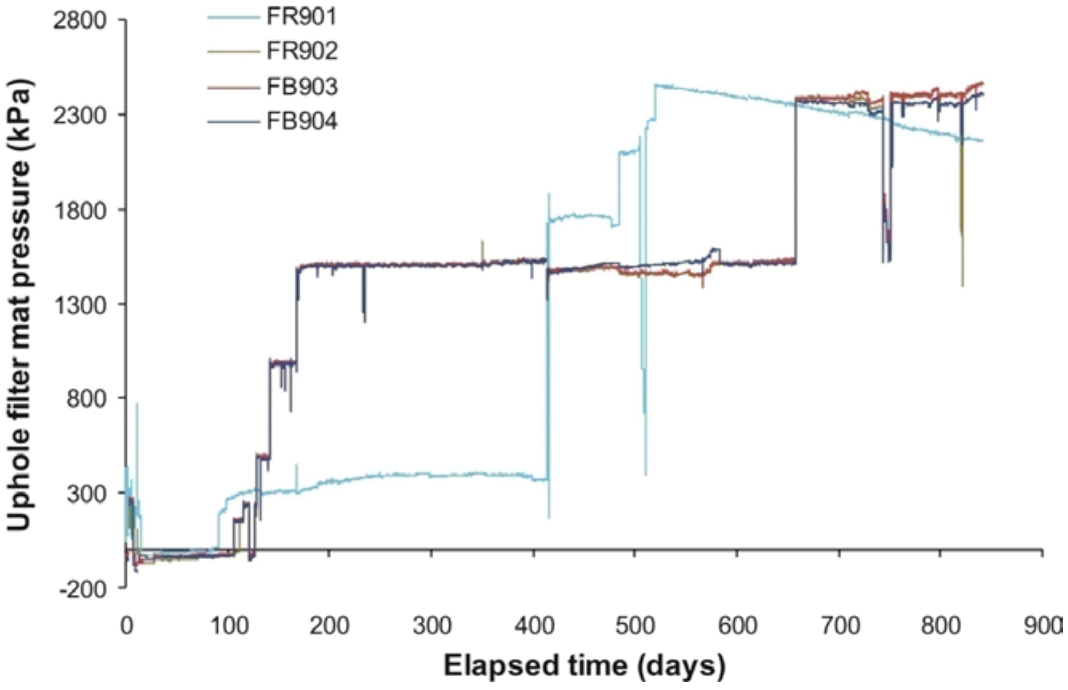

Figure 4-1. *Evolution of water pressure in the filter mats located on the borehole wall and within the bentonite blocks. Filter mat FR901 is in direct communication with the drain holes and was therefore allowed to evolve independently from the other filter mats.*

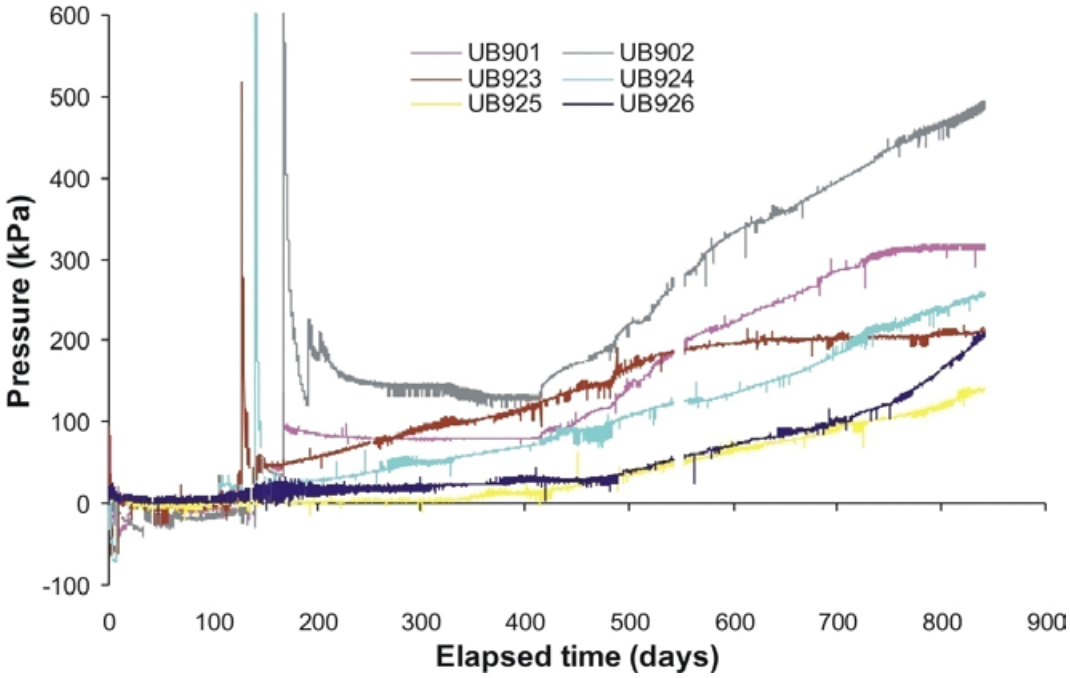

Figure 4-2. *Variation in porewater pressure within the bentonite at the 6 monitoring points. The large spikes in the data correspond with attempts to increase porewater pressure within the artificial hydration system early in the test history.*

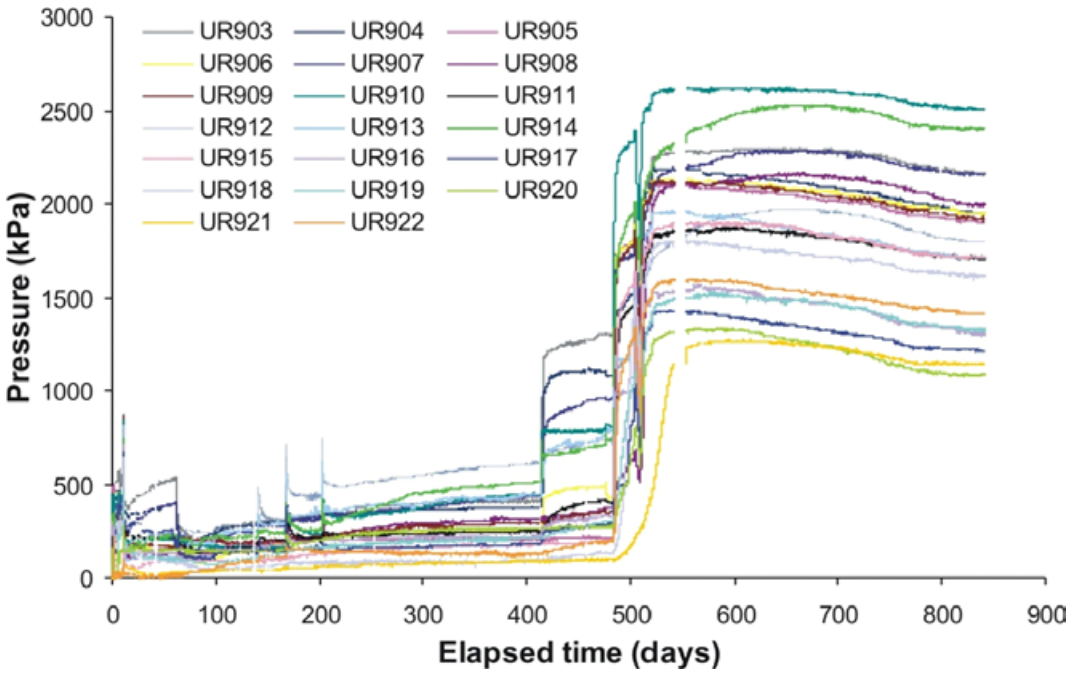

Figure 4-3. *Variation in porewater pressure with time measured at the rock face. The spikes in the data from day 141 to day 203 correlate with attempts to increase porewater pressure in the artificial hydration system. The rapid increase in pressure from around day 415 relate to changes in the boundary condition during the installation of packers in PRH-1 and 2 and their subsequent closure.*

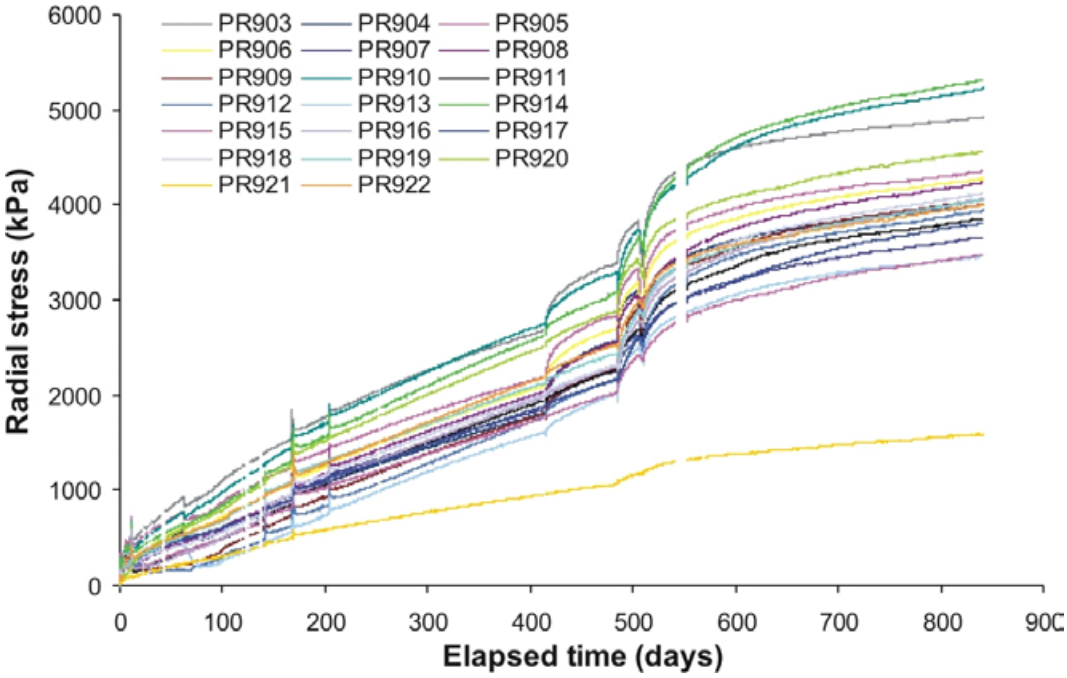

Figure 4-4. *Variation in radial stress with time. In the absence of preferential flow (piping), the rate at which total stress increases is insensitive to the absolute value of porewater pressure applied to the filters.*

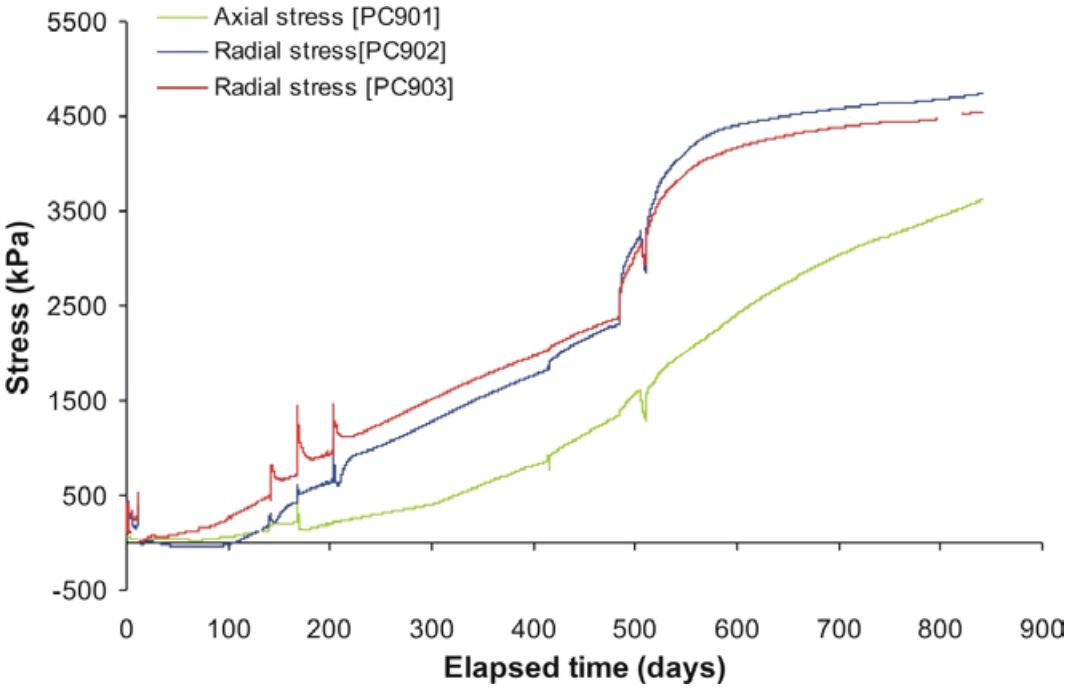

Figure 4-5. *Development of axial and radial pressure on the side and base of canister.*

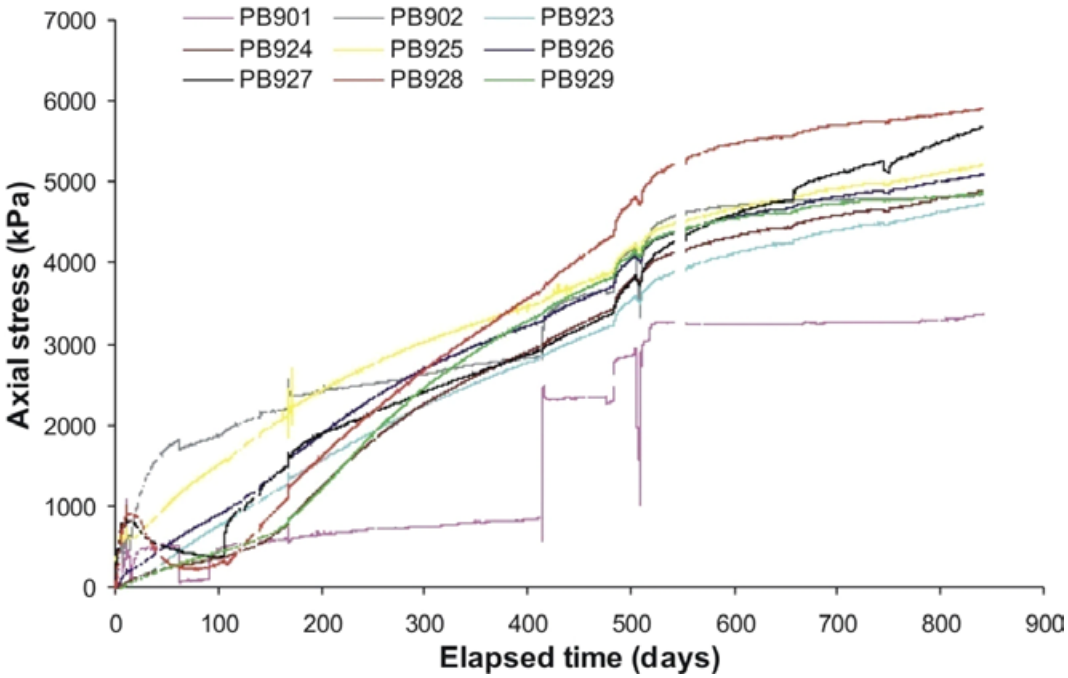

Figure 4-6. *Development of axial stress measured at 12 locations within the buffer.*

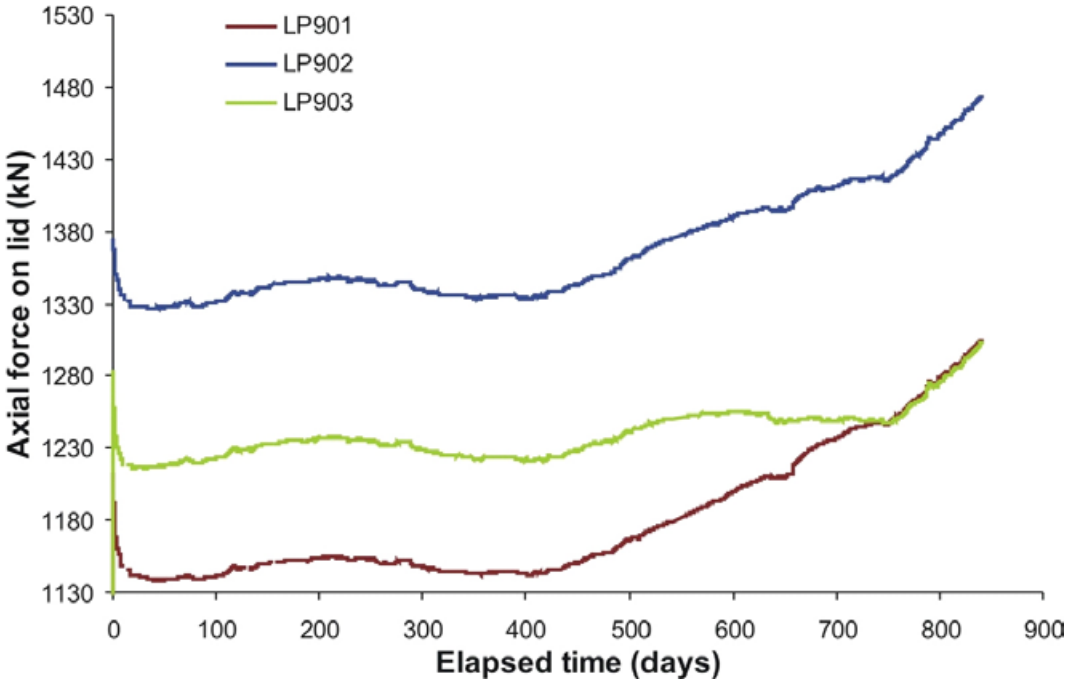

Figure 4-7. *Axial force acting on the steel lid measured by 3 Glotz load cells attached to separate rock anchors.*

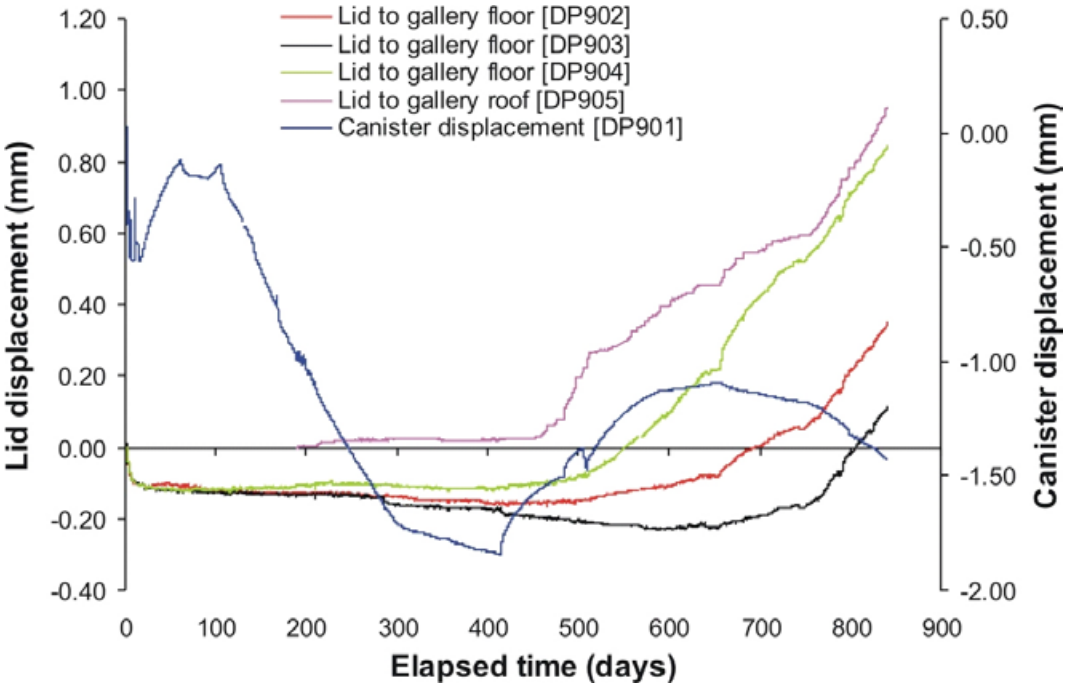

Figure 4-8. *Linear displacement of the steel lid and copper canister. Movements of the lid are measured relative to both the gallery floor and ceiling. Movements of the canister are measured relative to the steel lid.*

5 Hydraulic and gas injection tests Stage 1 (day 843–day 1,110)

The first Stage of hydraulic and gas injection testing was reported in the Lasgit Status Report for 2007 /Harrington et al. 2007/. However, /Harrington et al. 2007/ report was written prior to the completion of the second hydraulic test and before recalibration of the instrumentation was performed. Since then all data from this stage of experimentation has been quality control checked and certain reported values have now been modified. This section is an updated version of that previously reported; where values have changed these are clearly marked with a $^{\#}$ notation.

At the request of project stakeholders a preliminary gas injection history was undertaken in 2007 with a view to verifying the operation and data reduction methodologies outlined in the original concept report and to provide qualitative data on hydraulic and gas transport parameters for a bentonite buffer during the hydration process. It was decided that preliminary mass transport measurements would be undertaken in FL903, one of the 100 mm filters positioned in the lower canister array.

On 25th May 2007 (day 843), the lower filter arrays (FL901 to FL904) were isolated from all neighbouring test circuits by closing the appropriate valves and the pressures allowed to decay to provide information on the spatial distribution of local porewater pressures in the vicinity of each filter. Then on 21st June (day 870) a constant head test was started in FL903, with the pressure on that filter raised to 4.3 MPa. During this hydraulic test the remaining filters in the lower level remained isolated from the artificial hydration system and their pressure was allowed to evolve in order to provide temporal data on local porewater pressures within the buffer clay. At the same time, artificial hydration continued through all remaining canister filters and hydration mats. Pressure on FL903 was maintained at 4.3 MPa until 19th July (day 898), when it was reduced to 560 kPa and was then held constant until 7th August (day 917). During this period flow rates into and out of FL903 were monitored with time.

On 7th August (day 917) gas injection into FL903 began. Starting with an estimated gas volume of $1.26^{\#} \times 10^{-3}$ m^3, the gas was pressurised by introducing water into the gas reservoir at a steady rate until 20th August (day 930) when the test was temporarily stopped and the pressure held constant. This continued until 11th September (day 952) when the gas volume was re-charged to $1.337^{\#} \times 10^{-3}$ m^3 and pressurisation resumed, until 3rd October (day 974) when gas injection was stopped. The pressure decay in FL903 was then monitored through to the end of October. To examine the evolution of hydraulic properties following a gas injection event, a repeat hydraulic test was performed immediately after the cessation of gas injection. This had the additional benefit of flushing gas from the system and aiding the hydration of the clay.

5.1 Basline hydraulic test results (day 843–day 917)

The pressure responses at filters FL901 to FL904 during the course of the hydraulic test (day 843 to day 917) are shown in Figure 5-1 and the flow rates at FL903 during the two steps of the constant head test (day 870 to day 917) are shown in Figure 5-2.

For comparison, the porewater pressures on the deposition hole wall at sensors UR907 to UR910 are shown in Figure 5-3. These sensors are located at the same elevation as the injection filters FL901 to FL904. It can be seen that the pressures in all the injection filters rapidly drop well below pressures present at the deposition hole wall, strongly suggesting that a significant volume of the bentonite buffer near the canister remains in a partially saturated state. This explanation (rather than simple hydraulic disequilibrium) seems probable as it would require a much lower bentonite permeability to yield such low pressures (measured at FL901, 902 and 904) after extended periods of hydration. If such permeabilities were the case then the response to the shut-ins would take much longer than observed in Figure 5-1.

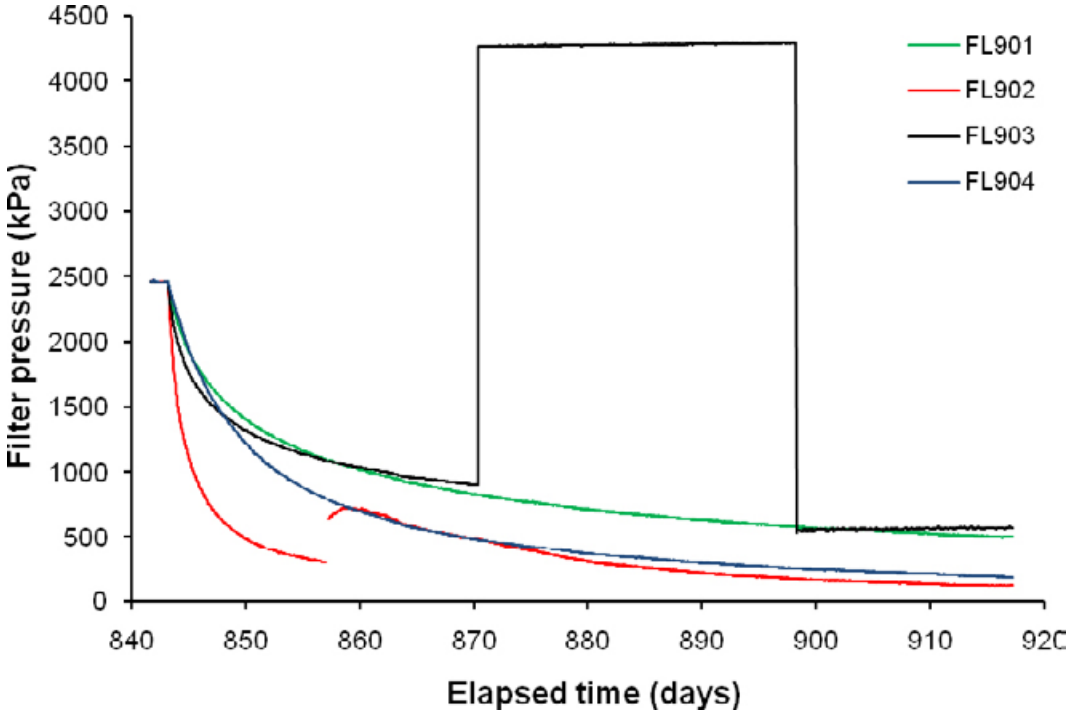

Figure 5-1. *Pressures observed at the lower canister filters FL901 to FL904 during the hydraulic test.*

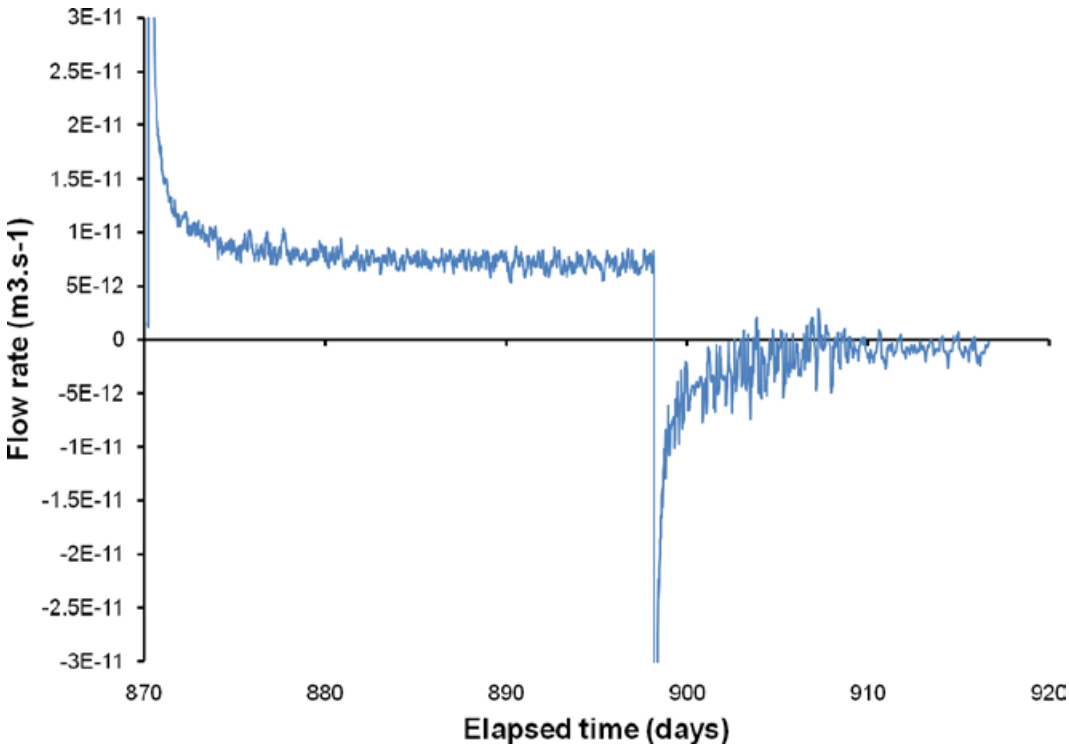

Figure 5-2. *Flow rate observed at lower canister filter FL903 during the constant pressure stages of the hydraulic test.*

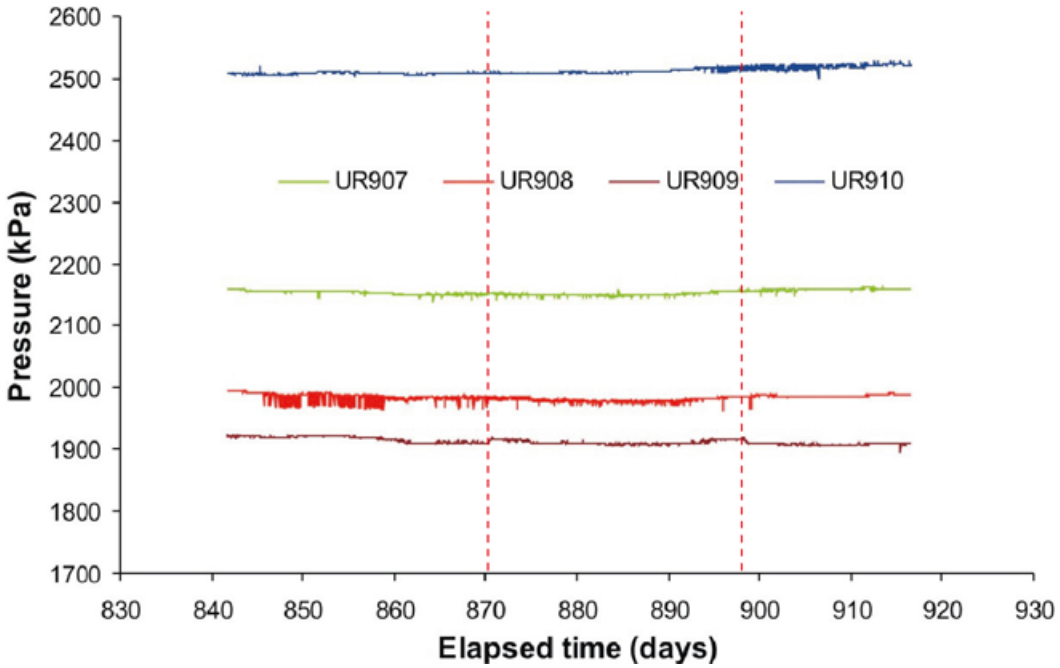

Figure 5-3. *Porewater pressures observed at deposition hole wall sensors UR907 to UR910 during the hydraulic test. Red dashed line shows start points of constant head stages.*

It can also be seen that the pressures at the various injection filters decline at different rates. These rates seem to reflect the sizes of the filters, with the smallest filter, FL902, falling most rapidly to about 300 kPa within 15 days of the start of the shut-in. The cause of the pressure discontinuity at day 857 in this sensor is not known. The two largest filters, FL901 and FL903, remain at the highest pressure at 870 days, at 820 and 900 kPa respectively, and the intermediate sized filter, FL904, falls to about 480 kPa by 870 days. These observations are consistent with the suggestion that the volume of bentonite around each filter that has been resaturated is proportional to the size of the filter. However the fact that the pressure at FL903 initially falls more rapidly than either FL901 or FL904 shows that additional factors may well be involved. One will be the differences in the porewater pressures at the deposition hole wall opposite each of the injection filters (Figure 5-3), which may have caused local variations in the degree of resaturation. Another may be some degree of heterogeneity within the buffer as it swells, which may also be affected by any eccentricity in the position of the canister with respect to the bentonite blocks.

The flow rate data in Figure 5-2 show that there is a transient of about 10 days after each of the two pressure changes in FL903 before the flows settle to a fairly steady level, although the data following the second pressure change at day 898 exhibits considerably more noise.

5.1.1 Hydraulic test modelling

In order to obtain estimates of the hydraulic conductivity and specific storage of the bentonite from these data it is necessary to develop a model of the flow processes occurring within the clay. As noted above, the data strongly suggest that a significant volume of partially saturated material remains around the canister at this time, and that the extent of this partially saturated zone varies with location around the canister. This means that the initial state of saturation of the system cannot be specified *a-priori*. Instead, it is necessary to model the whole of the hydration stage of the Lasgit project in order to arrive at a suitable spatial definition of the initial saturation state for the hydraulic test. Running such a detailed simulation with a full multi-phase model such as TOUGH2 would take too long for this preliminary assessment so a finite element porous media flow model parameterised in terms of hydraulic conductivity and storativity with a variable saturation capability was used for these calculations.

Attempting to model variably saturated flow in the full bentonite buffer in 3D with sufficient grid refinement to accurately resolve flow processes around filters as small as 10 mm in diameter was not feasible with the available resources. However, a preliminary model of one quarter of a cylinder centred on one filter and extending just 0.7 m vertically up and down the canister from the filter was constructed, in order to test the possibility of using such a model to interpret the test data (the initial void space around the canister was represented in the model). The mesh created contained 86,000 nodes on 507,000 tetrahedral elements and took about 5.5 hours to run a single simulation of the hydration and hydraulic test stages of the experiment. The results of a simulation of the hydration stage that assumed a hydraulic conductivity of 1.3×10^{13} m.s^{-1} and a specific storage of 1.5×10^{-4} m^{-1} is shown in Figure 5-4.

While this model gives a useful general picture of the likely saturation state of the bentonite around an injection filter at the end of the initial hydration stage, detailed examination of the solution suggests that the mesh is not sufficiently refined to give accurate results close to the filters. In addition run times are such that the model would be very difficult to use for data interpretation so a slightly simplified and more efficient approach was sought. After some experimentation, a 2D axially symmetric model was chosen, centred on an injection filter, with the axis of symmetry projecting perpendicular to the canister towards the deposition hole wall. Using a mesh of about 2,000 nodes on about 4,000 triangular elements a single simulation could be run in around 40 seconds. This makes it possible to obtain fits to data for each of the filters in a reasonable timescale. Figure 5-5 shows the fits obtained to the shut-in pressure data, using separate parameter values for each filter, with the parameter values given in Table 5-1 for each model. It can be seen that relatively similar values for hydraulic conductivity have been obtained but that there is quite a wide range of specific storage values.

The same model was also used to interpret the constant head steps applied to FL903, but in this case comparing the flow rate data to the model simulation. However, using parameters from the shut-in stage gave a poor fit to the flow rate data, as shown in Figure 5-6. A revised model provides a much improved fit with $K = 0.75 \times 10^{-13}$ m.s^{-1} and $S_s = 0.25 \times 10^{-4}$ m^{-1}.

These models used to derive the initial conditions for the filter shut-in calculations also give an indication of the progress of the resaturation of the bentonite in this part of the borehole. Figure 5-7 shows the simulated pressures, plotted as hydraulic heads, at each filter at day 840, close to the end of the hydration stage, the parameters for the individual fits from Table 5-1 being used in each case. In these plots the two darkest blue bands show the extent of unsaturated conditions. It can be seen that the unsaturated zone is much more extensive near the smallest filter, FL902, than near the larger filters FL901 and FL903.

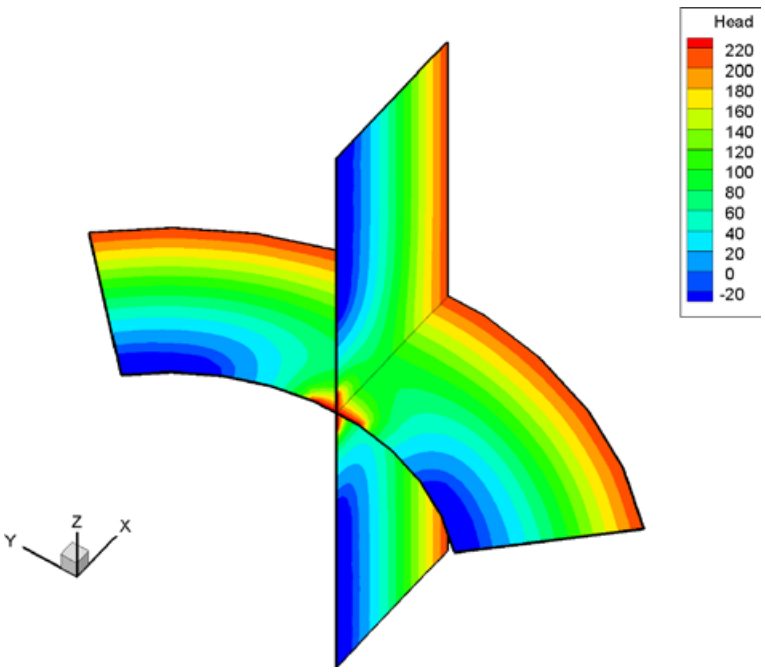

Figure 5-4. *Pressure heads in a finite element model of single phase variably saturated flow around filter FL901 after 840 days of hydration. Dark blue bands indicate remaining zones of partially saturated material.*

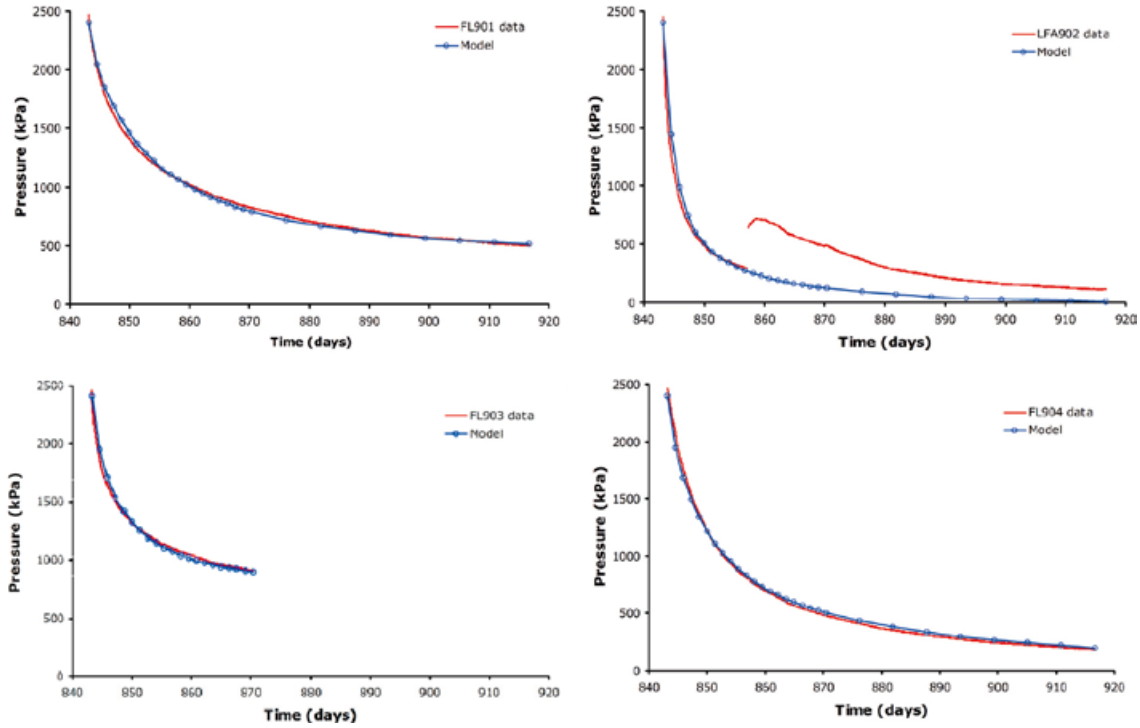

Figure 5-5. *Comparison of model simulations to shut-in pressure data for the injection filters FL901 to FL904 during the hydraulic test.*

Table 5-1. Hydraulic parameters obtained from fits to shut-in pressure curves for injection filters FL901 to FL904.

	K ($m.s^{-1}$)	S_s (m^{-1})
FL901	1.10×10^{-13}	1.20×10^{-4}
FL902	0.90×10^{-13}	5.50×10^{-4}
FL903	1.24×10^{-13}	0.55×10^{-4}
FL904	1.58×10^{-13}	4.00×10^{-4}

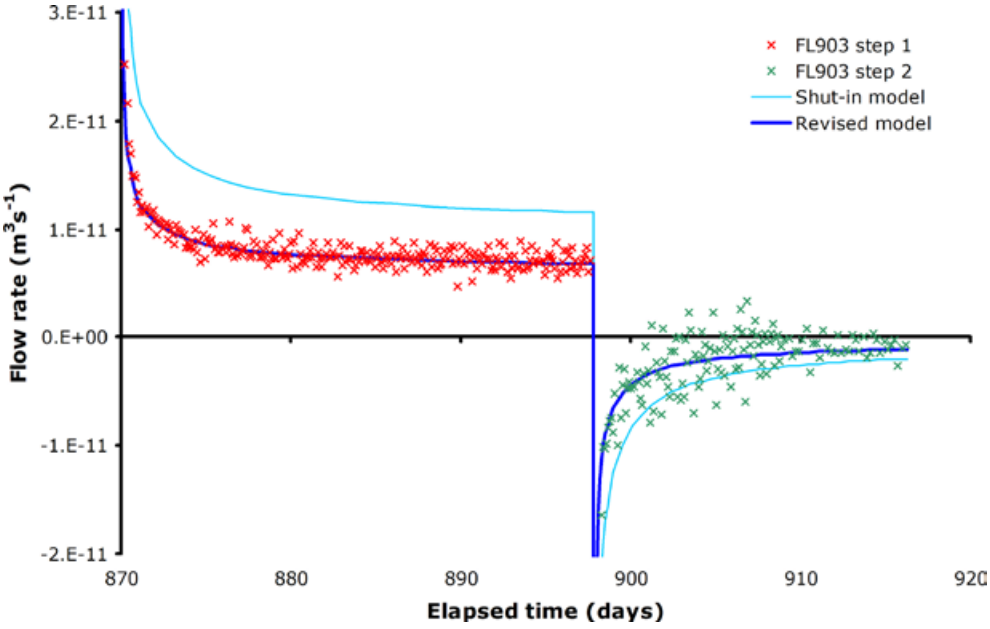

Figure 5-6. *Comparison of model simulations with flow rates at FL903 during the constant pressure test steps.*

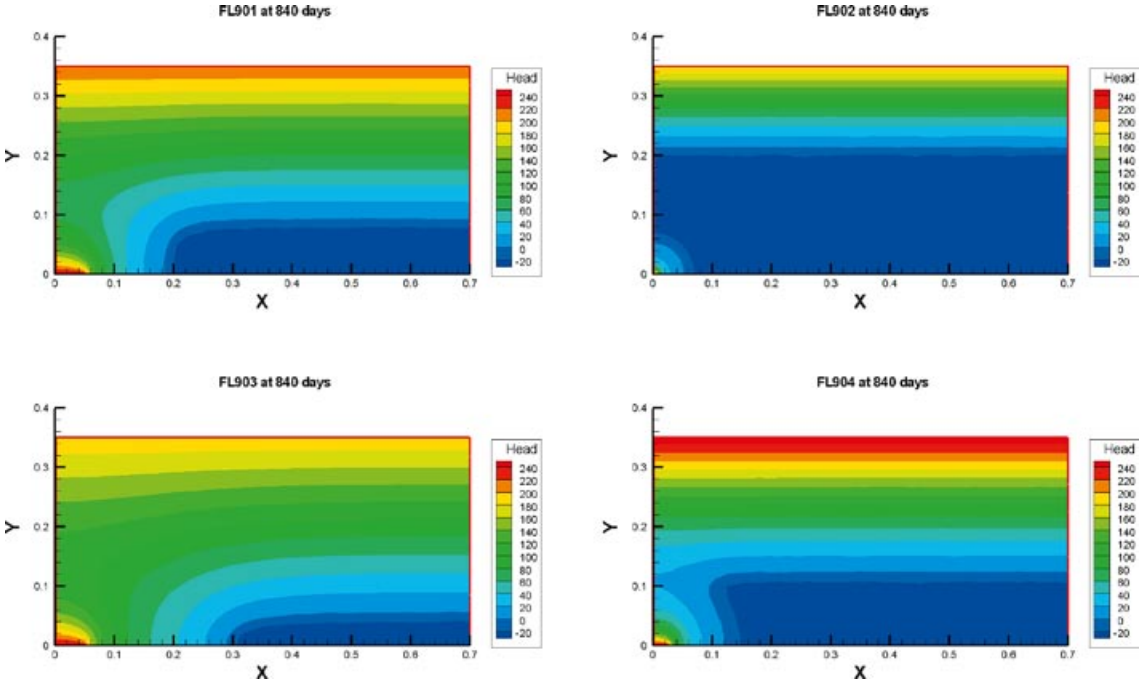

Figure 5-7. *Simulated pressure heads around each filter at 840 days, the end of the hydration stage.*

5.2 Gas injection test results (day 917–day 1,010)

Gas injection testing began on 7th August 2007 (day 917) through canister filter FL903. Gas with an initial volume of $1.26^{\#} \times 10^{-3}$ m^3 was introduced to the interface vessel and then pressurised by pumping water into the cylinder. On 20th August (day 930) the pressure in FL903 was held constant until 11th September (day 952) when the gas was re-charged to a volume of $1.337^{\#} \times 10^{-3}$ m^3 and pressurisation restarted. This second stage of pressurisation continued until 3rd October (day 974) when the filter was again isolated by means of closing a valve and gas pressure allowed to decay. The observed gas pressure at the filter is shown in Figure 5-8, which also shows the predicted pressure for a confined ideal gas undergoing constant flow operation of the confining system. *It should be noted both predicted gas pressure and the derived volumetric flow rate of gas into the deposition hole are strongly dependent on the start volume of gas*.

During the first stage of gas pressurisation (days 917–day 930) the observed pressure starts to depart from the pressure predicted for an ideal gas[2] at about day 924. As gas pressure increases the departure in predicted gas pressure cannot be explained by gas moving into solution and must be symptomatic of gas penetration of the buffer. Figure 5-9 shows this period in more detail together with the estimated rate of flow of gas into the clay. These data suggest that gas starts to flow into the buffer at a pressure of about $650^{\#}$ kPa, which is much lower than the expected gas entry pressure for saturated intact bentonite. It therefore seems likely that gas is flowing between the bentonite and the canister and possibly between bentonite blocks (the interface between bentonite rings 2 and 3 lies just 50 mm above the injection filter).

When gas pressurisation stopped at day 930 and the pressure was held constant, flow into the clay dramatically reduced by around 98.5%, indicating that propagation of the main gas pathway(s) practically ceases when the pressure stops rising. In its most basic form, this can be viewed as the expansion of gas pathway(s), conceptually little different to that of inflating a balloon, where the walls of the latter represent the pathway surfaces within the clay. The small continuous flux observed

[2] The initial start volume of gas was estimated by fitting the early predicted pressure response to that of the measured values from FL903. The start gas volume for the second test phase was estimated at the end of the test by displacing the remaining gas with water through the FL903 drain vent. Given the importance of this parameter, in future tests, additional effort will be placed on its measurement prior to gas injection.

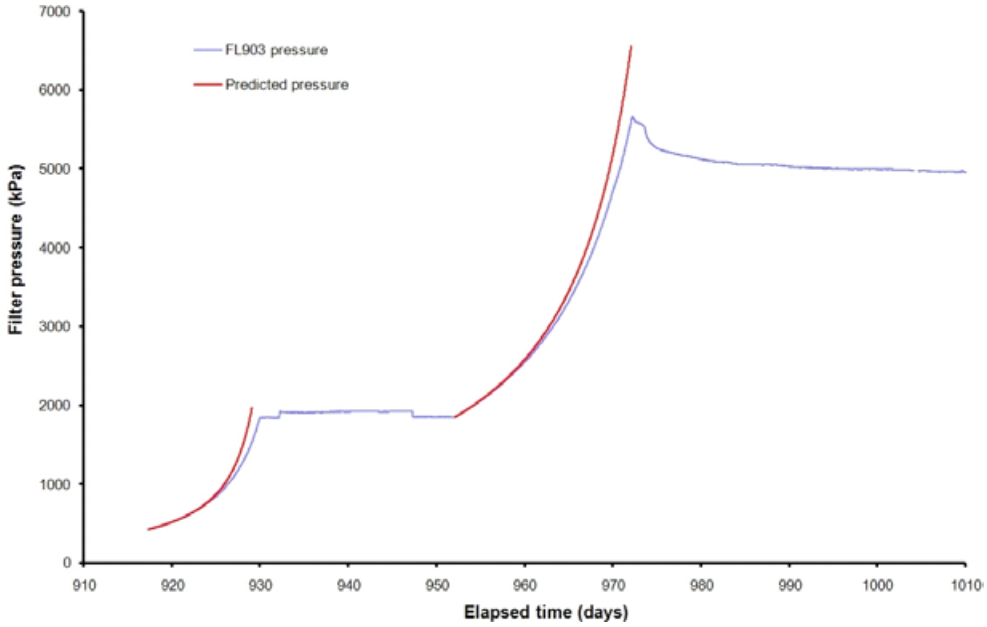

Figure 5-8. *Comparison of predicted and observed gas pressures at FL903 during the gas injection test.*

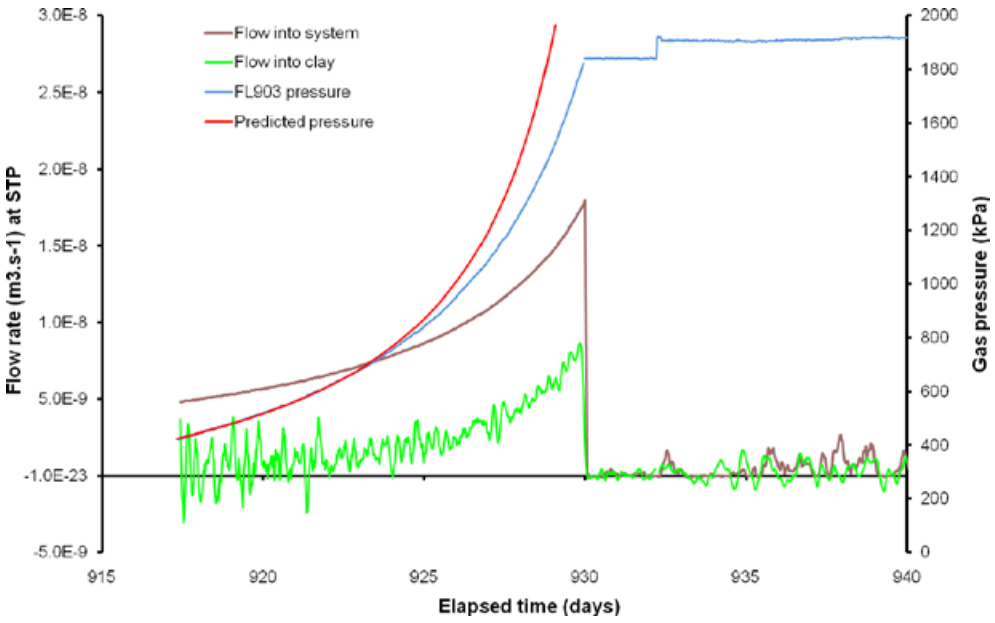

Figure 5-9. *Estimated rate of gas flow into the system and the clay compared to the predicted and observed gas pressures during the first stage of the gas injection test. Flow into clay is calculated using a combination of weighted moving average and time moving average (mean).*

following this event may result from the movement of gas along small-scale pre-existing features which are only present because the bentonite remains in suction and is not in hydraulic equilibrium. If correct, these fluxes should reduce in magnitude during later tests as hydration of the buffer progresses. Given the sudden reduction in flow, it seems clear from the data that gas is not flowing within the original porosity of the clay and that the initial network of gas pathways fails to locate an adequate sink capable of accommodating the previous in-flow of gas.

Following the onset of the second stage of gas pressurisation (day 952) the observed pressure starts to deviate from the predicted ideal gas compression curve almost immediately (see Figure 5-10), indicating that the pathway continues to extend without any delay. Gas flow into the clay during this second

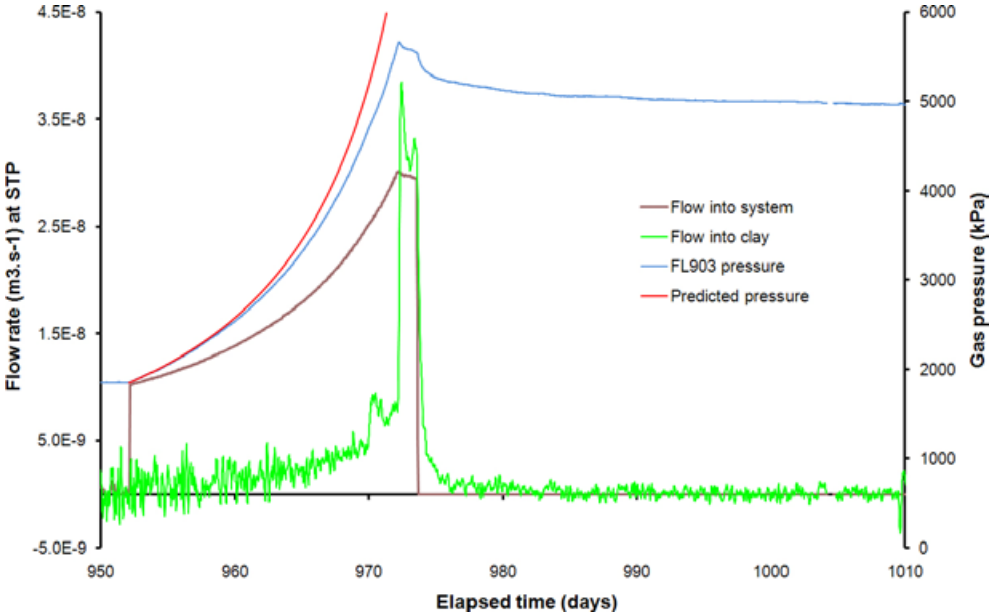

Figure 5-10. *Estimated rate of gas flow into the clay compared to the predicted and observed gas pressures during the second stage of the gas injection test.*

stage rises gradually with time until about day 970 at which point it rises much more sharply until gas pressurisation is stopped again at day 974. The sharp rise in flow rate occurs when the gas pressure is marginally greater (approximately 0.2# MPa) than the local total stress measured on the rock wall, but is around 0.25# MPa lower than the radial stress monitored on the canister surface at PC903. Axial stress measured at PB902 was also marginally higher than the gas pressure (around 0.3# MPa). Gas pressure continues to increase reaching a peak pressure of 5.66 MPa at day 972.3. This is followed by a small spontaneous negative transient leading to a quasi steady state illustrated in detail in Figure 5-11 at a gas pressure of around 5.5 MPa. This behaviour is qualitatively similar to results from laboratory scale tests reported by /Horseman et al. 1999, Harrington and Horseman 2003/.

The injection pump was stopped at day 974 and the gas pressure allowed to decay to provide an estimate for the apparent capillary threshold pressure. It can be seen in Figure 5-10 and Figure 5-11 that just before injection is stopped, the post peak gas flux exhibits dynamic behaviour (over and undershooting flux into the system) suggestive of unstable gas flow. Following the cessation of injection the flux declines rapidly at first but then enters an extended period of very small flows[3]. This is reflected in the pressure response which drops rapidly initially but then decays very slowly towards an asymptotic capillary threshold pressure, Figure 5-12, which is tentatively estimated to be around 4.9 MPa. This is very similar to the average radial stress measured on the canister which is also close to the axial stress measured at PB902. This result, if correct, suggests a strong correlation between gas transport and total stress and supports the observations reported by /Harrington and Horseman 2003/ based on laboratory scale tests. The breaks in slope in the pressure decay curve (Figure 5-12) are indicative of the sealing and temporary formation of highly unstable gas pathways.

However, this observation raises a simple question: why does the gas pressure appear to asymptote at a value far in excess of that required to initiate gas flow? To help answer this question we must return to the conceptual model of the “expanding balloon” mentioned earlier. Initial results (with gas pressure below total stress) demonstrate that in the absence of a sink, continued gas penetration of the buffer and or canister interface, required an increasing gas pressure to drive major pathway

[3] These fluxes are significantly smaller than that observed during the earlier constant pressure phase, which may have been previously related to flux along small-scale pre-existing features.

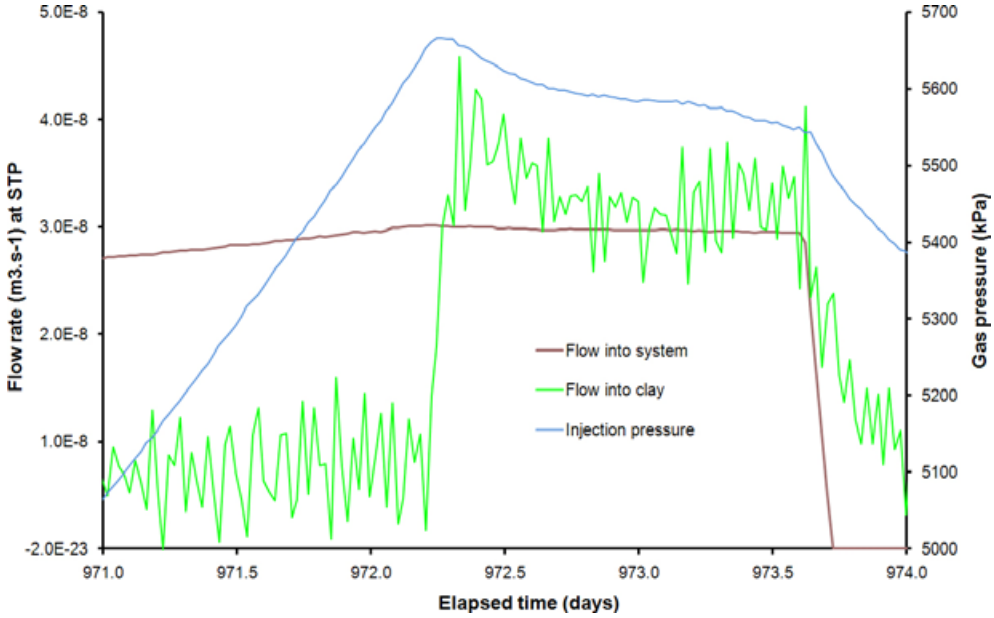

Figure 5-11. *Unsmoothed flow rate and pressure responses around peak gas pressure. Gas flow into the clay rapidly increases following the peak which is followed by a small spontaneous negative transient.*

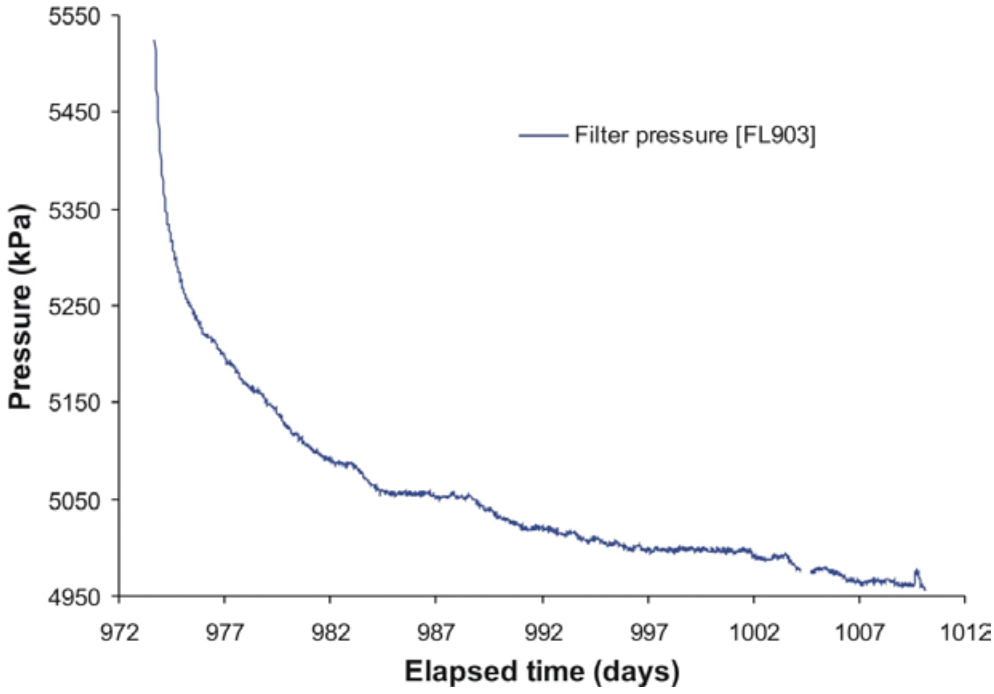

Figure 5-12. *Shut-in response for filter FL903. The inflections in the pressure decay response are suggestive of dynamic gas flow and pathway closure.*

propagation[4]. Analysis of the data indicates that only a relatively small amount of gas was injected into the clay during the test. The fact that the subsequent gas pressure asymptotes at a value close to that of the local total stress suggests that the majority of the gas remained resident in the buffer/deposition hole. As the pressure within the pathways decline, the effective gas permeability of the clay significantly reduces.

Figure 5-13 and Figure 5-14 show details of the radial stress and pore pressure responses to the sharp increase of gas flow, prior to and just after the peak gas pressure of the second gas injection stage, in a selection of sensors close to the injection filter FL903. It is notable that the most pronounced responses are seen in the sensors from Section 4 (see Appendix), which are 600 mm below the injection point, rather than the Section 5A sensors, which are 300 mm above it. Examination of the data indicates changes in stress and porewater pressure begin at the peak in gas pressure.

Figure 5-15 and Figure 5-16 show the temporal evolution in radial stress and porewater pressure during this time (normalised to zero at day 972.02). Figure 5-15 shows a well pronounced increase in radial stress around the entire base of the deposition hole, with the highest increase noted in the vertical plane below the point of injection. This indicates the gas preferentially moved downwards, probably along the interface between the canister and buffer. It is notable that the radial stress immediately adjacent to FL903 actually decreases during this time. A similar observation is also seen in the porewater pressure trace (Figure 5-16). The cause of this behaviour remains unclear.

Detailed inspection of the porewater pressure intensity plots (Figure 5-16) generally confirms the above observations, though initial results suggest that the pulse in porewater pressure dissipates at a faster rate than that of the radial stress. The rise in porewater pressure can be interpreted as a hydrodynamic response caused by the local increase in stress (Figure 5-13) around the gas pathways.

Analysis of the porewater pressure sensors located within the buffer show no obvious sensitivity to the injection of gas. In contrast, axial stress sensors located beneath and above the canister appear to register the passage of gas, probably detecting reflected stresses normal to the gas flow path (Figure 5-17). Indeed, the slow and then rapid increase in PB902 immediately following the peak gas pressure is strongly indicative of the time dependent propagation of gas pathways.

A small deflection (reduction) in the rate of increase in axial stress at the base of the canister (PB901) occurs around 0.85 days after the peak in gas pressure. A reduction in stress can only be caused by the removal of load. This would suggest some form of displacement has occurred within the system as a result of gas injection.

While it is difficult with the available data to make definitive statements regarding the exact direction and number of gas flow paths, it seems highly probable that the gas moved generally downwards away from the filter and then along the interface between blocks C1 and R1 and/or R1 and R2. The fact that the gas pressure asymptotes at a value close to the local total stress, may suggest that the small amount of gas injected during the test remained resident in the buffer/deposition hole. This observation compliments the findings of the predictive modelling work described in /Harrington et al. 2007/, which identified the effectiveness of the seal between canister and bentonite as a critical parameter in determining the overall time taken to resaturate the facility. This is also logical as there is a clear axial stress gradient running from high to low from the top of the deposition hole (PB928 ~6.0 MPa) to the lowest stress sensor (PB902 ~4.9 MPa). Under most conditions gas would be expected to propagate along such a stress vector.

However, the observed general coupling between gas, stress and porewater pressure at the repository scale is extremely important and is strongly indicative of pathway dilatancy as a gas transport mechanism. These observations are qualitatively similar to those reported by /Horseman et al. 2004/.

[4] The small continuous flux noted from the initial constant pressure gas test was probably along pre-existing small-scale features, which may be present because the bentonite remains in suction and is not in hydraulic equilibrium during this phase of testing.

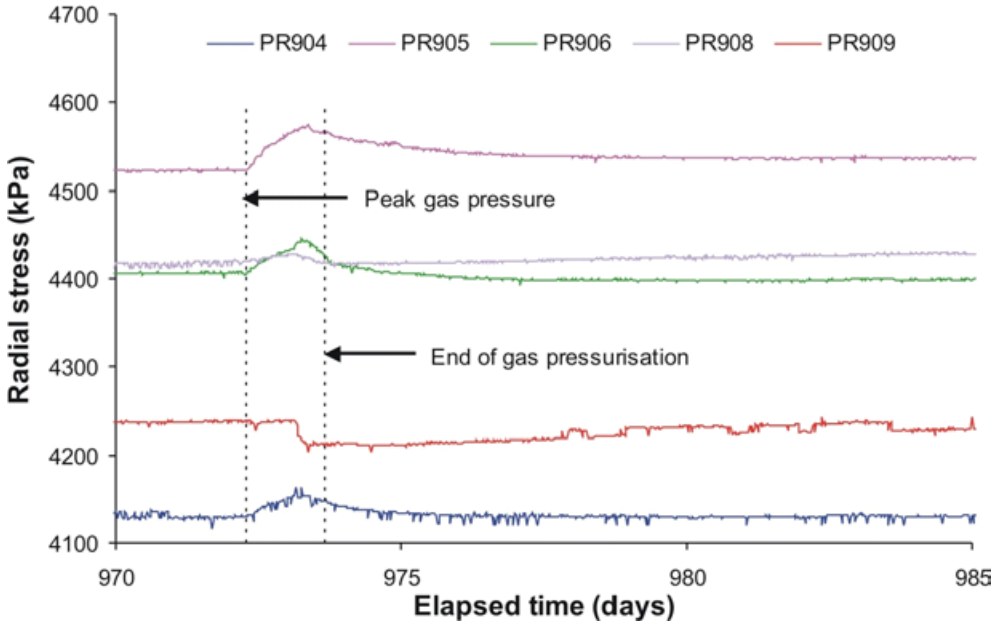

Figure 5-13. *Radial stresses observed in a selection of sensors close to FL903 at the end of the second gas pressurisation stage.*

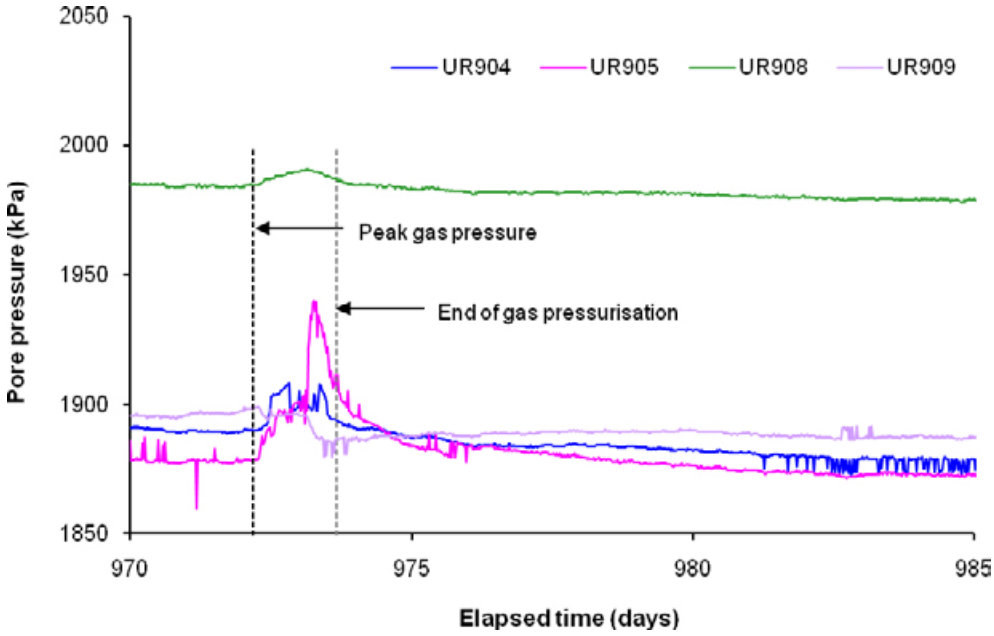

Figure 5-14. *Pore pressures observed in a selection of sensors close to FL903 at the end of the second gas pressurisation stage.*

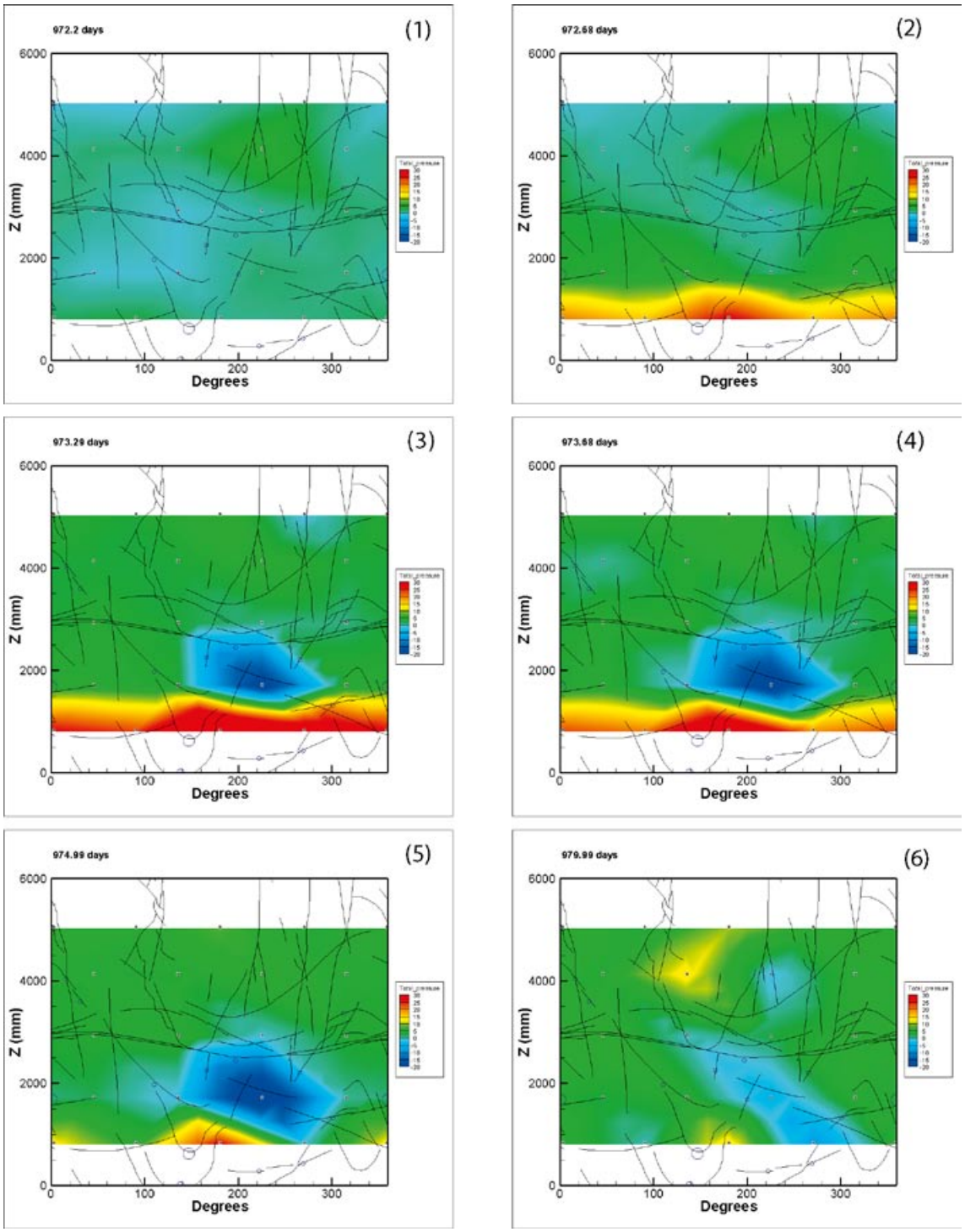

Figure 5-15. *Evolution in normalised radial stress around the deposition hole wall prior to and after the peak in gas pressure (days 972.2 to 979.99). The intensity plots indicate a general increase in radial stress around the base of the deposition hole. Adjacent to the filter radial stresses appear to decline momentarily.*

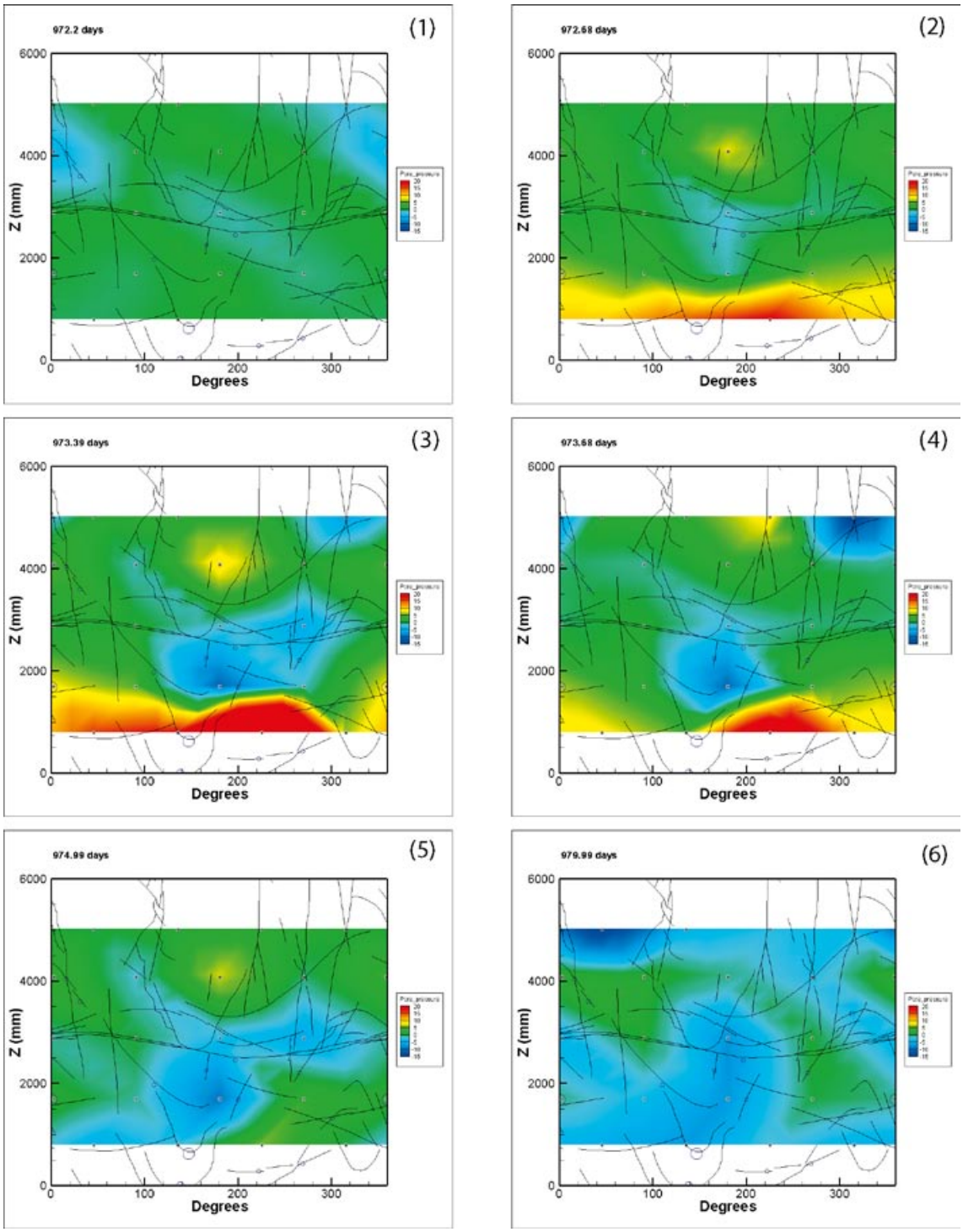

Figure 5-16. *Evolution in normalised porewater pressure around the deposition hole wall prior to and after the peak in gas pressure (days 972.2 to 979.99). The intensity plots indicate a general increase in porewater pressure around the base of the deposition hole focussed in the vertical plane of the source filter (FL903). Adjacent to the filter porewater pressure appear to decline momentarily.*

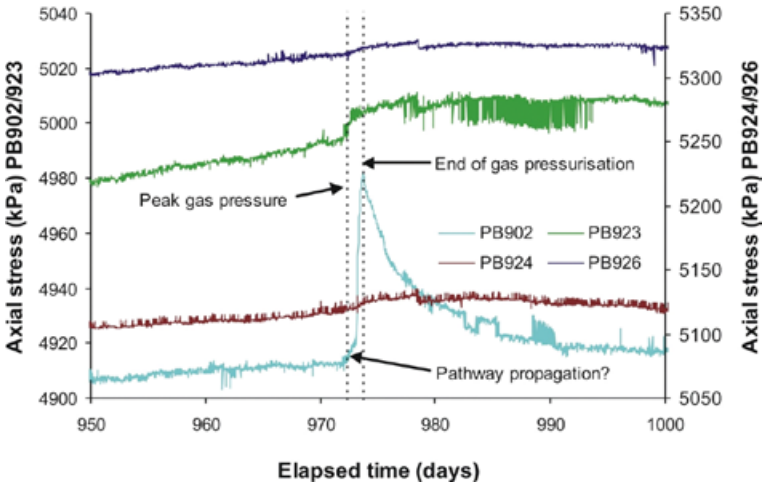

Figure 5-17. *Selected axial stress data during the second stage of gas injection. The strongest response is observed by PB902, which, located below the canister, exhibits signs of time depended pathway flow.*

5.3 Hydraulic test post gas injection (day 1,010–day 1,110)

To examine the affect, if any, on the hydraulic properties of the buffer following gas injection, a second hydraulic test was performed. Prior to the start of this test, the drain valve to FL903 was opened to atmospheric pressure and the gas in the test system vented. Water was then injected in order to help sweep residual gas from the injection system. Once a steady stream of water was discharged from the drain valve, it was closed and the hydraulic pressure in the test system raised to 4.4 MPa (very close to the original test pressure in Section 5.1). Once steady-state conditions were established, the hydraulic pressure was again reduced to 480 kPa and the recovery stage monitored. Figure 5-18 shows the evolution in flow rate from both hydraulic tests (pre- and post gas injection) plotted against the duration of each test.

While modelling of the post-gas hydraulic data has not been performed due to the uncertainties associated with defining an accurate saturation at the start of the test, a visual inspection of Figure 5-18 clearly indicates that little, if any, significant change in permeability has occurred because of the injection of gas. The slight offset in the red line is indicative of a small change in hydraulic storage. Based on the data available, the nascent gas pathways would appear to have no significant effect on the hydraulic performance of the buffer. This is not unexpected given the limited duration of the gas tests and the quantities of helium injected.

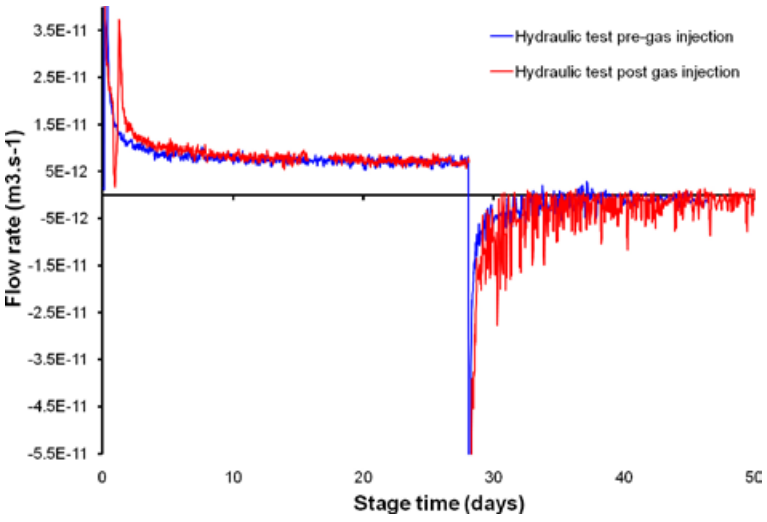

Figure 5-18. *Evolution in flow rate for hydraulic tests performed before and after gas injection.*

6 Hydration Stage 2 (day 1,110–day 1,385)

Hydration stage 2 was initiated after the system had been recalibrated fully on day 1,110. The lower canister filters (FL901–904) were re-pressurised in line with the other hydration filters and the second stage of hydration begun.

Below is a summary of noteworthy events that occurred during this stage of experimentation, some of which are discussed in more detail in the following sections of the report. It should be noted that discrete date events are quoted to 2 decimal places, whereas non-discrete events such as calibration, are quoted on the day the event occurred.

1. **Day 1,084:** Calibration was first attempted on Monday 21st January 2008 once the second hydraulic test had completed. At this time there was significant blasting activity within the HRL which prevented calibration.
2. **Day 1,105:** On Monday 11th February 2008 a second attempt was made to calibrate the system. This was again made problematic by blasting activity and battery issues with the calibration Fluke.
3. **Day 1,109:** Calibration was successfully achieved on Friday 15th February 2008.
4. **Day 1,110.0:** Following calibration, the system was re-configured so that all filters participated in the artificial hydration of the clay (Friday 15th February 2008). The observed slow reaction of FL903 to the increase in pressure suggested that the air actuated valve had failed. On inspection this was not seen to be the case.
5. **Day 1,122:** Starting on Wednesday 27th February 2008 at around 22:30, pressure sensor FM906 (PXG0FM906) began to drift. This appears to have lasted for approximately 8 days until 02:00 on Thursday 6th March 2008. After this time the pressure response of FM906 matched that of the other filter mat transducers. The decision to replace the transducer at the earliest opportunity was taken.
6. **Day 1,126.7:** Following biannual QC checking of the data, it became apparent that problems existed between the transfer of Geokon data to the Labview logging computer system. This meant that any issues with the Geokon data may not become apparent until after each biannual QC check. Measures were put in place and the problem was resolved on Monday 3rd March 2008 at approximately 11 am.
7. **Days 1,134.92–1,135.69:** The first of two planned power cuts to the entire Äspö laboratory occurred on Tuesday 11th March 2008 at approximately 15:00:00, with power returning by Wednesday 12th March 2008 at 10:39:40. During this period the lab PC failed to log, unlike the Geokon system which remained active.
8. **Days 1,135.96–1,136.63:** The second of the two planned power cuts occurred on Wednesday 12th March 2008 at approximately 16:00:00, with power returning by Thursday 13th March 2008 at 10:13:44.
9. **Day 1,157.17:** On Monday 31st March 2008 the configuration of the artificial hydration system was changed.
10. **Day 1,211.92:** The FM906 pressure transducer was replaced during a site visit on Tuesday 27th May 2008, with calibration occurring of the old and new FM906 pressure transducers. Calibration was complete by 16:05:32, with FM906 left with a high shut-in pressure of over 18 MPa (isolated from down-hole) in order to leak test the new pressure sensor. This elevated pressure remained until Thursday 17th July 2008 (day 1,262), when the sensor was reconnected to the hydration system; no leaks were noted. During the site visit it was also confirmed that there were no issues with the air actuated valve controlling FL903. All air actuated valves were checked and were found to be operating satisfactorily.
11. **Day 1,289.0:** Calibration of the complete system was conducted during a site visit on Tuesday 12th August 2008. Calibration was complete by 18:07:48.
12. **Day 1,289.0:** During the site visit two additional LVDT instruments were wired into the data acquisition system. The supports for the LVDTs were not complete, so the actual installation date was day 1,332 on Thursday 25th September, 2008. These two high precision instruments have been placed in order to observe lateral movements of the lid. The two new transducers are identified as LDS5 and LDS6.

13. **Day 1,291.7:** At approximately 10 am on Friday 15th August 2008, the compressor failed. This was initially observed as all air actuated valves are designed to close when air pressure in the receiver is depleted. This effectively shuts off the down-hole filter arrays from the laboratory and means that no artificial hydration can occur.
14. **Day 1,347:** The two new horizontal lid transducers (LDS5 and LDS6) were calibrated against LDVT calibration wedges on Friday 10th October, 2008.
15. **Day 1,351.88:** The new compressor was connected to the Lasgit system on Tuesday 14th October 2008 at approximate 15:00:00.
16. **Day 1,373.72:** The lab PC crashes during external connection from BGS on the 5th November 2008 at 11:13:33. The PC is successfully brought back online.

Data in this report has been included up to day 1,385 on Monday 17th November 2008, stage 2 of hydration was still ongoing at this time. It should also be noted that data between day 1,289 and day 1,385 have not been calibrated, nor have they been error checked. These data are reported for qualitative purposes only, although they are unlikely to significantly alter other than spike removal.

6.1 Failure of the compressor (day 1,289)

At approximately 10 am on Friday 15th August 2008 (day 1,289), the Spiralair KS1/T compressor failed. This was initially observed as a drop in system pressures caused by the closure of the air actuated valves once the compressed air in the receiver had been depleted. This effectively shut-off the down-hole filters from the laboratory preventing continued artificial hydration of the clay.

During the site visit of an engineer it was deemed necessary to replace the existing compressor. This resulted in a considerable time delay to the restart of the artificial hydration activities while the new compressor was ordered, delivered, and commissioned. Whilst this situation was not ideal, it allowed the pressure decay in all filters to be observed, giving an unexpected observation of the state of hydration of the bentonite buffer.

As can be seen in Figure 6-1, the compressed air reduced was off-line between days 1,291.7 and 1,351.88; a total of just over 60 days (marked as a grey band in all appropriate Figures). The re-start of artificial hydration was initiated once all pressures in the filters had achieved asymptotes. The compressed air data after day 1,351 shows that the new compressor behaves in a similar manner to the old unit. As the compressor is only a means of operating the air actuated valves it can be concluded that the change in compressor will have had no affect on the test results.

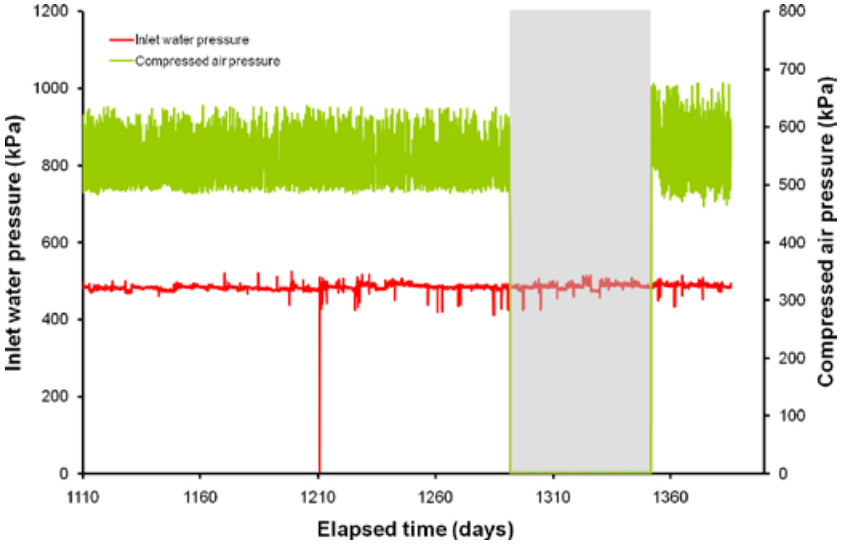

Figure 6-1. *Plot of inlet water pressure and compressed air pressure during hydration stage 2 (the grey band delineates the failure of the compressor). As can be seen, the compressor failed at day 1,289 and was not re-established until 60 days later at day 1,351. The behaviour of the compressed air before and after failure shows that the new compressor is identical to the existing one in operation.*

6.2 Pressure sensor drift and replacement

Soon after calibration had been completed, pressure sensor FM906 started to behave differently from the other pressure transducers, as seen in Figure 6-2 from day 1,122. At this time, examination of the data and experimental setup did not show anything of concern and the decision was taken to observe the seemingly erroneous result. Over the following 8 days the pressure transducer continued to drift in a linear manner, but by about day 1,130 the behaviour levelled, giving a similar response to all other filter mat pressure transducers.

The result for FM906 was carefully monitored to ensure that the drift was not a precursor to a more significant failure of the sensor or a true system response. No additional drift was observed and the transducer continued to mirror the behaviour of the other transducers, al be it with an offset in pressure. It was therefore concluded that the pressure transducer was only affected for an 8 day period and the decision was taken to replace the FM906 transducer to prevent any future drifts during more important experimental stages. This was done during a site visit on Tuesday 27th May 2008 (day 1,211).

The pressure transducer was calibrated before being changed. This data suggests that the transducer was behaving normally. The decision was taken to remove the drift from the FM906 dataset as there appeared to be no reason for the erroneous behaviour. A linear function was applied between day 1,122 and day 1,130 and a correction for the apparent drift of the transducer applied. This gives the result shown in Figure 6-3. The correction is not perfect as FM906 now appears to have a slightly lower pressure than the other filter pressures. However, it represents a best estimate for the parameter during this time.

The new pressure transducer for FM906 was attached and calibrated on day 1,211. FM906 was left with a high shut-in pressure of approximately 18.5 MPa (isolated from down-hole) in order to leak test the new pressure sensor on day 1,212. The raised pressure was allowed to decay and remained at an elevated pressure until Thursday 17th July 2008 (day 1,263), when the sensor was reconnected to the hydration system. No leaks were noted following installation of the new pressure transducer.

6.3 Blasting activity

The early part of 2008 saw considerable blasting activity within the Hard Rock Laboratory. This activity generally occurred at a depth of 450 m, several hundred metres from the Lasgit experiment. Vibration logs show that blasting or related activity occurred on 11th and 17th–19th December 2007, as well as 11th–13th, 16th, 19th, 21st and 24th February 2008. During these times data were thoroughly analysed to ensure that no detrimental effects were observed in the Lasgit experiment.

As will be outlined later (Section 7.2), there are many temporal effects of pore pressure oscillation that correlate with temperature. This makes it difficult to identify any changes in pore pressure as a result of the construction of the new tunnel at 450 m depth. As also discussed later (Section 6.7), it was deemed necessary to ensure that the measurements of canister lid displacement were also not influenced by blasting. An underpinning assumption of Lasgit is that the assembly hall roof is static; from here the roof to lid distance is accurately monitored. Stick-slip movement of the lid was observed during the period of blasting. These movements were fairly regular and some corresponded with blasting activity. However, a large number of blast events did not correlate with any observed displacement of the lid. As discussed later (Section 6.7), it can be shown that the gallery roof is indeed static and the observed movements in the Lasgit lid are very unlikely to be due to blasting.

In light of the available information it can be concluded that the blasting activity within the HRL has not had a detrimental effect on the Lasgit experiment. Pore pressure may have altered as a result of the construction of the new gallery, however long term data (introduced in Section 7) indicates that pore pressure within several boreholes in the 420–450 m depth range exhibit a long-term background decay in pore pressure.

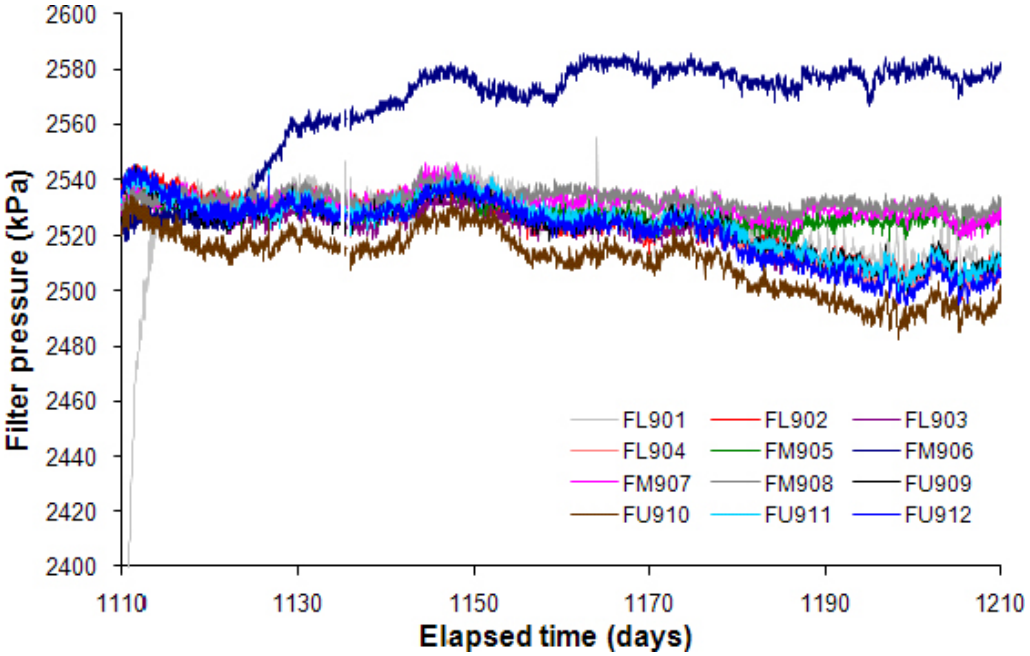

Figure 6-2. *Plot of canister filter pressures to illustrate the drift seen in FM906. This drift has been interpreted as a linear drift from day 1,122.19 to day 1,129.33, whereby the intercept of calibration coefficient has drifted. Compare this with the result in Figure 6-3 which shows FM906 after the data has been corrected. The removal of the 6 day drift brings FM906 in line with the other pressure transducers.*

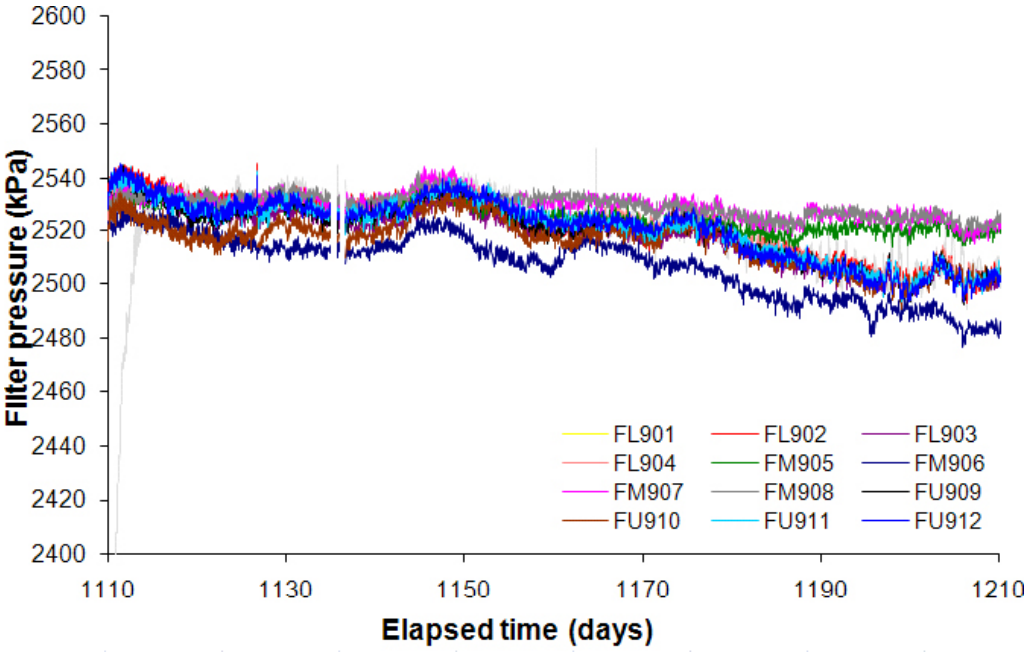

Figure 6-3. *Plot of canister filter pressures after FM906 has been corrected.*

6.4 Evolution of porewater pressure

The following sections describe the temporal evolution of porewater pressure in the Lasgit system, reflecting the complex interaction between artificial and natural sources and their cumulative role in the hydration of the buffer clay.

6.4.1 Canister filters FL901 to FU912

Data from the canister filters are shown in Figure 6-4. Artificial hydration continued in all filters after the lower filter array was brought back on-line at day 1,110 to a pressure of 2,500 kPa. Pressure in the filters quickly increased to the new pressure level with the exception of FL901 which exhibited a much more gradual increase in pressure compared to the other filters. This has been attributed to the non-operation of the air actuated valve that controls the water pumped into this filter. However, the valve was inspected during the site visit in May and appeared to be in working order. The slow build up in pressure therefore suggests that the valve was open but flow may have been restricted by debris in the system.

As can be seen in Figure 6-4, the pore pressure results are dominated by the pressure decay seen in all sensors as the compressor failed at day 1,289. This is shown in more detail in Figure 6-5.

Figure 6-5 shows that considerable drops in pressure are observed over the 60 day period of cessation of artificial hydration as a result of the failure of the compressor. These are presented in Table 6-1. The highest pressure drop is seen in one of the smallest filters, the 5 mm radius FL902 which records a drop in pressure of over 85% from 2,235 kPa to 380 kPa. However, the linear trend shown in Figure 6-6, which can be considered as the average pressure drop observed for each sized filter, exhibits the expected trend with a higher drop in pressure recorded for filters with a smaller surface area. It should also be noted that these results will be affected by local variations in saturation of the clay, which may help to explain anomalously large drops in pressure for certain filters. This general observation is in agreement with previous pressure decay tests (Section 5.1.1), which also observed rapid declines in pressure associated with the smallest filters.

6.4.2 Modelling canister filters FL901 to FU912 during compressor failure

Data from the canister filters during the ‘compressor failure’ event have been interpreted using the same 2D, axially symmetric, finite element model of variably saturated porewater flow presented in Section 5.1.1. The axis of the model is centred on each filter and extends out to the perimeter of the emplacement borehole. The curvature of the canister is ignored to make possible the application of cylindrical symmetry and the model radius is set to one eighth of the canister circumference. The model bentonite is initially set to 95% saturation and the porewater pressures at the filter and outer boundaries are applied as linear segment approximations to the respective measured pressures. The bentonite saturated permeability and specific storage are adjusted to try to get the model to reproduce the pressure decline at the filter during the compressor failure event. Table 6-2 gives the estimated parameter values and the plots in Figure 6-7 to Figure 6-9 show the fits obtained.

Data from FL903 were not considered since this filter was used for gas testing and the model used for interpretation is not able to simulate that event, being only a single phase flow model.

Care had to be taken in modelling FM906 as the pressure data includes the pressure shut-in used during leak testing of the replacement transducer. During this time there is no pressure data for FM906. It may be noted that the fits for filters FL902 and FU912 are rather poor. These are the two small 5 mm radius filters and it would seem that the approximations made by the model are particularly poor for these data.

It would appear from the results in Table 6-2 that the upper filters are indicating generally higher values for permeability and specific storage than elsewhere which suggests the clay in this region is less hydrated, with flow along the suction gradient increasing the rate of pressure decay compared to sections of the clay with a higher saturation. This is consistent with the observations from Hardenby (Section 2.1.1) which indicate a lower density of conductive fractures on the depositional hole wall in this section of the borehole. However, it is also possible that the approximations of the model are just having a different effect on the outcome at these locations. The parameter values obtained for filters FL901 and FL904 are quite similar to those obtained from the hydraulic test earlier.

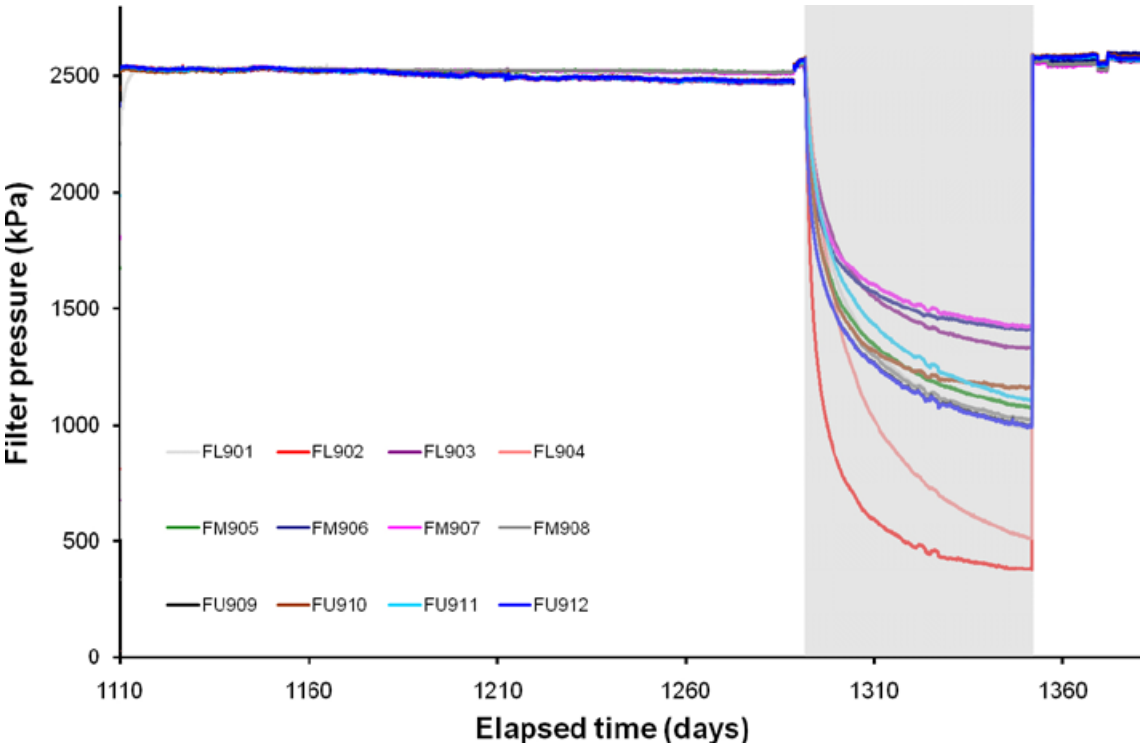

Figure 6-4. *Evolution of water pressure within the canister filters.*

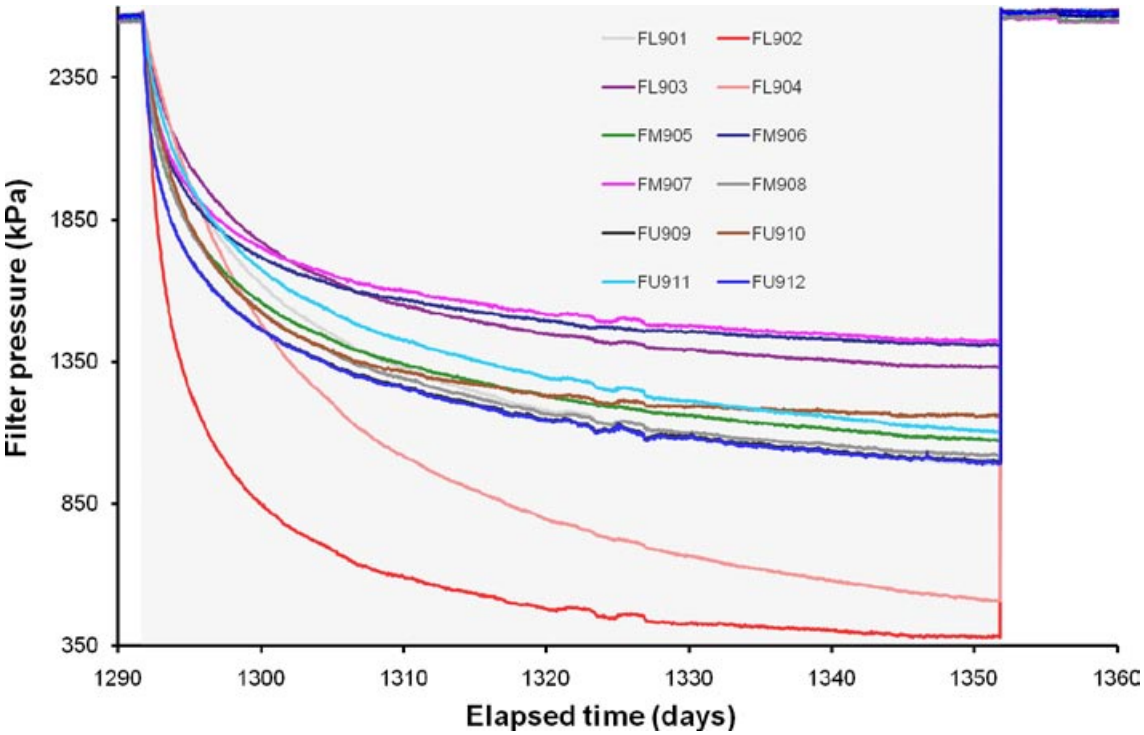

Figure 6-5. *Detail of the pressure decline seen in the canister filters during the period when artificial hydration had ceased. As can be seen, the rate of decline and the eventual plateau of the pore pressures are non-uniform.*

Table 6-1. Reduction in pressure seen in the filters and their corresponding dimensions.

Filter	Starting pressure (kPa)	End pressure (kPa)	Pressure reduction (%)	Filter radius (mm)	Filter area (mm^2)
FU909	2,238.8	996.2	61.3	50	7,854
FU910	2,397.7	1,158.7	54.9	25	1,963
FU911	2,426.7	1,105.8	57.0	50	7,854
FU912	2,238.3	991.7	61.4	5	79
FM905	2,314.2	1,076.5	57.8	50	7,854
FM906	2,350.3	1,410.6	44.8	50	7,854
FM907	2,353.6	1,425.7	44.1	50	7,854
FM908	2,334.2	1,024.5	59.9	50	7,854
FL901	2,432.7	989.2	61.3	50	7,854
FL902	2,234.8	377.9	85.3	5	79
FL903	2,449.8	1,331.1	48.0	50	7,854
FL904	2,482.7	509.2	80.2	25	1,963

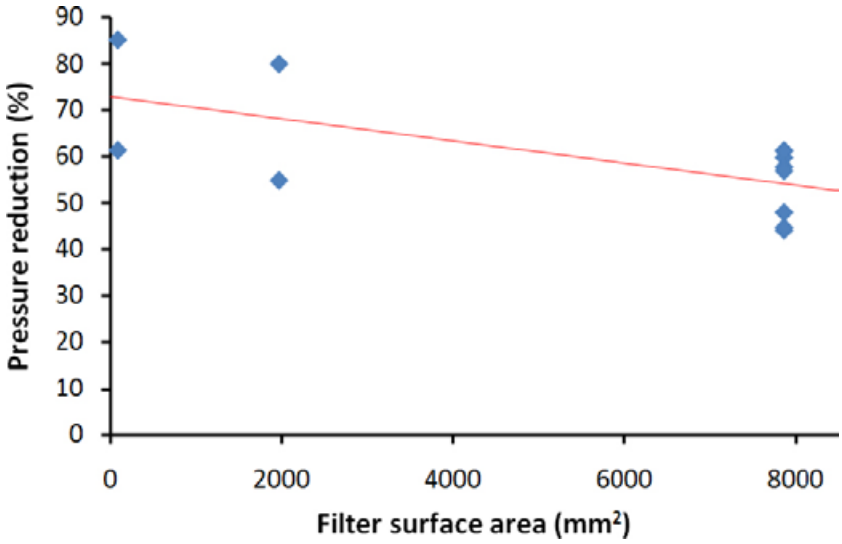

Figure 6-6. *Pressure reduction seen in each filter plotted against their surface area. As seen, the higher the surface area of the filter the greater degree of pressure reduction.*

Table 6-2. Parameter values obtained from model fits to data from each canister filter during the compressor failure event.

Filter id#	Permeability (10^{-21} m^2)	Specific storage (10^{-5} m^{-1})
FL901	8.0	9.0
FL902	7.2	5.0
FL904	13.5	45.0
FM905	7.0	3.0
FM906	8.1	3.5
FM907	6.7	3.0
FM908	5.8	3.0
FU909	9.0	7.5
FU910	50.0	33.0
FU911	23.0	17.0
FU912	33.0	30.0

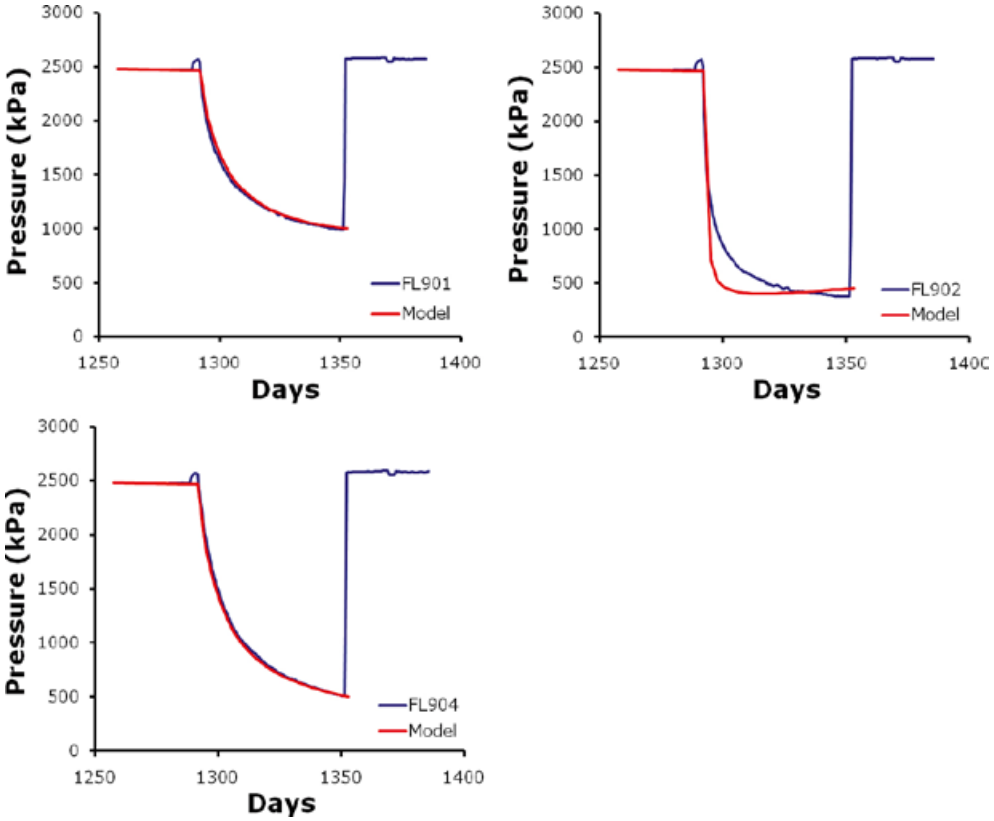

Figure 6-7. *Comparison of models to data for the lower canister filters, FL901, FL902, and FL904.*

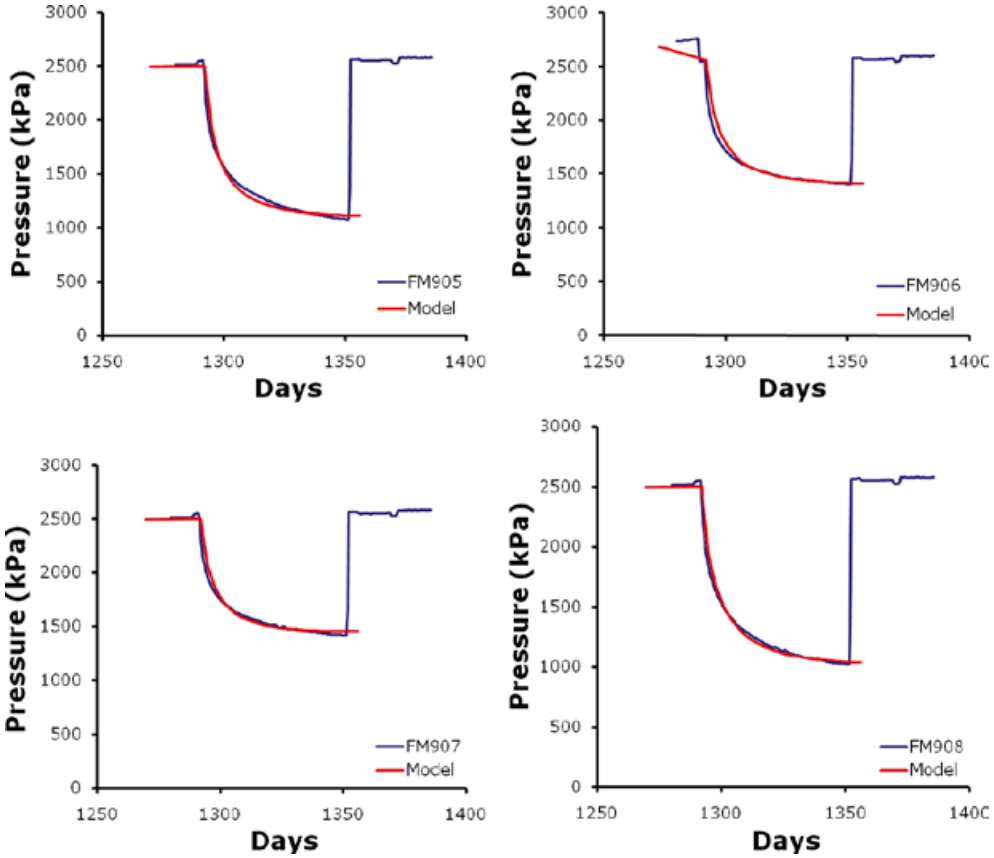

Figure 6-8. *Comparison of models to data for the middle canister filters, FM905 to FM908.*

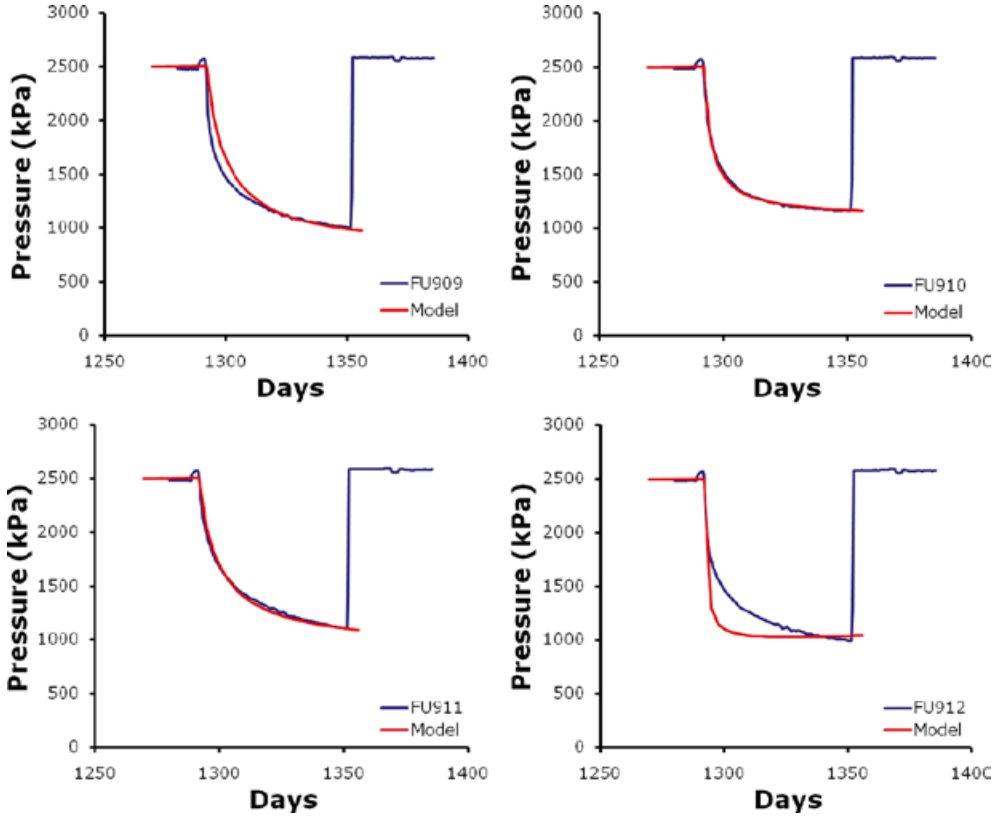

Figure 6-9. *Comparison of models to data for the upper canister filters, FU909 to FU912.*

6.4.3 Filter mats FR901, FR902, FB903 and FB904

Data from the filter mats generally show a steady pressure throughout this period of experimentation, with an occasional change in pressure due to the resetting of the control pumps, as shown in Figure 6-10. However, as with the results from the canister filters, the filter mats show a distinct drop in pressure when artificial hydration stopped.

As can be seen the two circular filter mats (FB903 and FB904), which are sandwiched between bentonite blocks C2–C3 and C4–C5 respectively, behave in a similar fashion (Figure 6-11), with a reduction in filter pressure from approximately 2,500 kPa to 1,500 kPa. Differences can be seen in the two filter mats that are emplaced along the wall of the hole (FR901 and FR902). The higher of these (FR902) drops very rapidly from 2,500 kPa to an eventual asymptote of almost 400 kPa (a drop of almost 84%). This suggests that this filter is well connected to some form of sink and that water injected at this point quickly drains The eventual filter pressure of 400 kPa is close to the pore pressure observed naturally in this location of the hole. Filter mat FR902 occurs at a height of 6.03 m from the base of the deposition hole (Appendix). Extrapolated pore pressures recorded in the pressure relief holes at this depth (Figure 6-12) indicate a pressure of between 400 and 500 kPa. It can be seen in Figure 6-11 that the two filter mats within the bentonite buffer have not reached an asymptote by the time the new compressor was commissioned and that pore pressure was continuing to slowly decay.

The history of filter FR901 has evolved differently from those of the other filter mats. This filter mat (located towards the bottom of the hole) was isolated from the hydration system due to the increase in pore pressure experienced early in the experiment (Section 4). No change in fluid pressure is seen during the period of cessation of artificial hydration. Therefore it can be deduced that no communication occurs between FR901 and any other filter array.

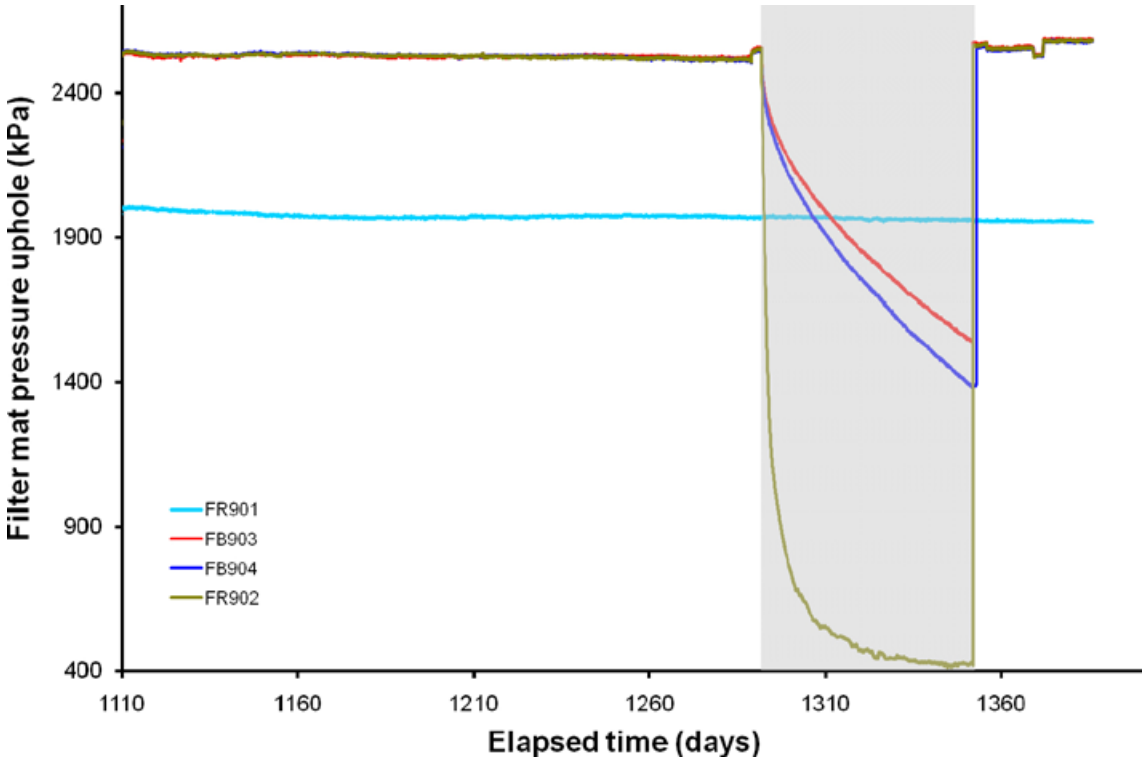

Figure 6-10. *Evolution of water pressure in the filter mats located on the deposition hole wall and sandwiched between the bentonite blocks. Filter mat FR901 (which is in direct communication with a number of packered intervals within the drain holes) was unaffected by the loss in artificial hydration pressure.*

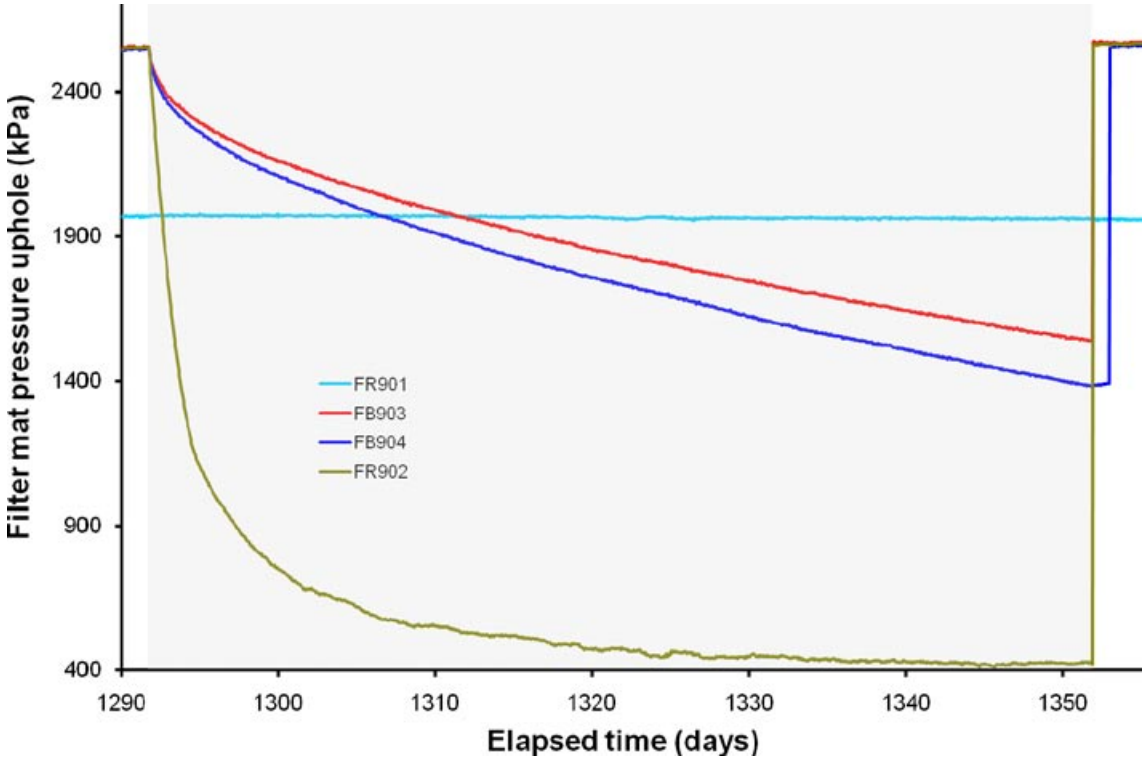

Figure 6-11. *Detail of the pressure decay seen in the filter mats during the period of cessation of artificial hydration. The two filter mats within the bentonite buffer had not reached asymptote.*

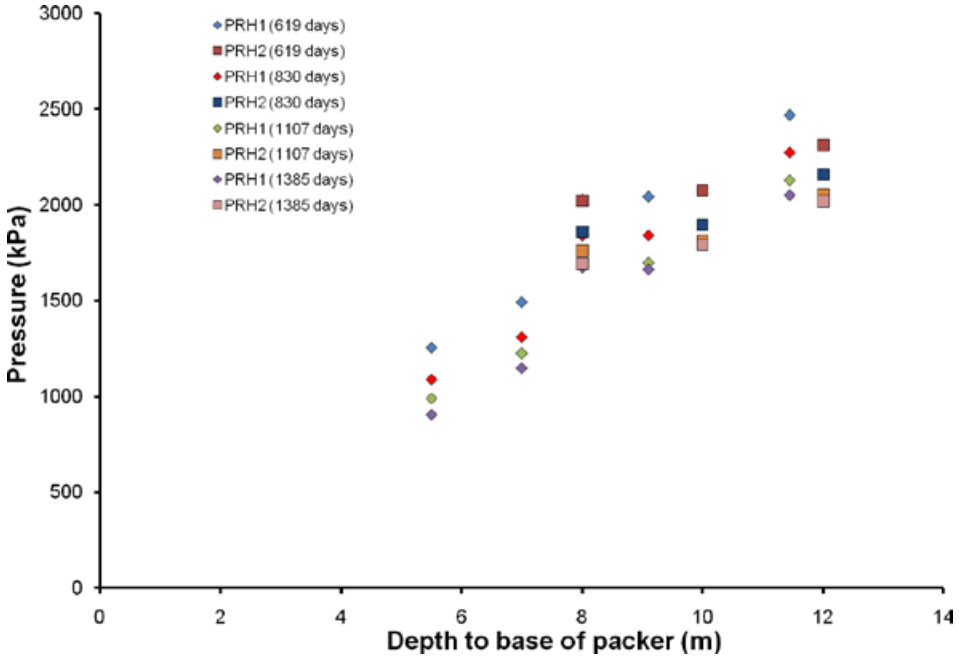

Figure 6-12. *Evolution of pressure in packered intervals within PRH1 and PRH2.*

6.4.4 Porewater pressure within the bentonite

Porewater pressure within the bentonite is measured at 6 discrete locations. As shown in Figure 6-13, three of the locations (UB901, UB923 and UB924) show a general slow increase in pore pressure during this period of experimentation. In contrast, the remaining three locations (UB901, UB902 and UB926) all show a conspicuous reduction in pore pressure. In each of these locations it can be seen that the reduction initiates between day 1,240 and day 1,280; which is prior to the compressor failure date and the cessation of artificial hydration (day 1,292). Thus the reduction in pore pressure at these times is not related to the compressor failure and must therefore be caused by some other event.

6.4.5 Porewater pressure measured at the rock wall (UR903 to UR922)

Porewater pressure is measured at 20 separate locations on the borehole surface and the data are shown in Figure 6-14. For seventeen of the twenty sensors (excluding UR903, UR907, and UR910) it can be seen that this period of experimentation exhibits relatively stable porewater pressures, with possible underlying seasonal variation (discussed in Section 7.2.3). The seasonal variation is best observed in UR914 in Figure 6-14.

Four unexpected events occurred during this period in pore pressure (see Figure 6-15):

- An almost instantaneous pressure rise of approximately 700 kPa occurred in UR907 at day 1,112, followed by a long decay of pressure.
- An almost instantaneous pressure rise of 300 kPa occurred in UR910 at day 1,135, followed by a long decay. A second event in UR910 occurred 109 days later at approximately day 1,244, when, over a 5 day period, the pore pressure slowly rose by 50 kPa to a new level.
- A pressure drop in UR903 of approximately 100 kPa occurred at day 1,368.

The first pore pressure "break-through" was observed at approximately 13:00 on 18th February 2008 (day 1,112.79) with a pressure jump from 2,140 to 2,790 kPa in UR907, as shown in Figure 6-16. After the event had been identified, close examination of the data showed that a precursor to the break-through occurred over the three days prior, as pressure built from approximately 2,100 to 2,140 kPa; although this may be the response as hydration restarted after calibration. The main feature is "instantaneous" with the 650 kPa jump observed between successive data points (logged hourly). Pressure decayed over the following 270 days to asymptote at a new pore pressure level of approximately 2,460 kPa, which is approximately 350 kPa higher than before the break-through.

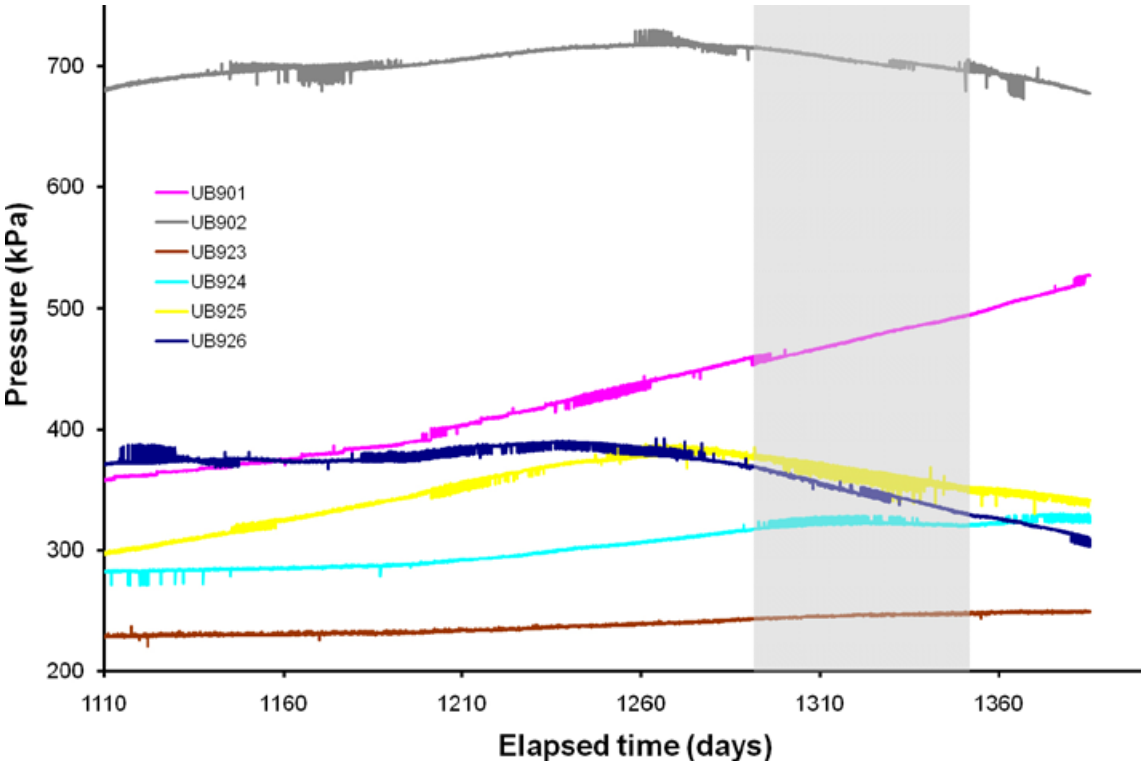

Figure 6-13. *Variation in porewater within the bentonite at the 6 monitoring points.*

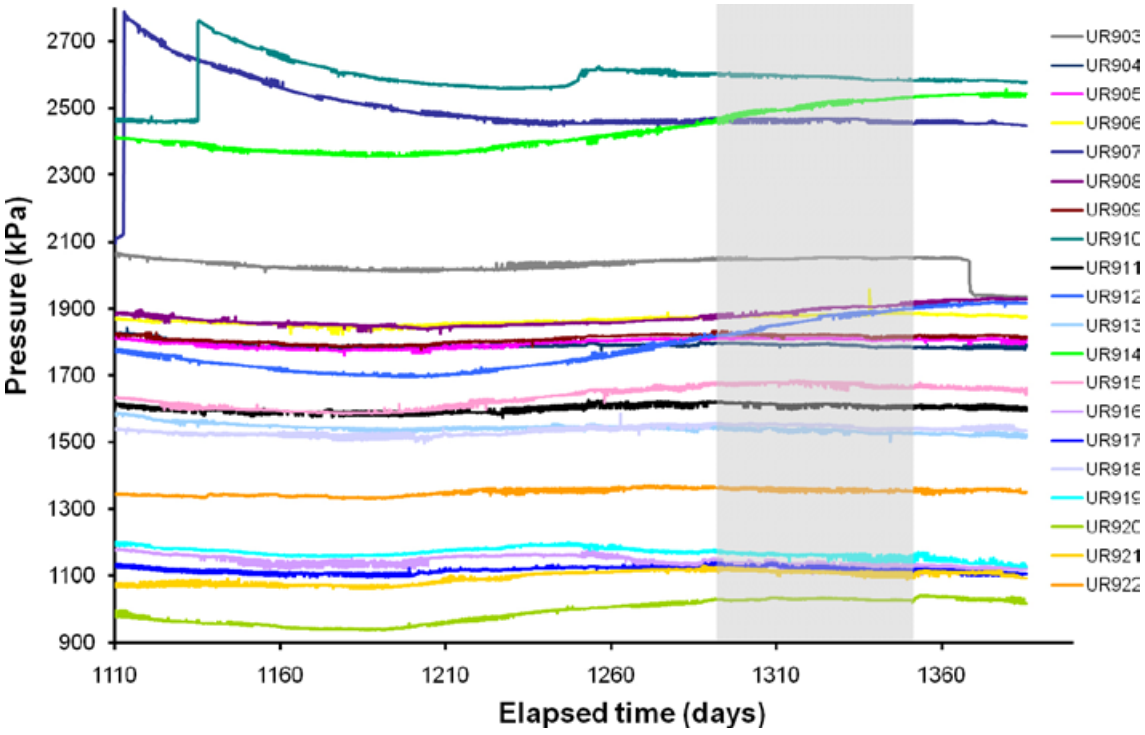

Figure 6-14. *Variation in porewater pressure with time measured at the rock face.*

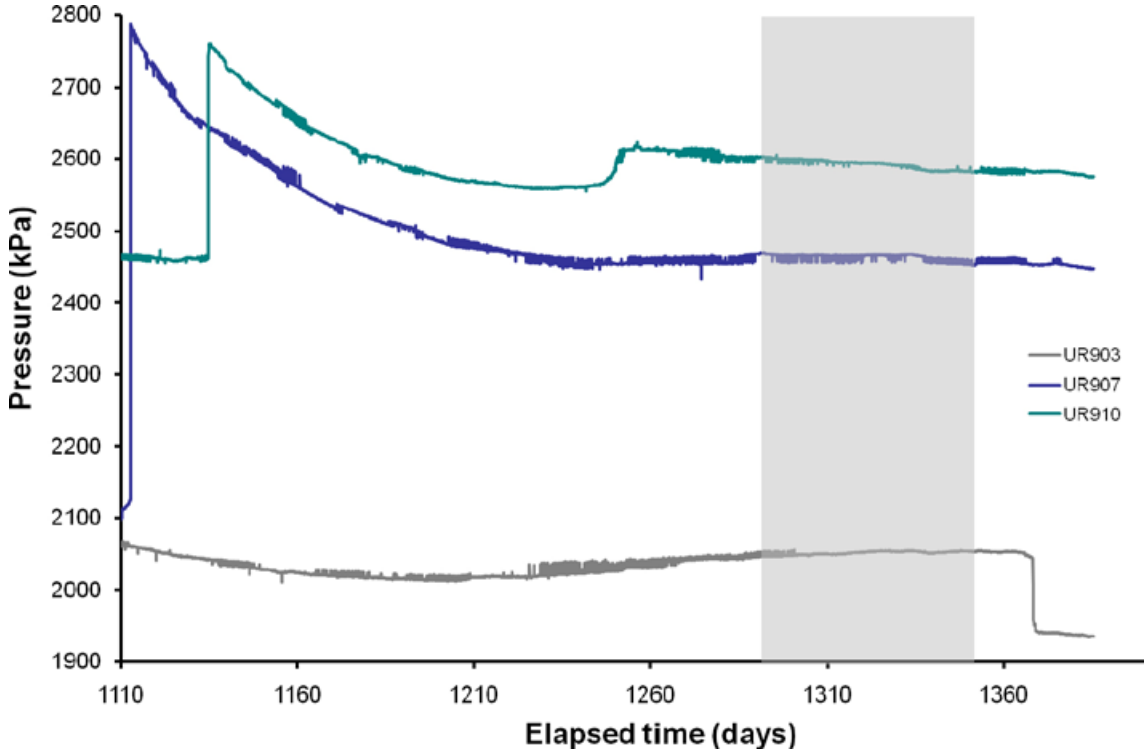

Figure 6-15. *Pressure changes observed in pore pressure sensors UR903, UR907 and UR910.*

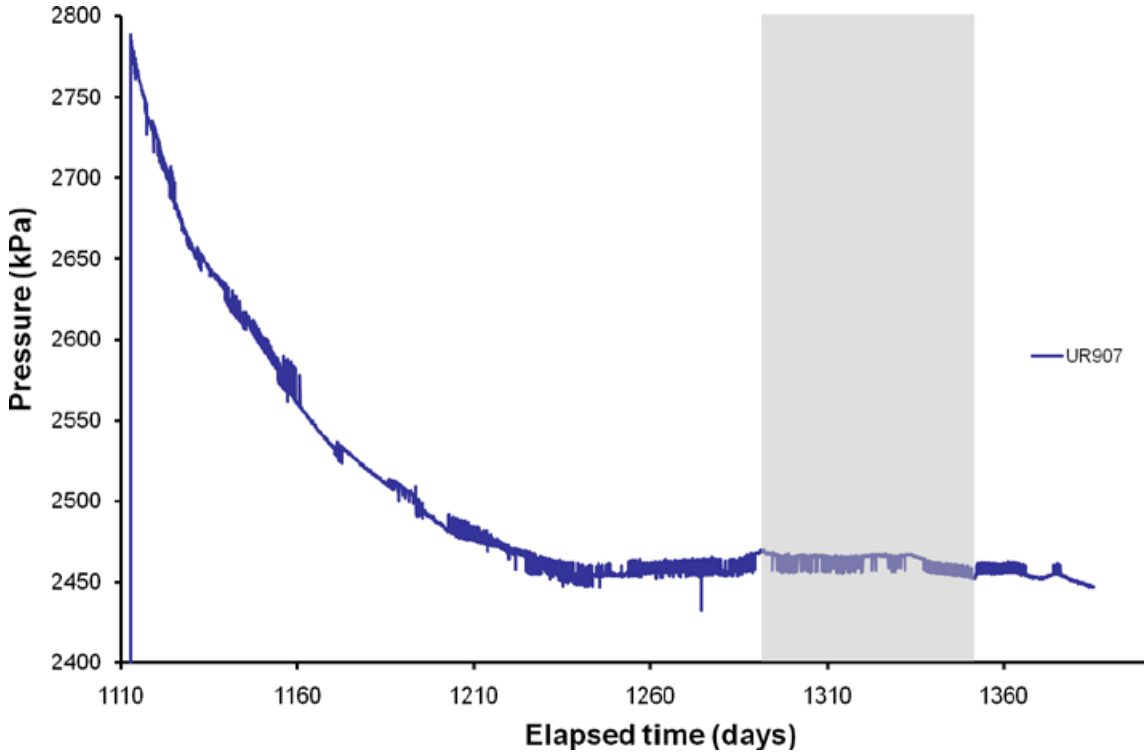

Figure 6-16. *Detail of pressure changes observed in pore pressure sensor UR907.*

This event resulted in a change to the daily data QC routine. Whereas previously all groups of data (i.e. UR or PR sensors) were plotted together, the procedure changed so that every channel is displayed in a separate graph of limited range. The purpose of this is to help identify subsequent pre-cursor events. Data is now checked viewing the previous 10 days only, allowing short term and low amplitude variations to be monitored.

The new QC arrangement also allows significant events to be marked and shown on all data channels, providing a powerful tool for observing correlations between different sensors. In the case of this event, it allowed careful scrutiny of the data leading to the conclusion that the pressure rise must have occurred in response to a 'real' event and not by an error associated with the experimental setup or measurement system. Examination of the fracture map (Figure 2-3) shows that sensor UR907 is located very close to a fracture. It seems highly probable that the pressure build up stems from external events outside of the Lasgit deposition hole, possibly related to the blasting events in the HRL (blasting was active at this time).

The second pore-pressure event was observed at approximately 19:00 on 11th March 2008 (day 1,135) in UR910, as seen in Figure 6-17. At this time pressure jumped from 2,465 kPa to 2,750 kPa, i.e. approximately 300 kPa. On this occasion, a precursor event was not observed prior to the increase in porewater pressure. In addition, pore pressure continued to rise and peak at a value of 2,760 kPa over the next few hours, before starting a pressure decay curve similar in form to that of UR907.

It should be noted that the total pressure observed during these events are very similar; 2,790 kPa for UR907 and 2,760 kPa for UR910. This is significant for two reasons; 1) the pore pressure peak is considerably (200 kPa) higher than that imposed by the artificial hydration system, 2) pore pressure prior to the break-through event was much higher for UR910, at approximately 2,450 kPa, compared with approximately 2,150 kPa for UR907. It is also interesting to note that the decay curve for both sensors is of a similar form following the initial break-through (Figure 6-15). This suggests similar storage and permeability coefficients of the bentonite, which is not surprising as both sensors occur on the same level, separated by 90 degrees.

The location of UR910 is not near a mapped fracture. However, the continuation of an existing nearby fracture would intercept the sensor very closely. It is possible that the full extent of this fracture has not been identified.

Whilst everything described for UR910 is similar to that seen in UR907, differences start to occur around day 1,240 (24th June 2008), when pressure slowly increased over a ten day period by approximately 45 kPa, from ~2,560 kPa to 2,605 kPa. Pressure over the remaining 135 days decays in a similar manner to UR910. The cause of this event is unknown.

The final significant pore pressure event occurred in UR903 and was observed on 31st October 2008 (day 1,368), as shown in Figure 6-18. Over the previous day, pore pressure decayed from 2,050 kPa to 2,045 kPa and then dropped spontaneously a further 85 kPa in one hour before levelling over the next few hours to 1,945 kPa. All previously described events have been pressure increases (and subsequent pressure decays), this is different in that pressure only decayed. The nature of this feature would indicate that it is a real pressure event and not a spurious sensor reading.

As shown in Figure 6-14, pore pressure variation on the rock wall has been minimal during the second stage of hydration; apart from the four pressure events described above. Figure 6-19 shows a series of intensity plots for day 1,110, day 1,250 and day 1,385. These show little variation in the spatial distribution of pore pressure during this time. While porewater pressure has increased in magnitude, the spatial distribution of pressure remains similar to that prior to gas testing (Section 4).

The presence of mapped or extrapolated fractures close to the three pore pressure sensors that displayed break-throughs (i.e. UR903, UR907 and UR910) suggest these features play a significant role in the observed behaviour. Mechanistically, it is hard to conceive of an event within the deposition hole that could result in the generation of porewater pressures that are significantly in excess of those imposed through the artificial hydration system. It seems more probable that events outside of the Lasgit deposition hole are in some way responsible for the behaviour noted above. While a direct correlation to external events such as blasting cannot be made, it is reassuring to note that the measurement system within the deposition hole is sufficiently accurate to register these occurrences, which bodes well for future gas testing.

The observations described above, are symptomatic of a highly dynamic and temporally evolving complex fracture network surrounding the deposition hole. This has remained unaffected by gas testing exemplified by the fact that the geospatial distribution of pore pressure has remained largely unchanged.

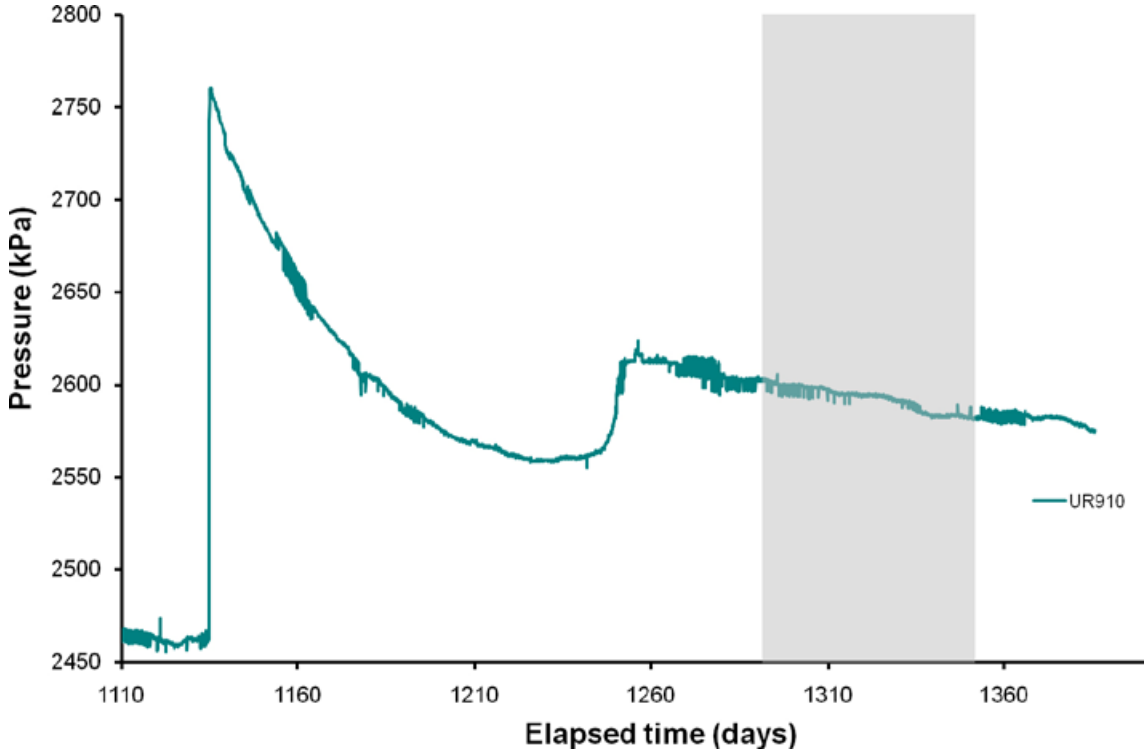

Figure 6-17. *Detail of pressure changes observed in pore pressure sensor UR910.*

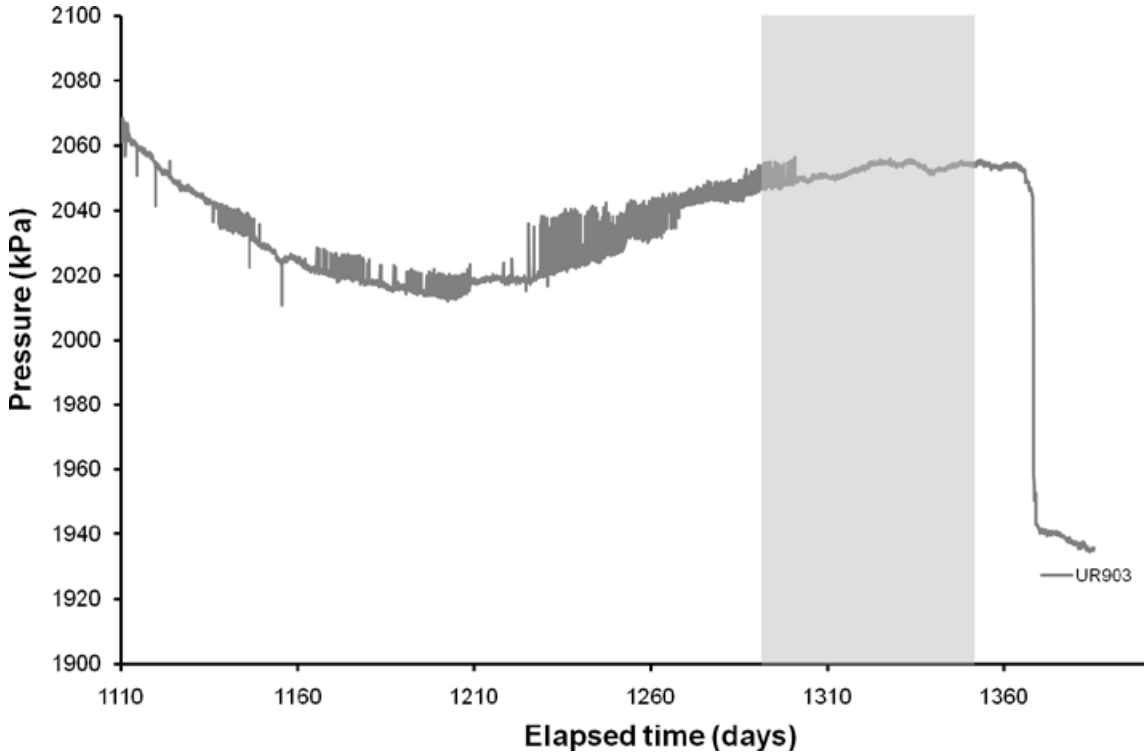

Figure 6-18. *Detail of pressure changes observed in pore pressure sensor UR903.*

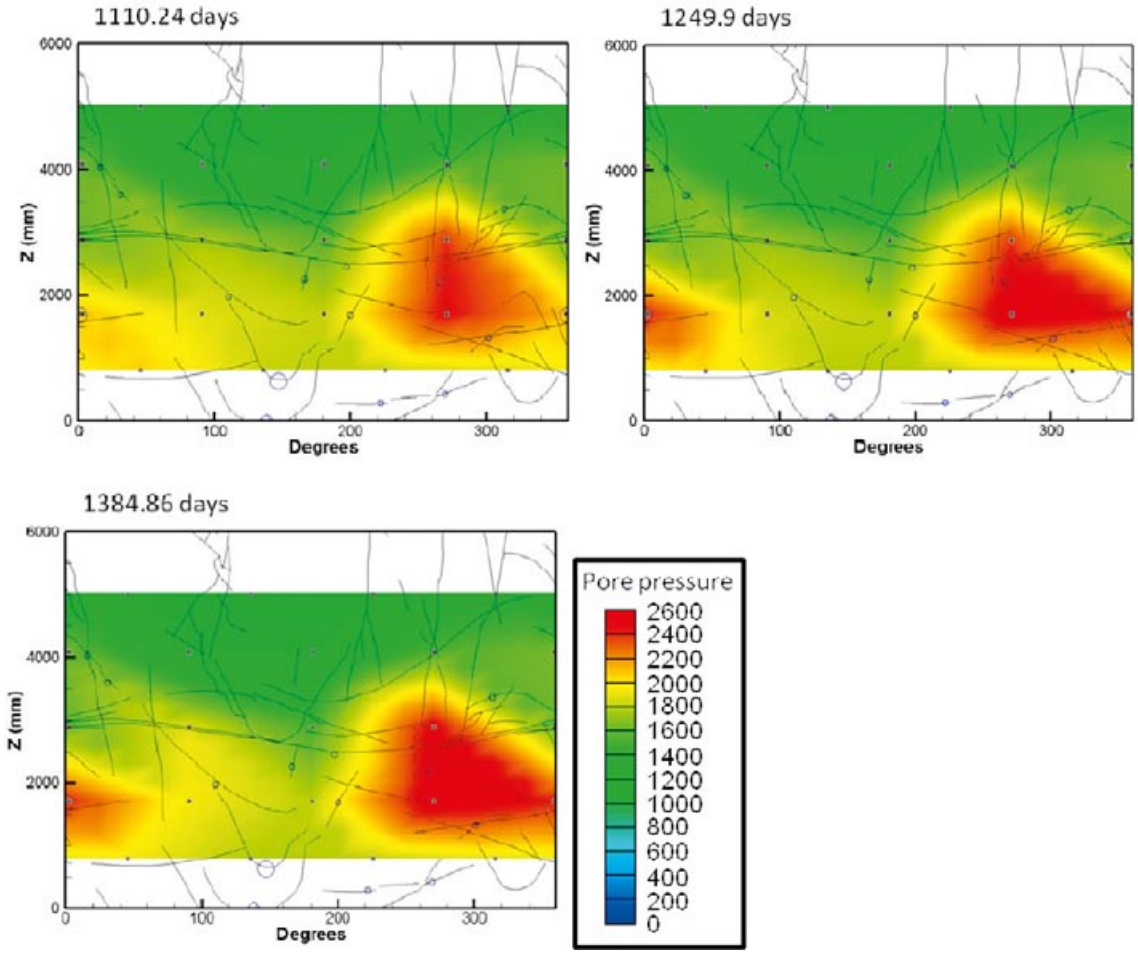

Figure 6-19. *Evolution of pore pressure at the deposition hole wall from day 1,110 to day 1,385.*

6.4.6 Porewater pressure in the pressure relief holes

Pressure data from the individual packered sections of the two pressure relief boreholes are shown in Figure 6-20. All pressure readings show a general decline during this period of experimentation, with no individual decrease greater than 100 kPa. The data suggest that intervals PRH2-1 and PRH2-2 are in equilibrium, with only minor decreases in pressure noted in PRH2-3, PRH1-2 and PRH1-3. It is possible that part of the change in pressure relates to seasonal variations as discussed in Section 7. However, it is also likely that this reflects the general decline of porewater pressure seen in the HRL (Section 7.2.5).

The data show that there is still great variation within the packered sections, with PRH1-1 exhibiting the highest pressure of approximately 2,100 kPa and PRH1-5 having the lowest pressure of almost 900 kPa. This is consistent with drawdown around the tunnel opening.

While interesting, the short-term fluctuations seen in certain packered sections (such as PRH1-3) are not mirrored in the deposition hole. Further inspection of the data shows small-scale features with a periodicity of approximately one day are observed towards the end of this stage of experimentation. The cause of these events is unknown, but may relate to diurnal variations in HRL temperature.

6.5 Evolution of total stress

Total stress within the Lasgit system is measured at 32 locations within the deposition hole. Sensors mounted on the canister, rock wall and within the clay can be used to determine both the axial and radial components of stress and the distribution of values throughout the borehole.

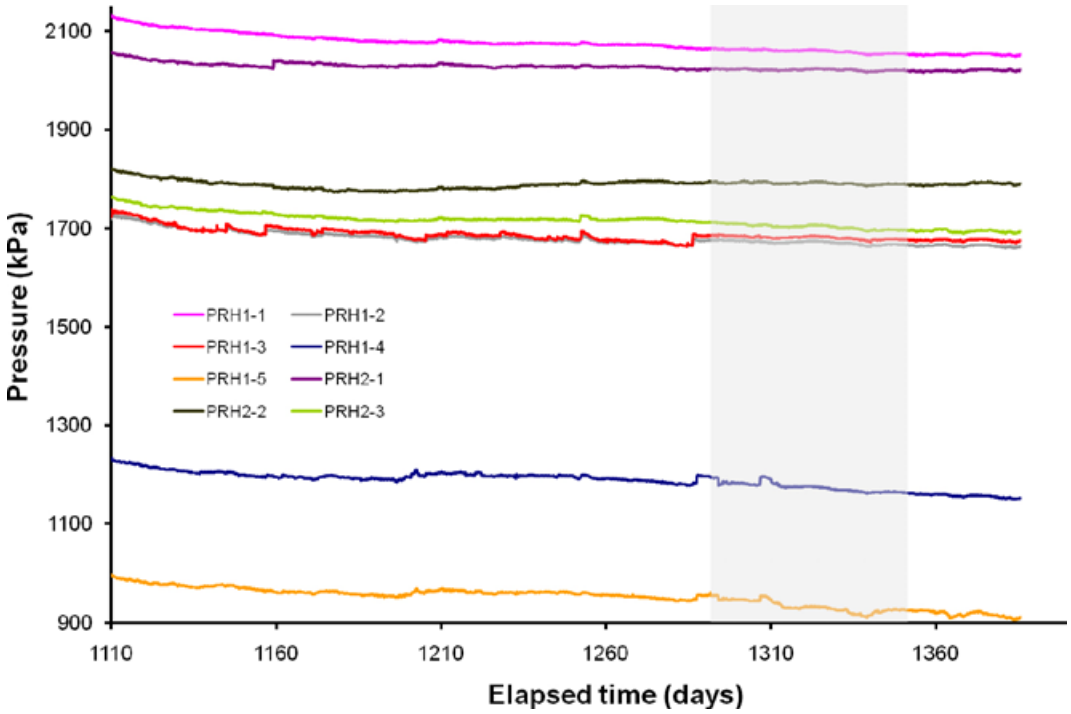

Figure 6-20. *Porewater pressures measured in the packered sections of the pressure relief boreholes.*

6.5.1 Radial stress measured at the rock wall (PR903 to PR922)

Data from the 20 total pressure sensors PR903 to PR922 are plotted in Figure 6-21. As can be seen, all radial stress sensors show a slow increase in total stress of no more than 100 kPa during this stage of the experiment. Long-term variations are noted, but as will be discussed later these can be attributed to seasonal variations in radial stress (see Section 7.3.1).

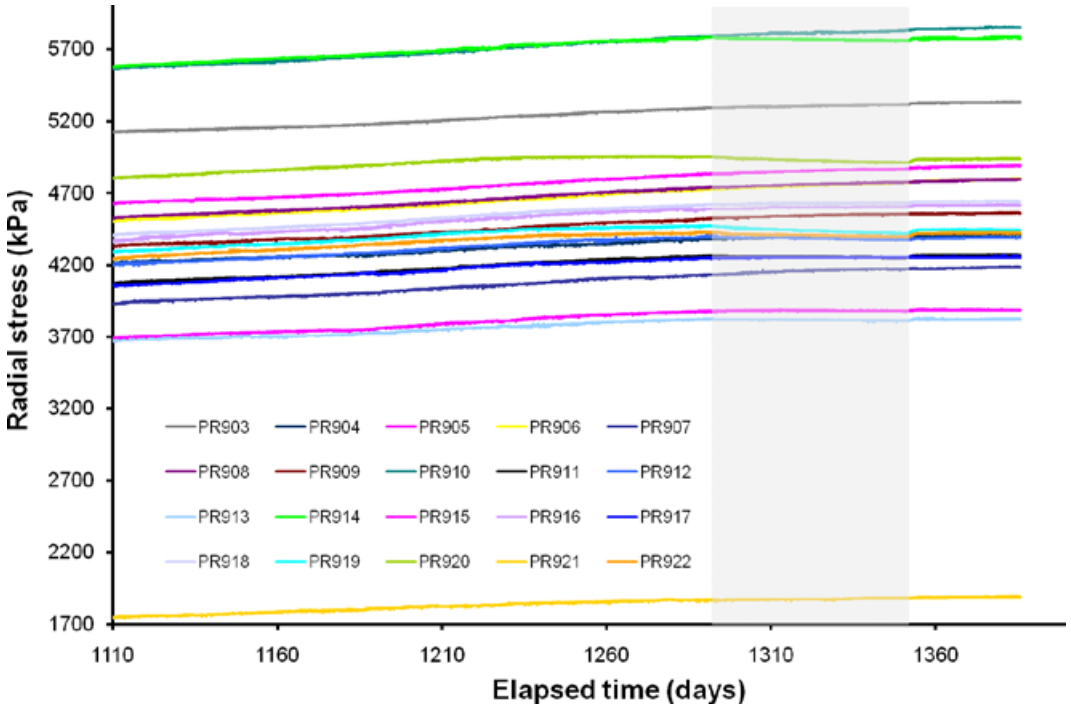

Figure 6-21. *Variation in radial stress with time. In the absence of preferential flow (piping), the rate at which total stress increases is insensitive to the absolute value of porewater pressure applied to the filters.*

The three intensity plots in Figure 6-22 show the spatial and temporal evolution in radial stress measured at the rock wall from day 1,110 to day 1,385. No significant variation in radial stress is observed, as all the radial stress sensors increase at a similar rate.

Figure 6-22 shows the variation of effective stress on the deposition hole wall for day 1,110, day 1,250 and day 1,385. The spatial distribution of effective stress remains fairly constant through this time with only small variations noted, primarily caused by the spontaneous increases in porewater pressure described in Section 6.4.5. The data indicates effective stress generally changes around the circumference of the depositional hole and does not exhibit any significant correlation to depth. The data suggest that the development of effective stress is related to the distribution and frequency of fractures.

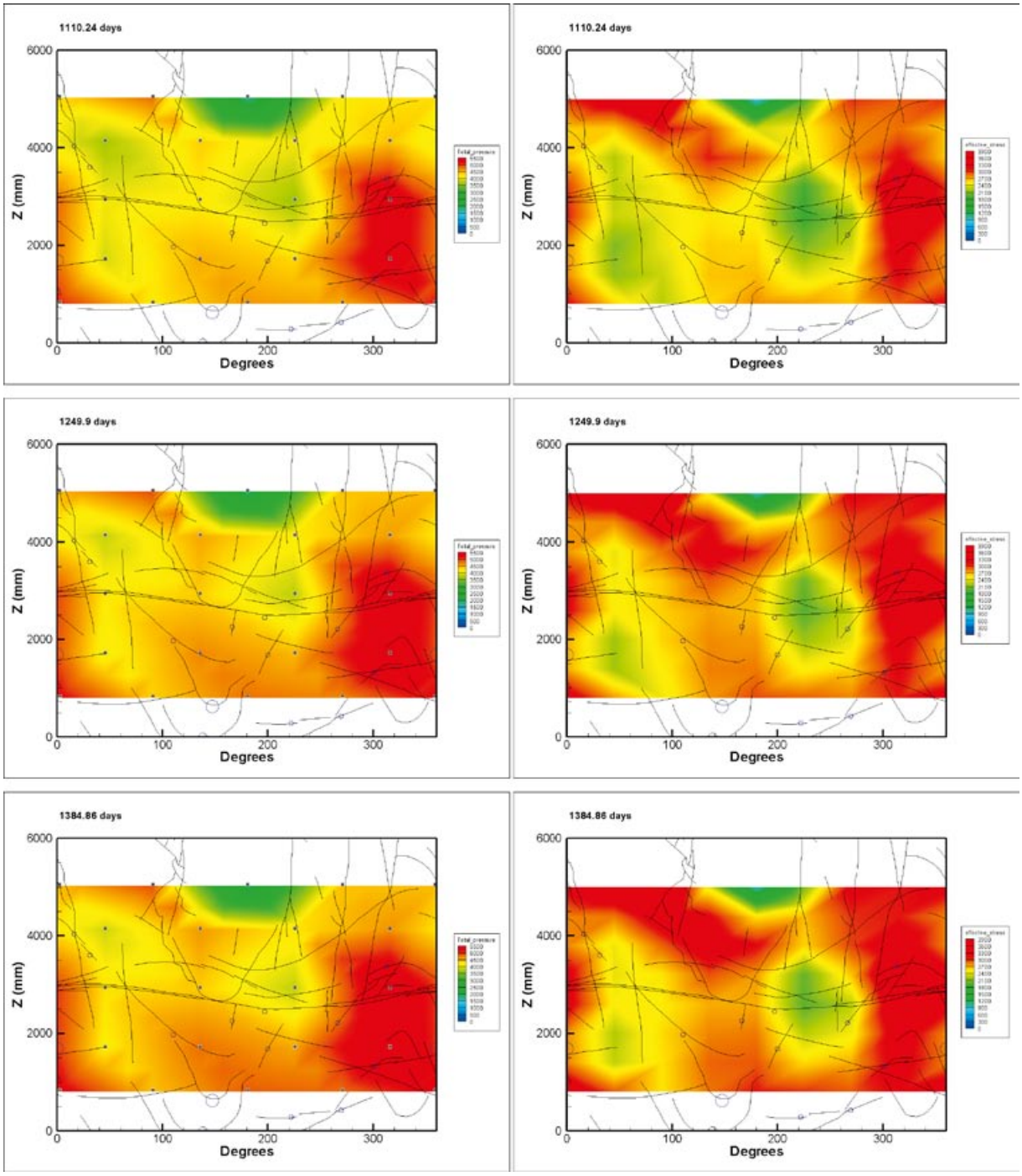

Figure 6-22. *Evolution in radial stress (left) and effective stress (right) around the deposition hole wall from day 1,110 to day 1,385.*

6.5.2 Radial and axial stress on the canister (PC901 to PC903)

Axial and radial stress around the canister has increased steadily during the course of the hydration stage (Figure 6-23). At the start of this experimental period stress ranged from 4,540 kPa to 5,070 kPa, which then increased to between 5,055 kPa and 5,380 kPa. The increase in radial stresses mirror one another, whereas axial stress has increased at a much greater rate, such that it now represents the intermediate principal stress acting on the canister. The change in slope in axial stress seen at approximately day 1,350 corresponds with the switch-on of the new compressor and the recommencement of artificial hydration. Detailed analysis of the stress gradient for axial stress shows a clear change in slope at the time when the compressor failed (day 1,291). However, PC902 and PC903 suggest only some sensitivity to the cessation of hydration on radial stresses. It should be noted that there is significant "noise" in the data and it is difficult to differentiate between seasonal and experimental variations at such low stress gradients.

6.5.3 Axial stress within the bentonite (PB901, PB902, and PB923 to PB929)

Data from the axial stress sensors within the bentonite are shown in Figure 6-24. At the start of this stage of experimentation axial stress ranged from 4,190 kPa to 6,300 kPa. In six of the nine sensors stress increased, while in three (PB928, PB902 and PB929) it remained approximately equal. The increase in axial stress continued until artificial hydration was stopped when the compressor failure at day 1,289. At this point total stress ranged from 4,650 kPa to 6,565 kPa.

During this period it can be seen that two of the stress sensors (PB902 and PB929) remain stable, whilst all other sensors exhibit either an absolute decrease in total stress or a reduction in the rate of stress increase. The most prominent stress drop occurred in PB927, which decreased from 6,560 kPa to 6,215 kPa; a reduction of nearly 350 kPa. All other sensors observed a smaller reduction in axial stress. Sensor PB927 is located at the top of the bentonite buffer at the interface with the concrete plug. Also occurring at this level is PB928 and PB929, which as shown in Figure 6-24 show very small pressure drops. This suggests that stress build up at the top of the bentonite buffer has become very heterogeneous. As pore pressure within the filter mat FB904 (located directly below PB927) drops, the total stress decreases in response to the change in pore pressure. Similar drops in stress are not observed in PB928 and PB929, which lie outside of the footprint of the mat, which therefore has less of an impact on the development of stress at these points within the bentonite.

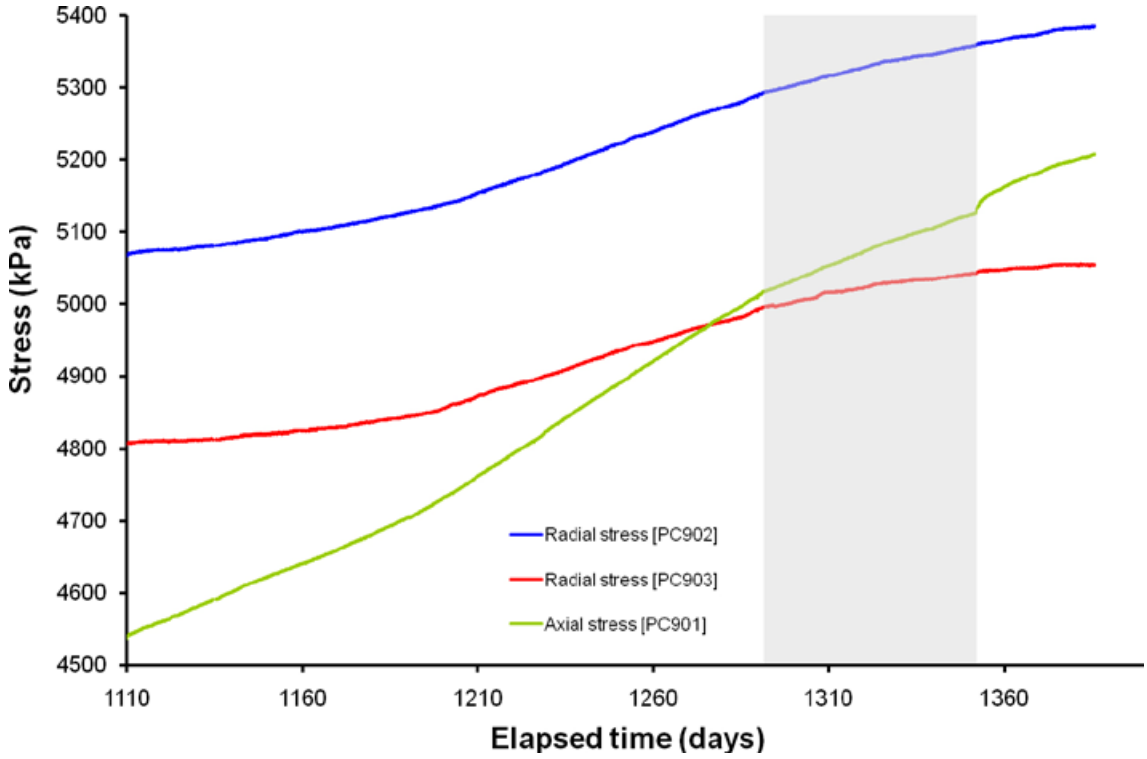

Figure 6-23. *Development of axial and radial pressure on the side and base of canister.*

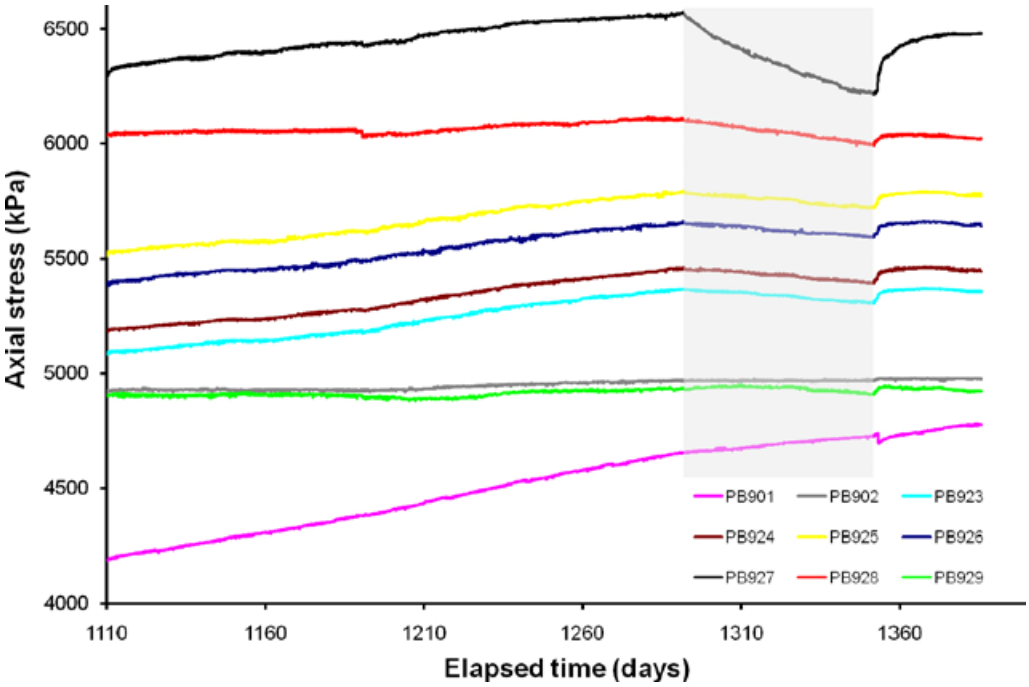

Figure 6-24. *Development of axial stress measured at 12 locations within the buffer. The affect on total stress caused by the compressor failure is variable depending on a number of factors in particular the location of the sensor in relation to sources of artificial hydration.*

After re-starting the artificial hydration at day 1,351, axial stress rapidly increases. However, Figure 6-24 indicates that by the end of the reporting period (29 days following the restart of hydration), most of the stress sensors have reached a plateau. This is contrary to expectation, as perceived wisdom would suggest stress sensors would exhibit similar stress gradients to those before and after the cessation and restart of hydration. For some locations, in particular PB927, the end stress level is significantly less than at day 1,289 when the compressor originally failed. However, examination of recent data indicates a general trend of slow pressure increase with all sensors recording pressures equal to or greater than before the compressor failure (with the exception of PB927 and PB928).

The intensity plots shown in Figure 6-25 have been constructed using the axial stress data from all sensors, except PB901. The plot clearly shows that axial stresses remains non-uniformly distributed across the major axis of the emplacement hole, as originally reported in /Harrington et al. 2007/. The increase in stress at PB927 provides an explanation for the minor differences in lid displacement observed in Section 6.7. It is interesting to note that the interruption in artificial hydration has not had a major effect on the distribution and direction of stress, but has had an effect on the magnitude of stress.

6.6 Axial force acting on the steel lid

Figure 6-26 shows a plot of the axial force (measured by the Glotzl cells) acting on the lid. As can be seen, at the start of the reporting period the forces were 1,280 kN, 1,390 kN and 1,555 kN in LP903, LP901 and LP902 respectively. Therefore forces on the canister lid are anisotropic.

Two very significant events occurred at day 1,190 and day 1,200 with force drops observed in LP901 and LP902 respectively. The first of these occurred in LP901 which for one day showed an increase in axial force, followed by an almost instantaneous drop in force from 1,425 kN to 1,405 kN, a drop of approximately 20 kN. Close examination of all canister lid data shows that this force drop is observed in all three Glotzcells and has a corresponding movement in all displacement sensors. One possible explanation for a drop in axial force is the movement of the Glotz cell laterally, which can relieve force on one set of tie-rods, or from the failure of a tie-rod. As movement is observed instantaneously in all lid data it strongly suggests that this stress drop occurs as a result of an event within the hole and not as a result of failure of the lid. Force drops are also observed in the PB sensors within the bentonite.

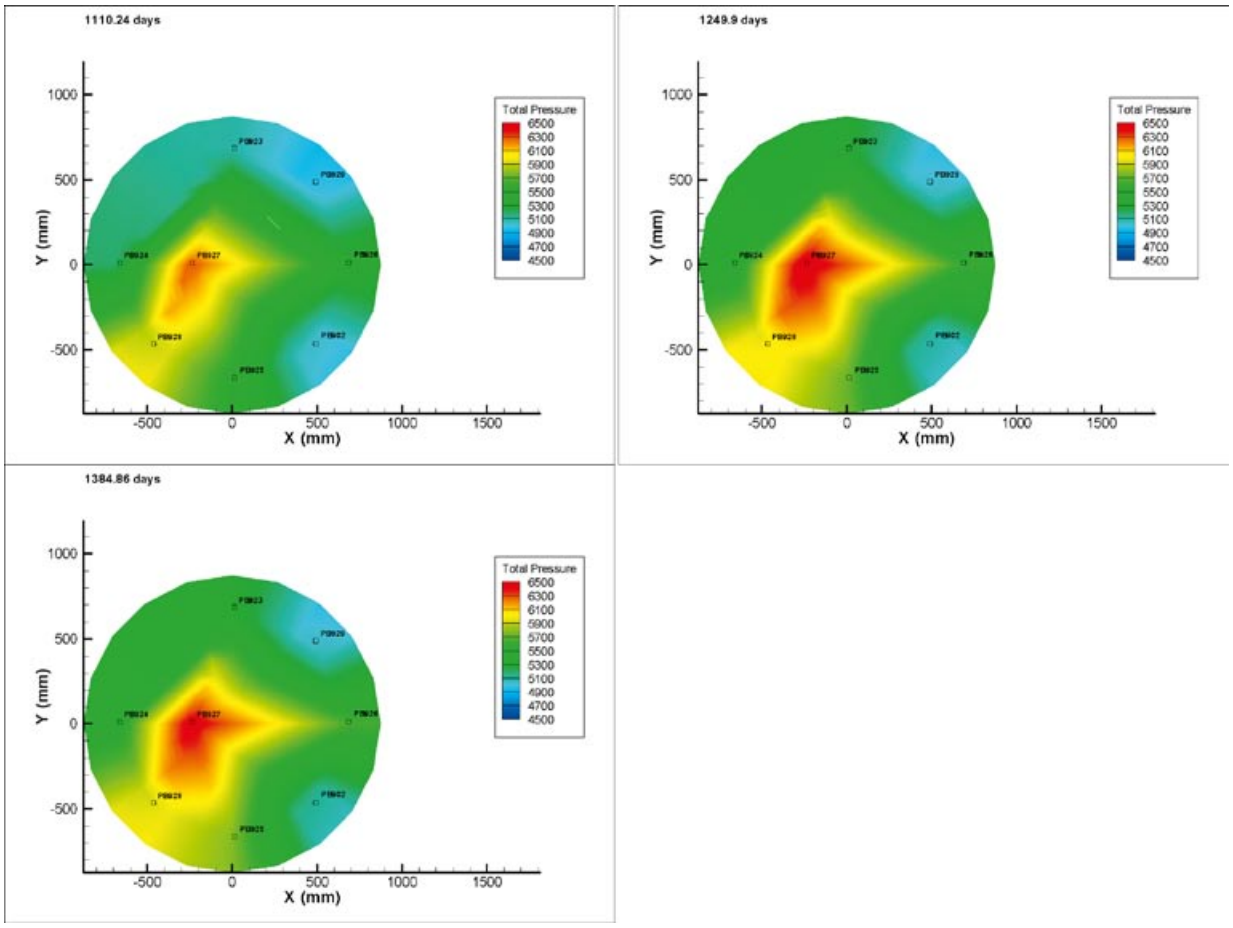

Figure 6-25. *Intensity plots showing the distribution of axial stress across the borehole from day 1,110 to day 1,385.*

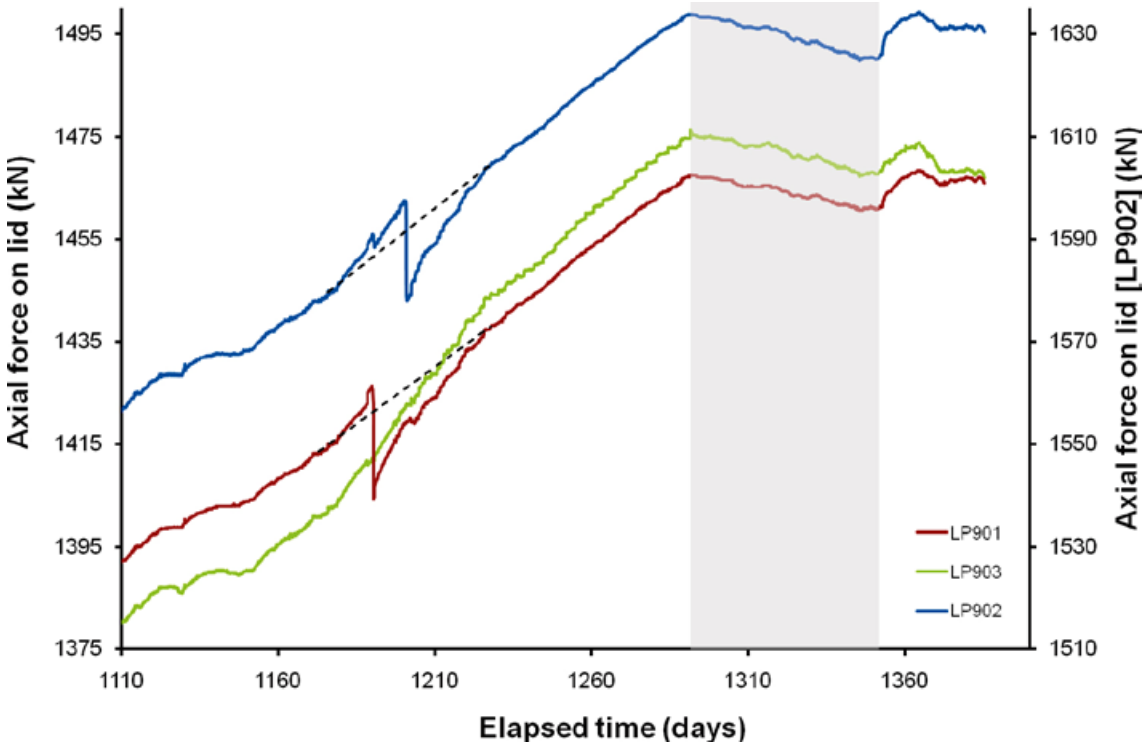

Figure 6-26. *Axial force acting on the steel lid measured by 3 Glotz load cells attached to separate rock anchors.*

The second force drop event occurred some 10 days later at day 1,200 with an instantaneous drop in force on LP902 from 1,595 kN to 1,575 kN; a drop of approximately 20 kN. Unlike in the earlier event, no changes in force are seen in the other LP sensors, only two of the four lid displacement sensors show any movement and these are not as significant displacements as observed in the earlier event. This can be explained by possible stick slip movement of the conical concrete plug, which may also help to explain some of the variations in axial stress recorded in the upper PB sensors. The hypothesis of stick slip is further supported by the analysis of the gradient of the axial force pre- and post-force drop (dotted lines in Figure 6-26), observed as a recovery in force over a 30–40 day period.

As shown in Figure 6-26, axial stress continued to build at a rate of almost 0.5 kN a day up until the point of compressor failure at day 1,289. During the period of no artificial hydration the axial force on the lid decayed in a linear manner at a rate of approximately 0.1 kN a day. Once hydration was restarted at day 1,351 the axial force began to rise, but soon peaked and fell to a new level and remained at this new force level.

Careful observations have been made of axial force once the compressor was brought back on line at day 1,351. The improved daily quality control check of the data allows all parameters to be cross checked easily. As shown in Figure 6-27 it was noted that the changes in axial force closely correlated with the temperature observed within the HRL. This can be explained by the temperature dependency of the Glotz cells or the thermal expansion of other system components (e.g. steel lid, tie rods). However, it is highly probable that the observed effect relates to the Glotz cells, which operate by measuring the pressure of a reservoir of fluid within the device. While the transducers are thermally compensated, there is no allowance for the thermal expansion/contraction of the fluid.

6.7 Displacement of lid and canister

Data from sensors DP901 to DP905 are plotted in Figure 6-28. Sensors DP902–905 continuously monitor movement of the steel lid relative to both the gallery floor and ceiling whilst DP901, attached to the Monel pipe and lid, yields relative changes in canister position. As shown, sensors DP902–DP905 show similar results, in general mirroring one another up to the point when artificial hydration stopped at day 1,289[5]. This shows that the lid movement is homogeneous, indicating the even movement of the lid as the bentonite swells within the hole. Whilst this observation may appear counterintuitive given the non-uniform distribution of axial stress within the hole, it can be explained as non-uniform stresses act on the base of the rigid concrete plug which then behaves as a piston resulting in uniform displacement of the lid.

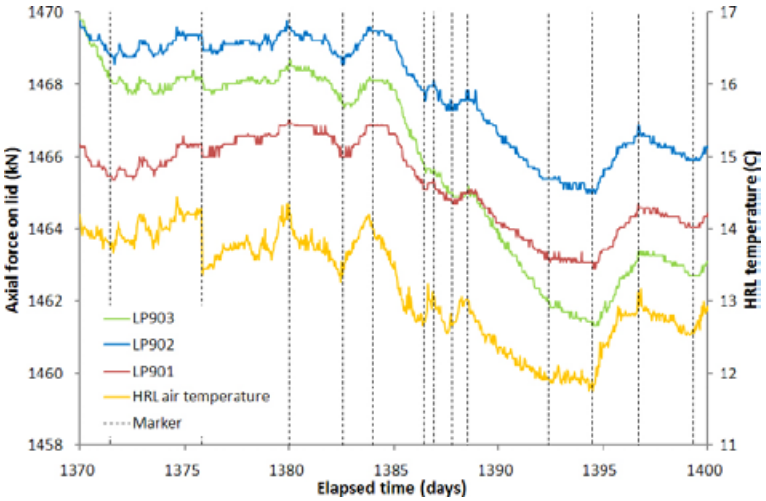

Figure 6-27. *Axial force acting on the steel lid plotted with temperature of the HRL.*

[5] The exception to this occurs at day 1192 in DP903, when it shows a reduction in displacement in contrast to all other sensors that exhibit an increase in value. This could be explained by tilting of the lid.

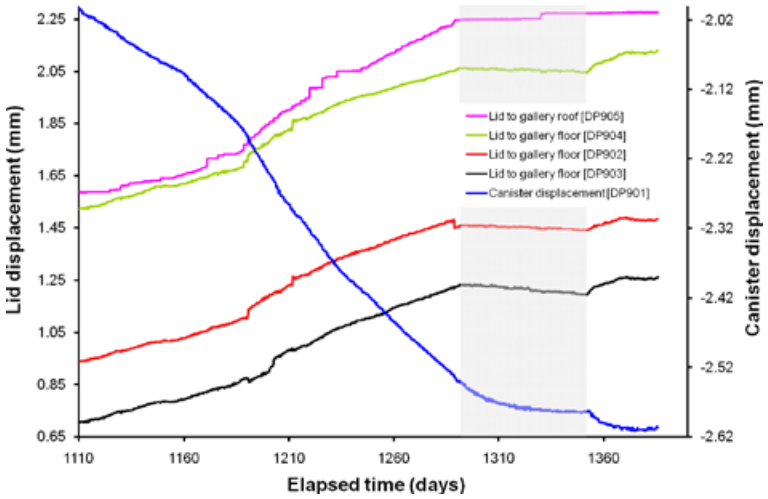

Figure 6-28. *Linear displacement of the steel lid and copper canister. Movements of the lid are measured relative to both the gallery floor and ceiling. Movements of the canister are measured relative to the steel lid.*

As shown in Figure 6-29, data for DP905[6] shows stick-slip movement of the lid throughout this period of testing. These small displacements are not always accompanied by movement recorded by the three displacement transducers at the edge of the lid (DP902–DP904). This suggests that the lid is buckling with the central portion bowing upwards. The data could also be explained by movement of the gallery roof, which is currently assumed to be static. However, with blasting occurring during this stage of experimentation it is possible that movement of the gallery roof has indeed taken place[7]. Since stick-slip movements occur with regular frequency it is possible to correlate some with the blasting events. However, the vast majority of movements occur when no blasting takes place. This scenario (i.e. movement of the roof) was discounted from examination of data accrued during the compressor failure and the accompanying cessation in artificial hydration. During this period the lid remained stationary for a prolonged period of time, strongly suggesting that the vast majority of observed deformations were as a direct result of actual lid movement.

It can be seen that the three displacement transducers around the edge of the canister lid all show a slight reduction in lid height during the cessation of artificial hydration. During the same period, the high resolution lid to gallery roof transducer (DP905), showed no drop in height and remained constant, with the exception of one slip event.

Considerable effort has been afforded to studying the movement of the lid. To aide this process, it was decided to add lateral displacement sensors in order to be able to describe fully in 3-dimensions the movement of the lid. While movement of the lid may be viewed as a secondary issue (i.e. merely offering confining pressure to the experiment), it is in fact a vital component, dictating the boundary condition to the test. Changes to this boundary will impact on both the results of gas injection and the subsequent modelling of the data.

It can be seen that when the compressor failed at day 1,289 the lid slowly settled as the stresses within the hole changed. Once the compressor was re-started at day 1,351 the lid quickly began to move at a similar gradient of that observed prior to compressor failure, but within 20 days reached a plateau which continued to the end of this reporting period. Preliminary analysis of recent data (up to February 2009, day 1,470) suggests that the system exhibits considerable hysteresis with all of the sensors now showing increasing displacement at this time. This type of behaviour has been reported by /Harrington and Horseman 2003/ and is the current focus of ongoing experimental laboratory work.

During the reporting period the canister continued to drop relative to the lid, with over 0.6 mm of movement observed. This strongly indicates preferential swelling of the clay has occurred above the canister. Intuitively this is to be expected given the availability of water from the artificial hydration system located in the upper section of the deposition hole.

[6] DP905 is the sensor measuring the gallery roof to the centre of the lid and currently has the highest resolution of the displacement sensors.

[7] Blasting occurred on 11-13/2/08 (day 1105 – day 1107) , 19/2/08 (day 1113)

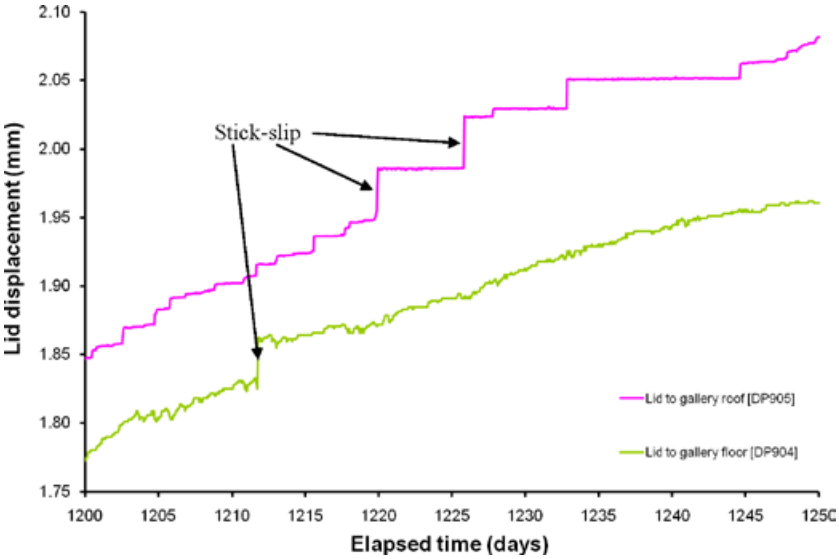

Figure 6-29. *Illustration of stick-slip movement of the canister lid from sensors DP904 and DP905.*

6.8 Laboratory utilities

Temperature in the Gas Laboratory, canister and Assembly Hall area are continuously monitored by a series of thermocouples (Figure 6-30). Apart from minor failures of the air-conditioning system at elapsed times of day 1,317 and day 1,324, temperature within the laboratory is continuously controlled. However, the air conditioning unit has not performed consistently during this reporting period. It can be seen that the temperature in the office area was very stable between day 1,110–day 1,186 and day 1,331–day 1,380. Between day 1,186 and day 1,331 temperature varied by over a degree. Temperature within the laboratory has been variable throughout the period and correlates with the temperature within the HRL, which shows a clear annual variation, cycling between about 10°C and 16°C. The canister also shows an annual variation, but with a much smaller range of 12.8°C to 13.6°C, and with a phase offset of about 90 days from the HRL temperature data.

Analysis of step changes in laboratory temperature (e.g. Day 745.0) show that these events have no significant effect on any of the sensor outputs recorded within the lab. Almost all recorded devices are either thermally compensated (pressure transducers) or use an internal thermocouple located with the device (e.g. all Geokon equipment) to correct for minor changes in temperature.

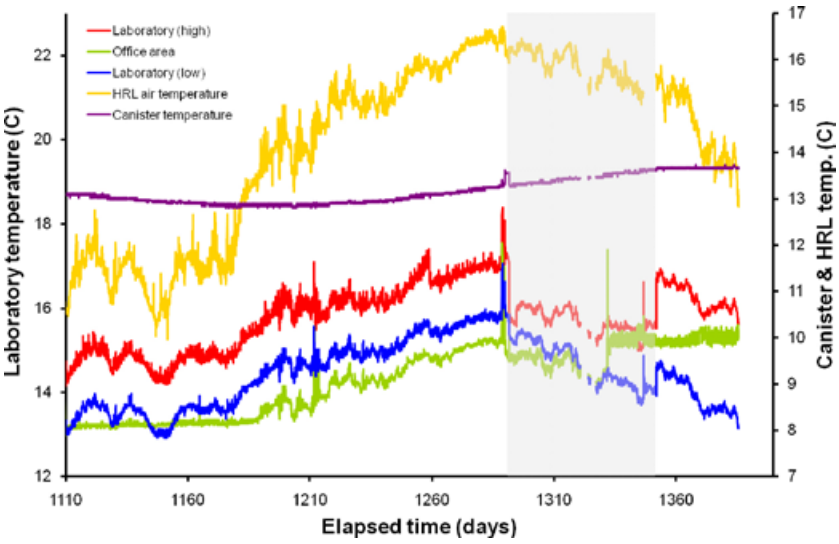

Figure 6-30. *Temperatures recorded in the Gas Laboratory, office, canister, and HRL.*

7 Complete test history

The Lasgit status report for 2007 contained all data from day 1 through to approximately day 915 /Harrington et al. 2007/. In Section 5 of this report, we have updated our observations of the gas stage of testing and given a full description of this stage of experimentation up until day 1,110. This was followed in Section 6 by a detailed description of the second stage of artificial hydration from day 1,110 to day 1,385. In this section of the report we take a more holistic view of the Lasgit data and examine the various parameters from day 1 through to day 1,385. It should be noted that not all events will be discussed, especially those introduced earlier in this report, but linked observations which underpin all data will be presented in the following sections.

7.1 Annual cyclicity and variation of properties

Dealing with short intervals of data that are often less than a year in duration, the impact of seasonal variations in temperature within the data are not always apparent. Now that Lasgit has been in operation for in excess of 1,385 days (3.7 years) it is clear that seasonal variations are occurring in certain parameters. These are introduced separately.

7.1.1 Temperature

Figure 7-1 shows the temperature variation in the gas laboratory, office, canister and HRL during the full duration of the Lasgit experiment. As can be clearly seen, the HRL and canister temperatures show very strong seasonal variation (note that the vertical black dashed lines denote the 1st January of each year that Lasgit has been running). The HRL temperature variation has ranged from approximately 10 degrees to just above 16 degrees. It can be seen that the winter of 2006/07 was not as cold as previous winters, with 2005/06 having a very short cold snap. In contrast, the summers have been consistent in their maximum temperature and their duration. The temperature in the canister has consistently lagged the HRL temperature by approximately 90 days and has ranged only ±0.5°C from 13.3°C throughout the test period. Some variation can be seen year on year. However variations of only 0.2°C are seen between temperatures for successive winter lows or summer highs. This clearly shows that the canister is free from major year on year temperature variations and a change of only ±0.5º over the year is not considered significant.

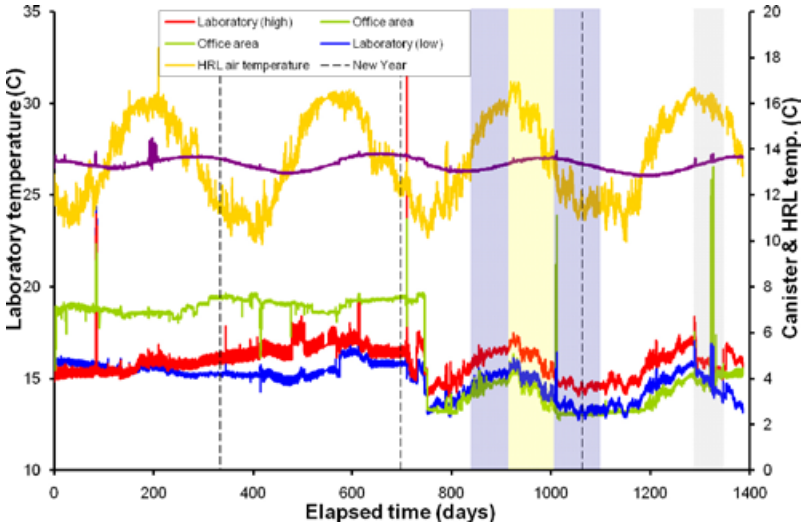

Figure 7-1. *Temperatures recorded in the Gas Laboratory, office, canister, and HRL during the complete experimental duration. The blue/purple coloured areas show the time of hydraulic testing, the yellow area shows the time of gas testing, and the grey area signifies the period when the compressor failed and there was a hiatus in artificial hydration.*

Of concern in the temperature data is the variation seen in laboratory and office temperatures. Prior to day 745 the air conditioning of the laboratory was well controlled with little significant variation. Since this date, the temperature results have shown the same seasonal variation as the HRL. Such variation could have an impact on data recorded within the gas laboratory and may be difficult to correct for. However, this problem has since been resolved by the air-conditioning manufacturer and laboratory and office now exhibit stable temperatures. It should be noted that temperature in the office air-conditioning unit was reduced by 3 degrees on day 745 in order to reduce the load on the system.

7.2 Evolution of porewater pressure

The following sections describe the temporal evolution of porewater pressure in the Lasgit system, reflecting the complex interaction between artificial and natural sources and their cumulative role in the hydration of the buffer clay.

7.2.1 Canister filters and filter mats

Figure 7-2 shows the canister filter pressure throughout the entire history of the experiment. As can be seen, there is no long-term observation of seasonal variation within this data and no other conclusions can be drawn in addition to those stated for each individual test period. This is to be expected as the canister filters are controlled and should not be influenced by seasonal variations. Data from the filter mat sensors are shown in Figure 7-3 and similarly shows no influence of seasonal variation.

7.2.2 Porewater pressure within the bentonite

Porewater pressure within the bentonite is measured at 6 discrete locations, as shown in Figure 7-4. The majority of the response seen is as a result of the artificial hydration, which appears to show little seasonal variation when viewed for a limited period of time. Following close scrutiny of the data it can be seen that longer duration fluctuations are present in the pore pressure responses which may originate from seasonal variations. These are especially obvious in UB902, UB926 and UB925 with oscillations of approximately 1 year. It can be seen that since approximately day 1,300, these three pore-pressure sensors have shown a distinct drop in pressure. Figure 7-4 clearly shows that the drop in bentonite pore pressure started before the failure of the compressor and the cessation of artificial hydration. Preliminary analysis of recent data (up to February 2009, day 1,470) suggests that UB901 and UB902 are evolving to equal pore pressures, indicating homogenisation of pore pressure within the bentonite at the base of the deposition hole.

7.2.3 Porewater pressure measured at the rock wall (UR903 to UR922)

Porewater pressure is measured at 20 separate locations on the borehole surface and the data are shown in Figure 7-5. As seen, many of the pore pressure sensors show obvious seasonal variation after the pore pressure of the artificial hydration system was raised to its final level at about day 500. Pore pressure has shown a general linear reduction from approximately day 600. The removal of this linear trend clearly shows the underlying sinusoidal variation of pore pressure, as shown in Figure 7-6. As one would expect, the general sinusoidal oscillations correspond more closely with the temperature observed in the canister and not with the HRL air temperature.

Close inspection of the data in Figure 7-6 shows that the oscillations of UR920 and UR915 are offset by approximately 20 days from that of UR912 and UR914. These latter pair of sensors (UR912 and UR914) occur on the same level of the hole (Section 7), but are 180º separated (position 90º and 270º respectively). Sensors UR915 and UR920 are situated higher in the hole (Section 9 and 10 respectively) and are situated at positions of 0º and 135º respectively. This suggests that the thermally induced pulse in pressure propagates vertically down the hole, evidenced by the fact that in Figure 7-6 the variation in pressure of UR920 predates the increase in canister temperature.

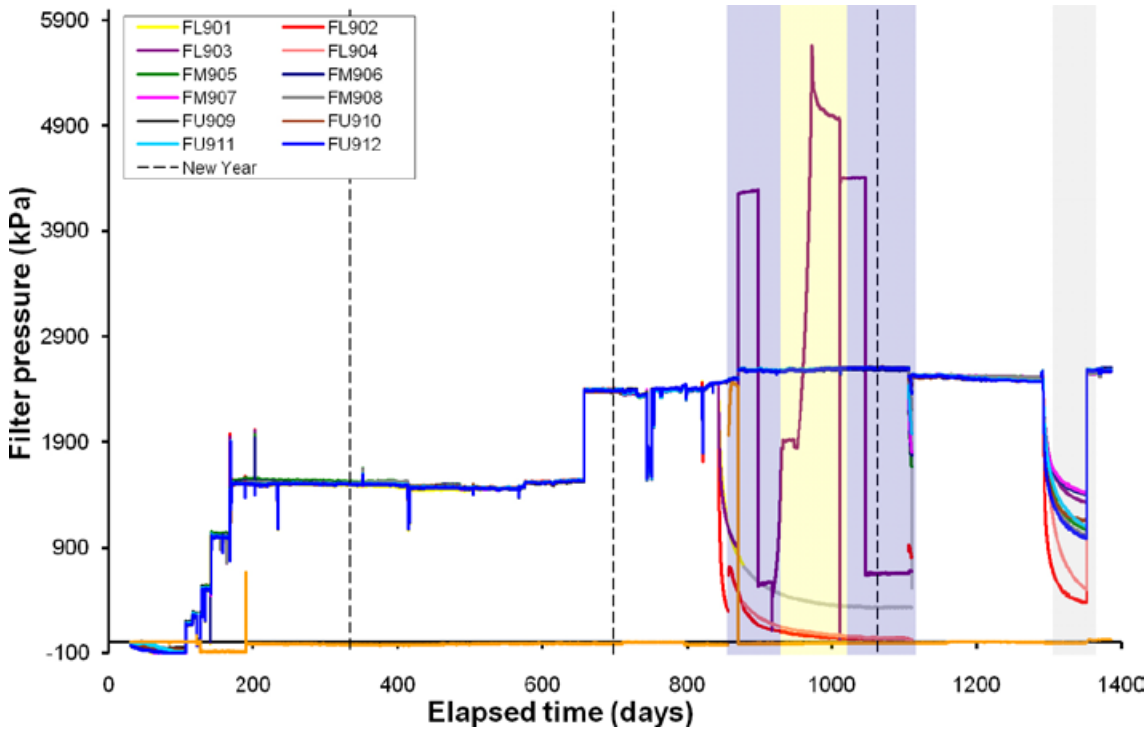

Figure 7-2. *Evolution of water pressure within the canister filters.*

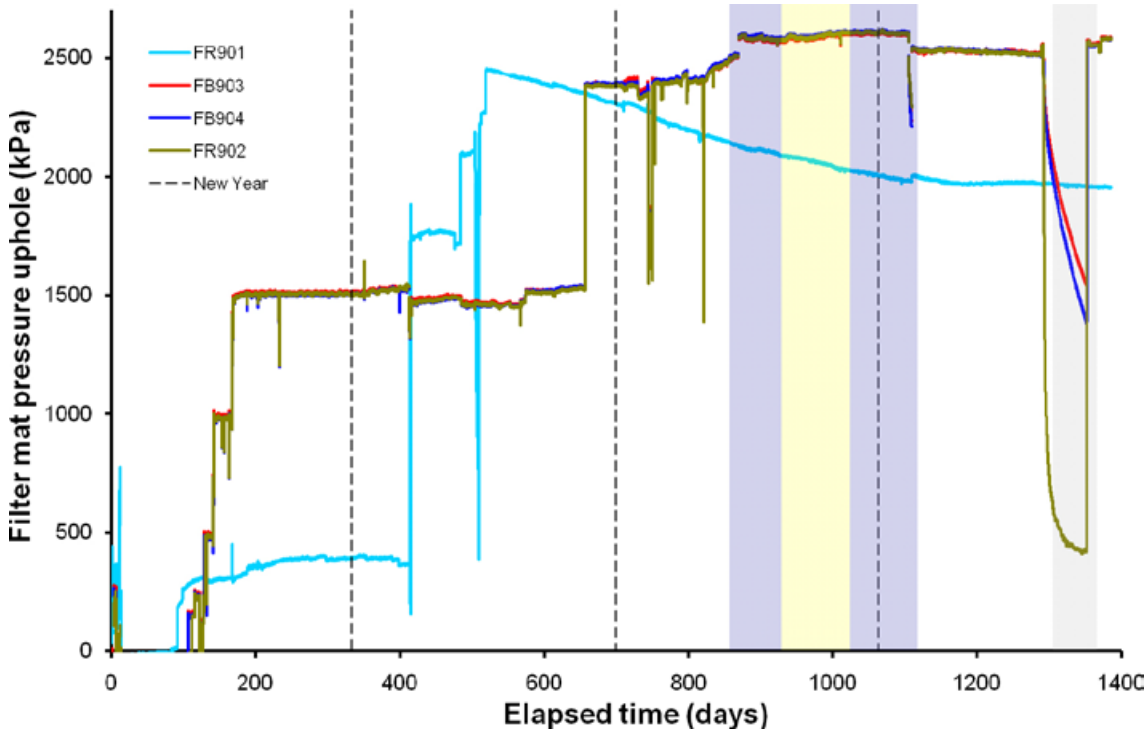

Figure 7-3. *Evolution of water pressure in the filter mats located on the borehole wall and within the bentonite blocks. Filter mat FR901 is in direct communication with the pressure relief holes and was therefore allowed to evolve independently from the other filter mats.*

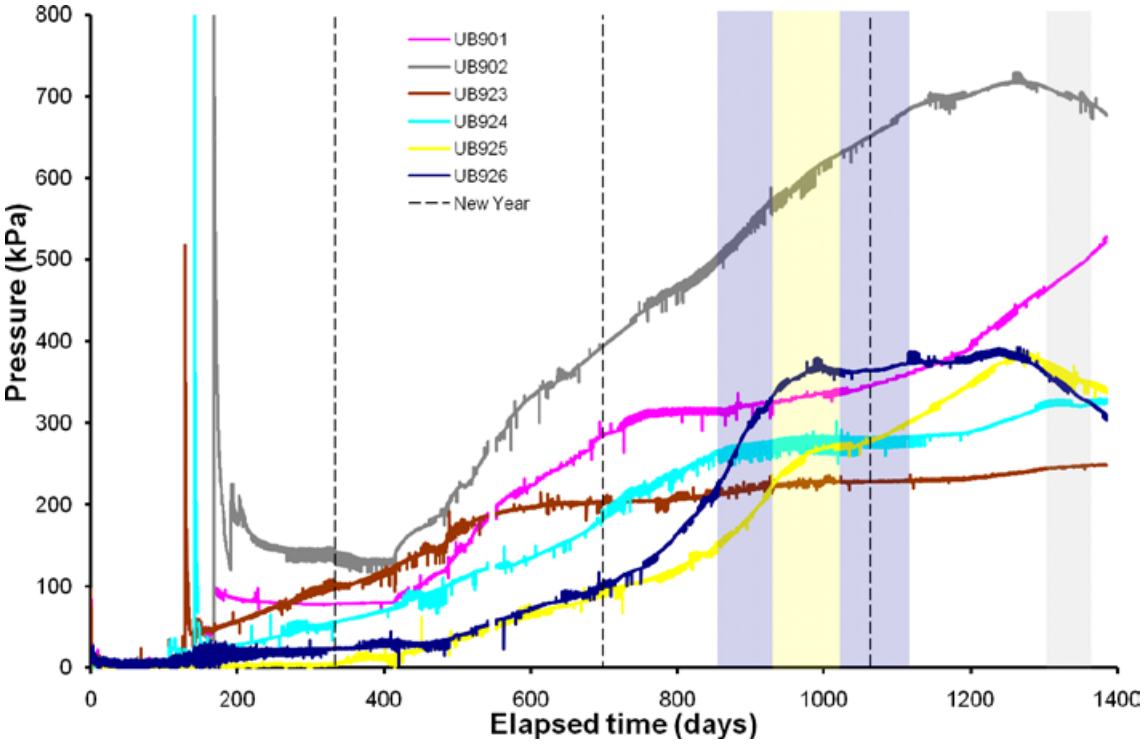

Figure 7-4. *Variation in porewater pressure within the bentonite at the 6 monitoring points. The large spikes in the data correspond with attempts to increase porewater pressure within the artificial hydration system early in the test history.*

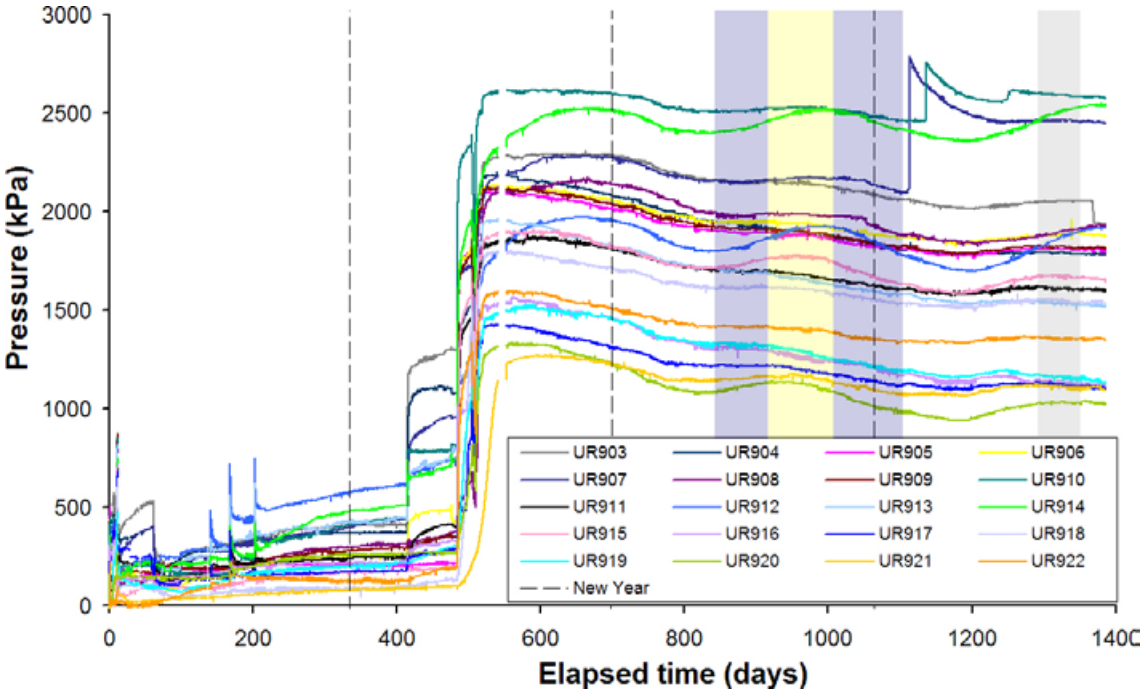

Figure 7-5. *Variation in porewater pressure measured at the rock face with time. The pore pressures clearly show a general decline. This is discussed later in Section 7.2.5.*

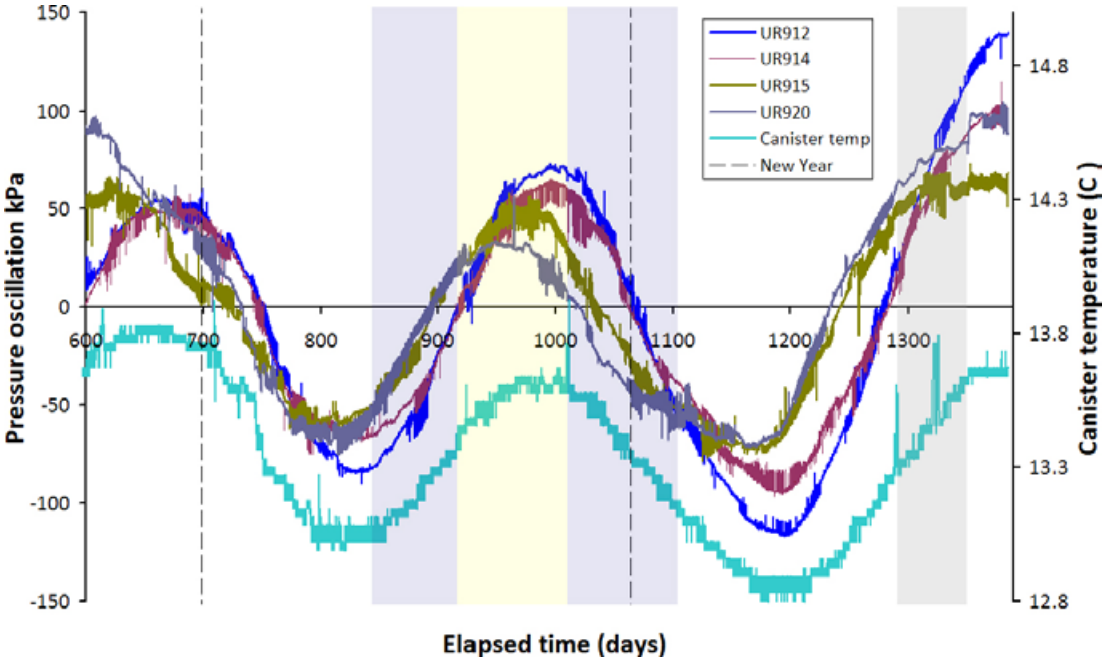

Figure 7-6. *Seasonal variation in porewater pressure measured at the rock face for four sensors with long term variation removed. It can be seen that UR912 and UR914 have no lag as these devices occur at the same level. When viewed in total the system displays lag that can be explained as a thermal pulse propagating down the deposition hole.*

7.2.4 Porewater pressure in the pressure relief holes

Pressure data from the individual packered sections of the two pressure relief boreholes are shown in Figure 7-7. Analysis of the data exhibits subtle seasonal variations in pressure; of most significance is the general decay in the local porewater pressure within the host rock from about day 425, which is discussed in Section 7.2.5. The data suggest that certain intervals may be approaching a plateau (e.g. PRH1-3) and that a stable hydraulic boundary condition will evolve in the near future.

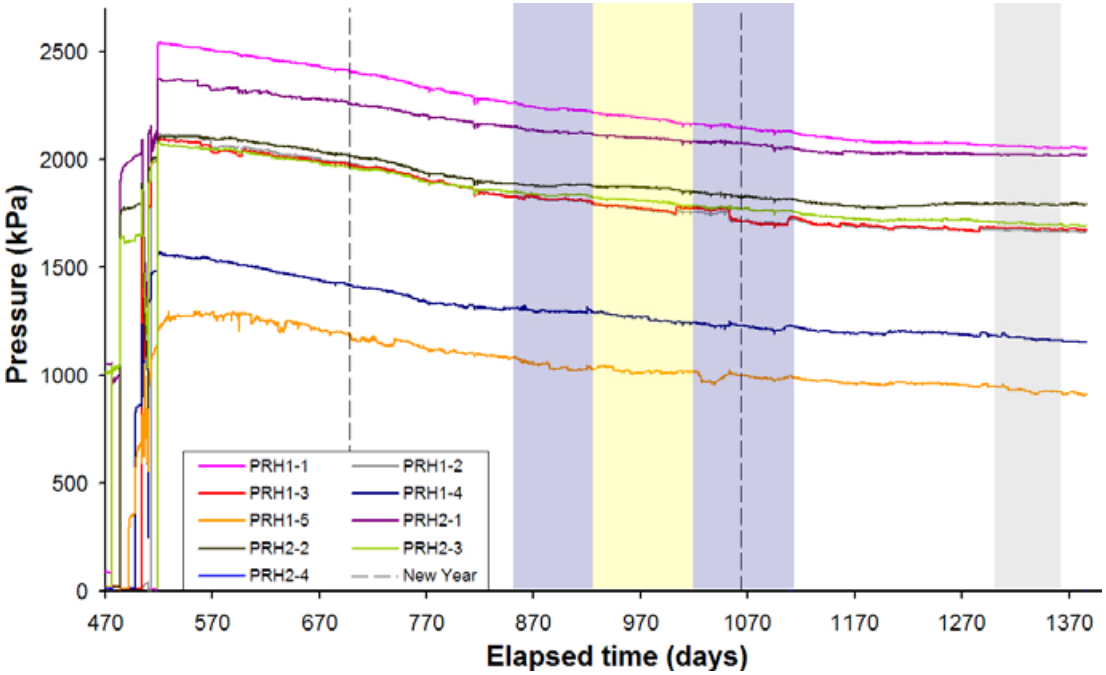

Figure 7-7. *Porewater pressures measured in the packered sections of the pressure relief boreholes.*

7.2.5 Comment on porewater pressure decay

Figure 7-5 and Figure 7-7 both show long term decay in porewater pressures at the deposition hole wall and in the pressure relief boreholes. This is of concern and could be symptomatic of a problem with the Lasgit experiment. However, close inspection of pore pressure data from other locations in the HRL also exhibit a long-term decay in porewater pressure that predates Lasgit, especially between the 420 m and 450 m depths. Figure 7-8 shows pore pressure data from borehole KA3105A located close to the Lasgit deposition hole. This clearly shows the slow time-dependent decay of pore pressure and a general declining trend within the HRL between the 420–450 m level. At present the cause for this temporal behaviour, which appears to predate Lasgit, is unclear, but it provides an example of the quality of the data (and its wider impact) being obtained from the Lasgit study, as it was this data that alerted staff at Äspö to this problem.

7.3 Evolution of total stress

Total stress of the Lasgit system is measured at 32 locations within the deposition hole. Sensors mounted on the canister, rock wall and within the clay can be used to determine both the axial and radial components of stress and the distribution of values throughout the deposition hole.

7.3.1 Radial stress measured at the rock wall (PR903 to PR922)

Data from total pressure sensors PR903 to PR922 are plotted in Figure 7-9. Significant stress growth has occurred throughout the entire history of the experiment, with the most obvious changes occurring as the experimental parameters are altered. After approximately day 600 the experimental parameters have remained mainly unchanged and seasonal variations can be seen within the continually increasing stress conditions. These oscillations are most obvious in PR914, PR915, PR919 and PR920, which are displayed in Figure 7-10 following the removal of the swelling stress component. The seasonal transients are less well defined than those previously described, but do have a period of one year. As seen, PR915 closely correlates with the HRL temperature, whereas PR914 has a lag of approximately 30 days.

The correlation of PR915 with HRL temperature is unexpected as it occurs at Section 9 of the deposition hole, approximately halfway up the holes length, a considerable distance from the influence of the gallery environmental conditions. It is possible that the influence in these parameters is actually a considerable lag of 50–100 days from the temperature observed at the canister. It can be noted that a negative correlation is seen between radial stress and canister temperature, i.e. radial stress has a negative oscillation when temperature is highest. This may relate to thermal contraction of the bentonite as the temperature increases.

7.3.2 Radial and axial stress on the canister (PC901 to PC903)

Axial and radial stress around the canister has increased steadily during the course of the hydration history (Figure 7-11), with one major perturbation at approximately day 500. Seasonal variations can be clearly seen in the data from about day 600 onwards. These may be present in the early history of the test, but, due to the rate of change in stress combined with changes in boundary condition during artificial hydration, mean that further analysis such as Fourier transformation would be required to illicit these responses. The removal of a simple linear trend shows oscillations with a period of approximately 1 year, as shown in Figure 7-12 . The stress oscillations appear to correlate with canister temperature. It should be noted that axial stress lags radial stresses as the sensor is located on the base of the canister and is further evidence of the propagation of a thermal pulse down the deposition hole.

7.3.3 Axial stress within the bentonite (PB901, PB902, and PB923 to PB929)

Figure 7-13 shows the history of axial stress within the bentonite. In general, the history is quite complex and is dominated by changes in experimental parameters. However, some of the stresses appear to show a seasonal variation (e.g. PB923, PB924). The development of axial stress has been more complex than for other parameters and as such it is not possible to remove a linear trend .

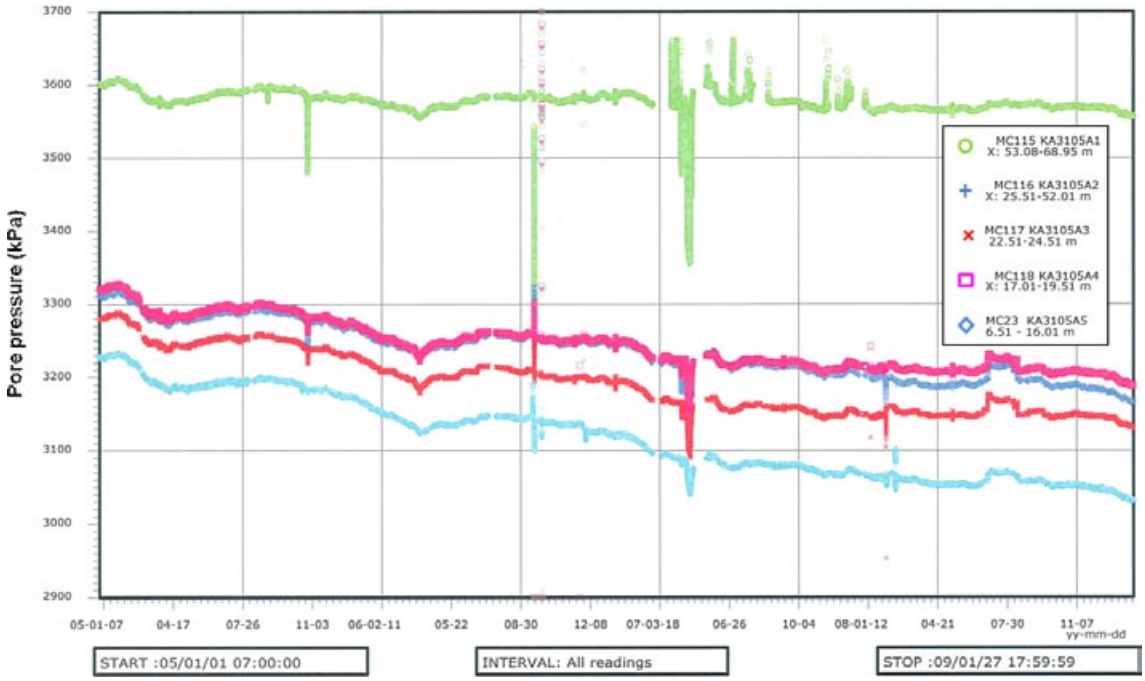

Figure 7-8. *Porewater pressures measured in nearby borehole KA3105A.*

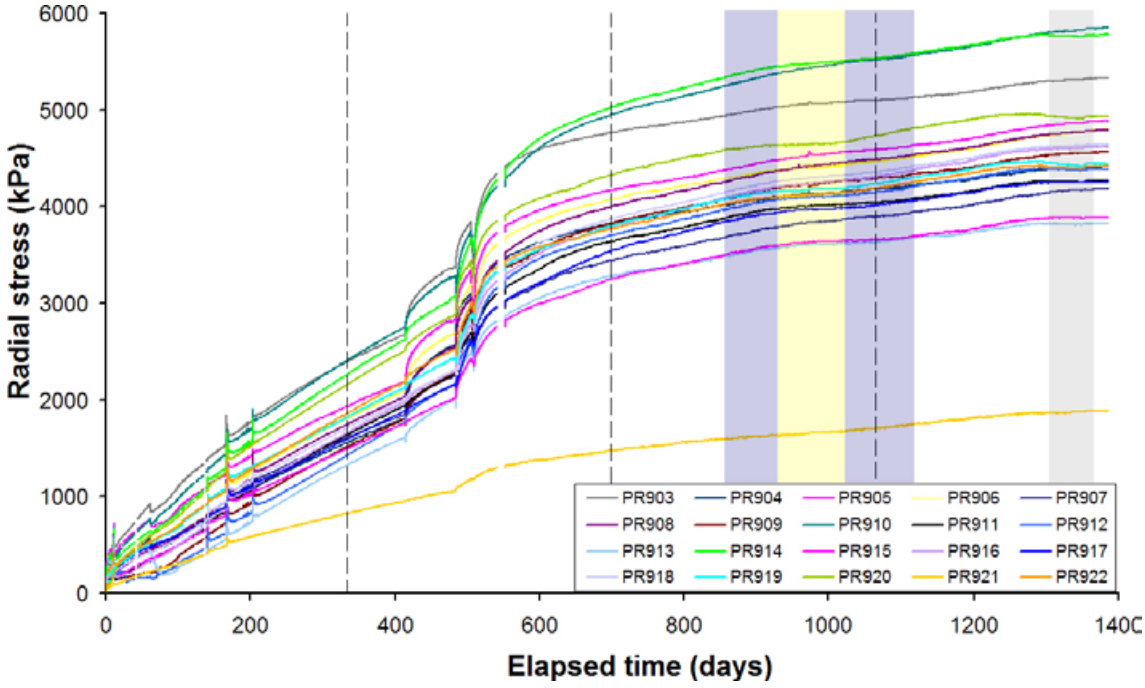

Figure 7-9. *Variation in radial stress with time for sensors PR903 to PR922 showing a general increase in stress with time.*

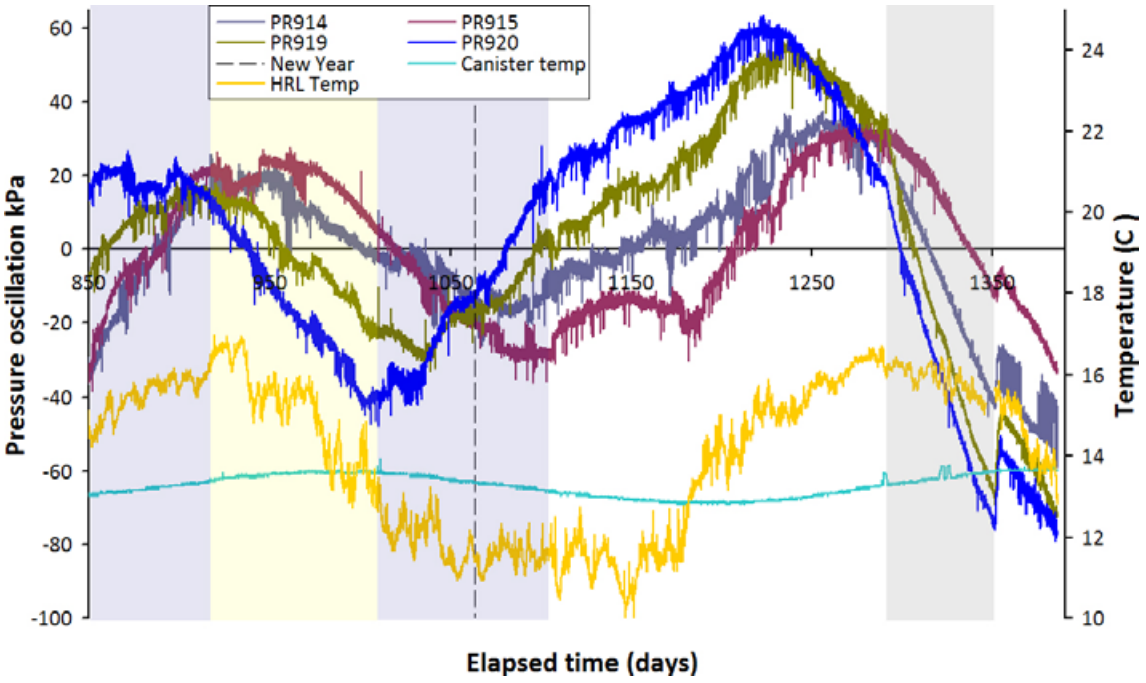

Figure 7-10. *Variation in radial stress with time after the removal of increasing stress component.*

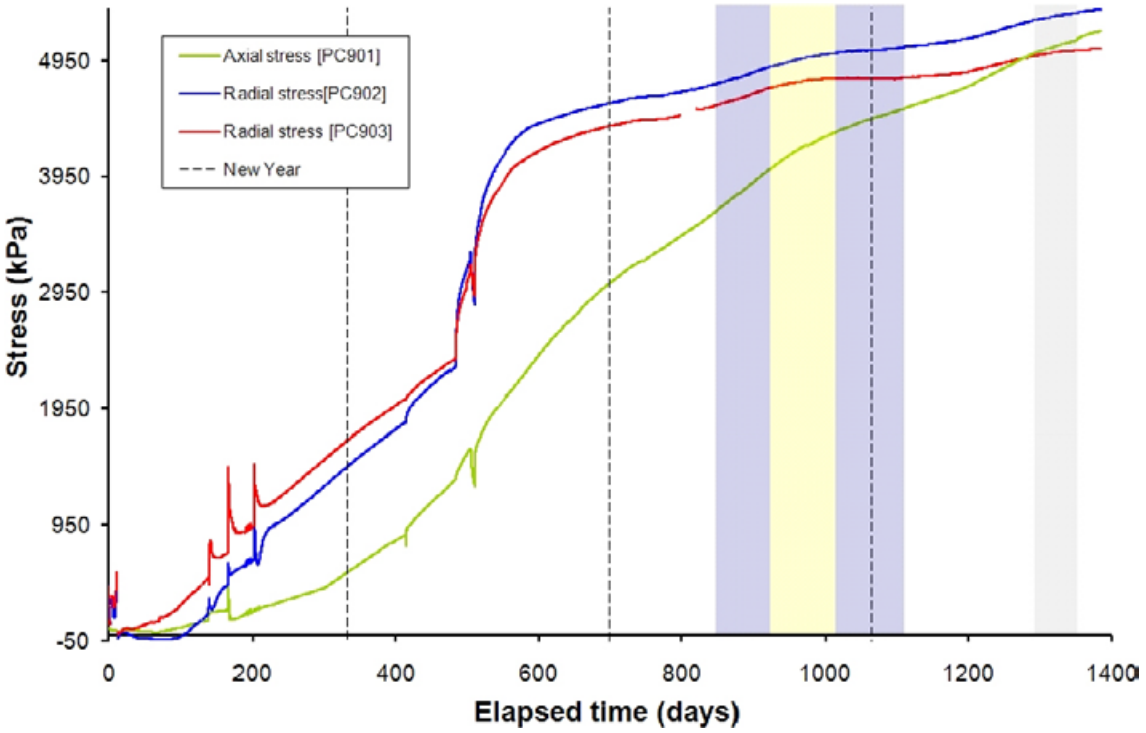

Figure 7-11. *Development of axial and radial stress on the side and base of the canister.*

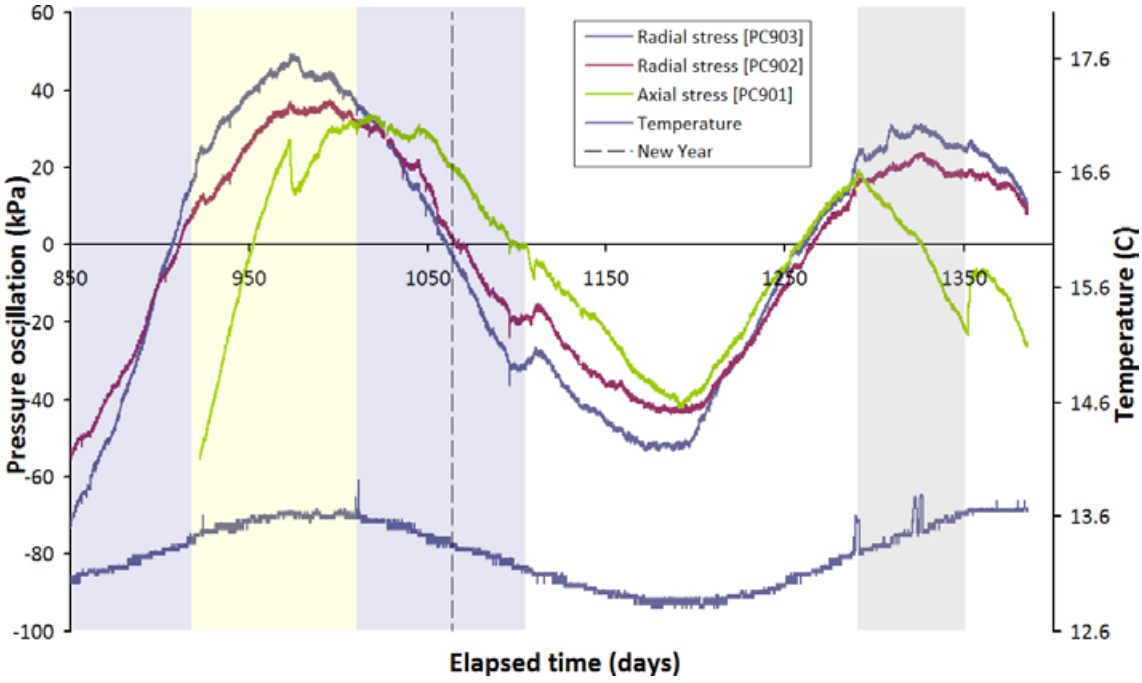

Figure 7-12. *Pressure oscillation observed in axial and radial pressure on the side and base of canister.*

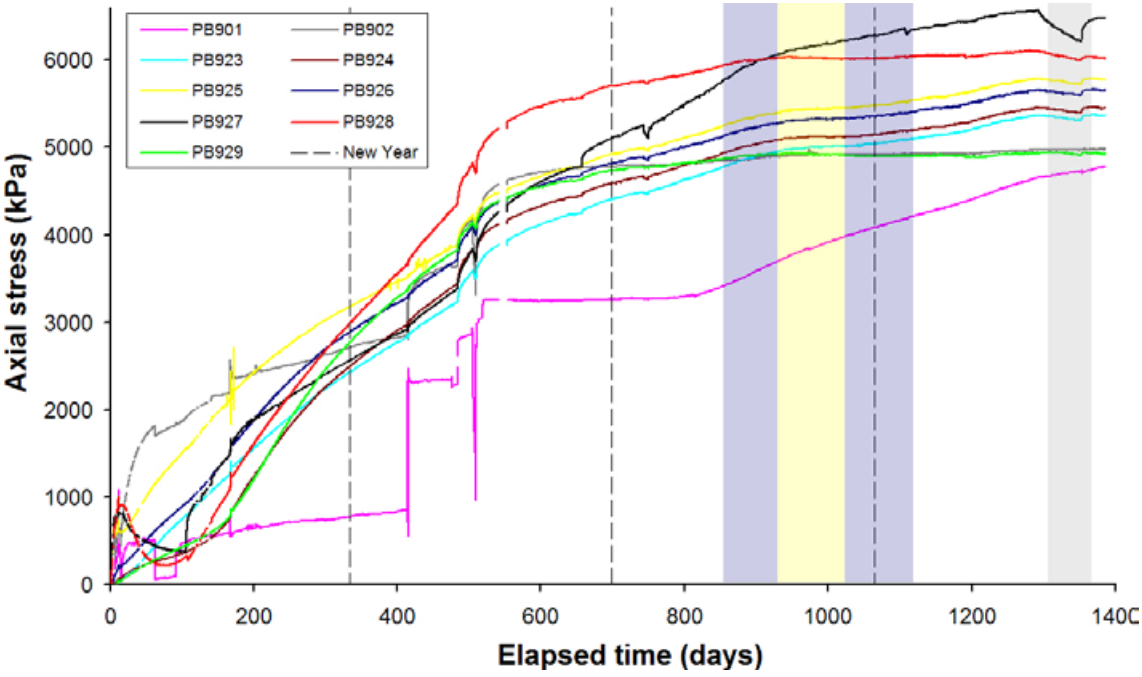

Figure 7-13. *Development of axial stress measured at 12 locations within the buffer.*

7.3.4 Net horizontal stress

As reported in /Harrington et al. 2007/, it is apparent from the intensity plots that high radial stresses are concentrated along the part of the deposition hole wall at about 300º and that stress varies mainly with angular position rather than with depth. This can also been seen in the stress plot shown in Figure 6-22 for the second stage of hydration. To examine this in more detail the data were divided into 16 angular strips and the stress values averaged over depth. This gives a set of pressures that can be represented as vectors in the horizontal plane as shown in Figure 7-14. Since these pressures act upon equal area segments of the hole wall they can be added vectorially to give a net horizontal force acting on the hole. The data from PR903 to PR922 have been used to generate this net force vector throughout the entire history of the experiment. Its magnitude as a function of time is plotted in Figure 7-15 and its locus in the horizontal plane is shown in Figure 7-16.

It can be seen in Figure 7-15 that the magnitude of the net force reached a well-defined plateau by about the time that packers were installed into the pressure relief holes. During installation of the packers there are significant changes in net stress, which afterwards, increases more rapidly. This has now levelled off once again, but there is no sign yet of it reducing, as would be expected of the system as it approaches an equilibrium state. This end point in the evolution of the system may, in reality, be impractical to attain (certainly within the life-span of the project), given the variability in composition of the bentonite blocks, their position in relation to the side-wall of the hole, the dependence of the system on the availability of water, and importantly their inherent shear strength.

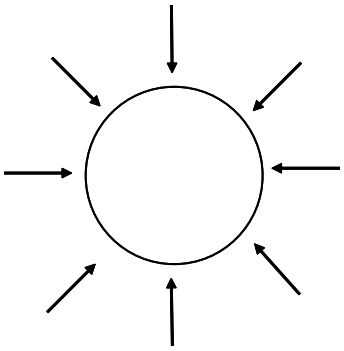

Figure 7-14. *Depth averaged radial stresses represented as vectors in the horizontal plane.*

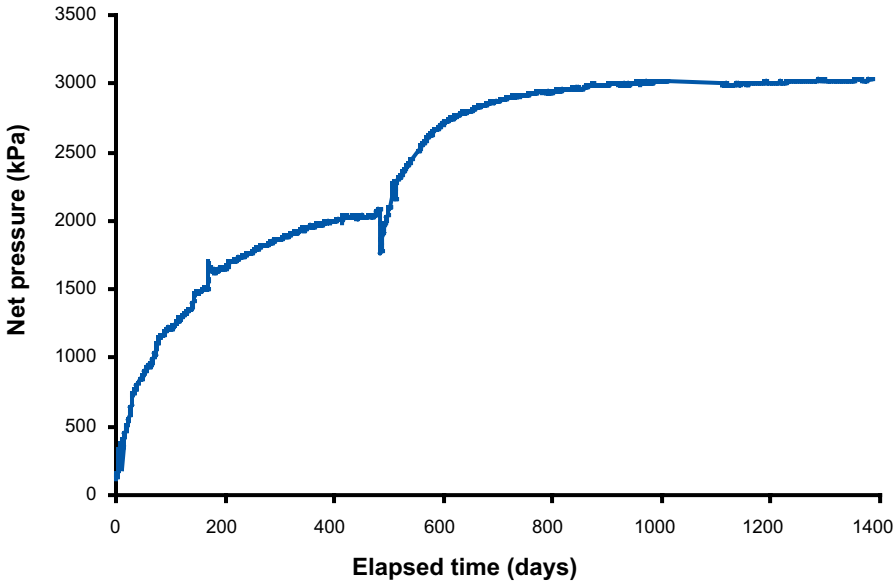

Figure 7-15. *Variation of magnitude of net pressure with time.*

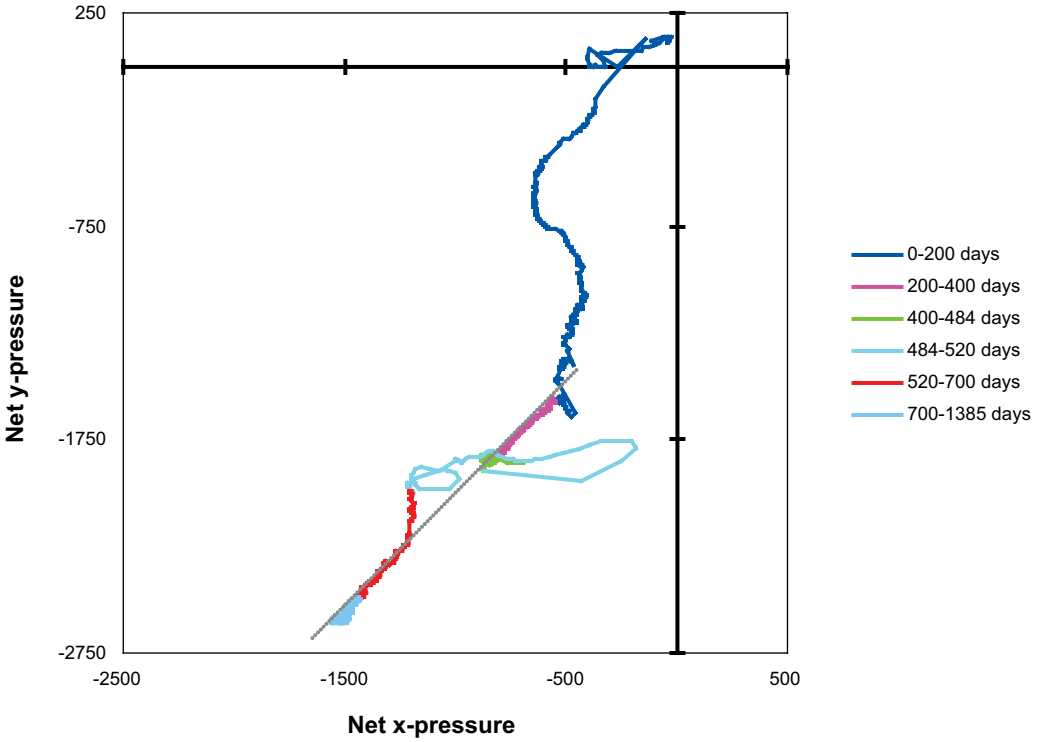

Figure 7-16. *Variation of net pressure direction with time.*

The locus plot in Figure 7-16 shows a fairly erratic path during the first 200 days of hydration which then settles to an almost linear path between day 200 and day 400. The packer installation is shown as a further period of erratic change in the net pressure locus, but thereafter, the path (shown by the red line) returns to the previous gradient observed from day 200 to day 400. It is interesting to note that the rate of movement has greatly slowed during the last 800 days but there is clearly no indication of a return to the origin as one would expect for a true equilibrium condition.

7.4 Evolution of suction in the bentonite buffer

Figure 7-17 shows the suction pressures recorded at the seven psychrometers WB901 to WB907 embedded at locations within the bentonite buffer (Section 3.2.7 and Appendix). While suction at each location continues to decrease (confirming ongoing hydration of the clay), the rate of hydration appears to be slowing. Greatest progress in hydrating the clay has been made near to the filter mats above the canister, whilst the least progress has occurred just below the canister. There is no data available yet for WB903 which was found to be defective following closure of the hole. While a number of psychrometers appear to be levelling (e.g. WB906), close inspection of the data reveals a steady downward trend, indicating that most, if not all of the clay, remains in some degree of suction.

It is anticipated that when the bentonite is fully saturated, psychrometer values will plateau at a finite (positive) suction, reflecting the natural salinity of the Äspö groundwater. However, the system is unlikely to be in hydraulic equilibrium at this time as the development of porewater pressure lags well behind the saturation of the clay. Ideally, in relation to future testing, the clay should be in a state of hydraulic equilibrium, otherwise, the suction introduces an unknown variable in the interpretation of the results.

No seasonal variation is noted in the data, as expected.

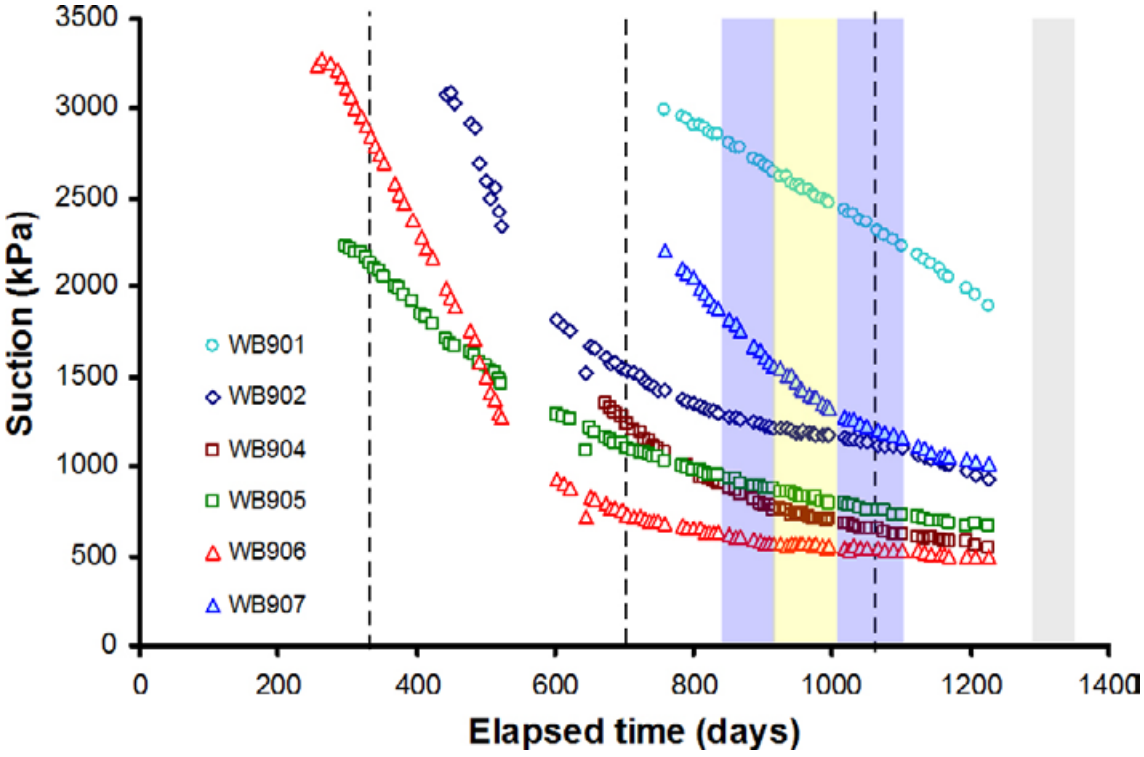

Figure 7-17. *Suction pressures recorded at sensors WB901 to WB907 for the entire test.*

7.5 Volumetric flow rate into artificial hydration system

Artificial hydration of the clay began on the 18th May 2005 at an elapsed time of 106 days. The pressure in each hydration filter was initially controlled using pumpset RP2. During the course of the hydration procedure, porewater pressure was increased in a series of steps. The uncorrected volumetric flow rate into the hydration system is shown in Figure 7-18. Inspection of the data clearly shows that flow rate into the system spontaneously increases as the pressure is raised. This is then followed by a well defined negative transient leading to a slow and extremely protracted reduction in volumetric flow (the general trend of decline is shown as a red dashed line). If a linear decay is assumed between day 800 and day 1,250, extrapolation suggests that a no-flow condition will be achieved about day 1,800. However, the assumption of a linear trend is highly questionable for the projection of future flow behaviour. Analysis of the data shows that the rate of flux into the system is not particularly sensitive to the modest pressures applied to the filters, confirming the predictive modelling work presented in /Harrington et al. 2007/.

7.6 Axial force and displacement of the steel lid

Figure 7-19 shows a plot of the axial force (measured by the Glotzl cells) measured at the lid. Considerable seasonal variation can be observed. Over periods of 1 year, maximum force can be seen to occur at approximately day 200, day 580, day 900 and day 1,300. This is clear cyclicity with a period of 1 year. These are times when the temperature is at its maximum within the HRL (see Figure 7-22).

Data from sensors DP901 to DP905 are plotted in Figure 7-20. After the early history of the experiment (day 1 to 600), all lid displacement sensors show a positive gradient, while in contrast the canister exhibits a negative displacement gradient. This is consistent with preferential swelling of the clay above the canister in close proximity to the filter mats /Harrington et al. 2007/, resulting in the upward displacement of the lid and downward movement of the canister.

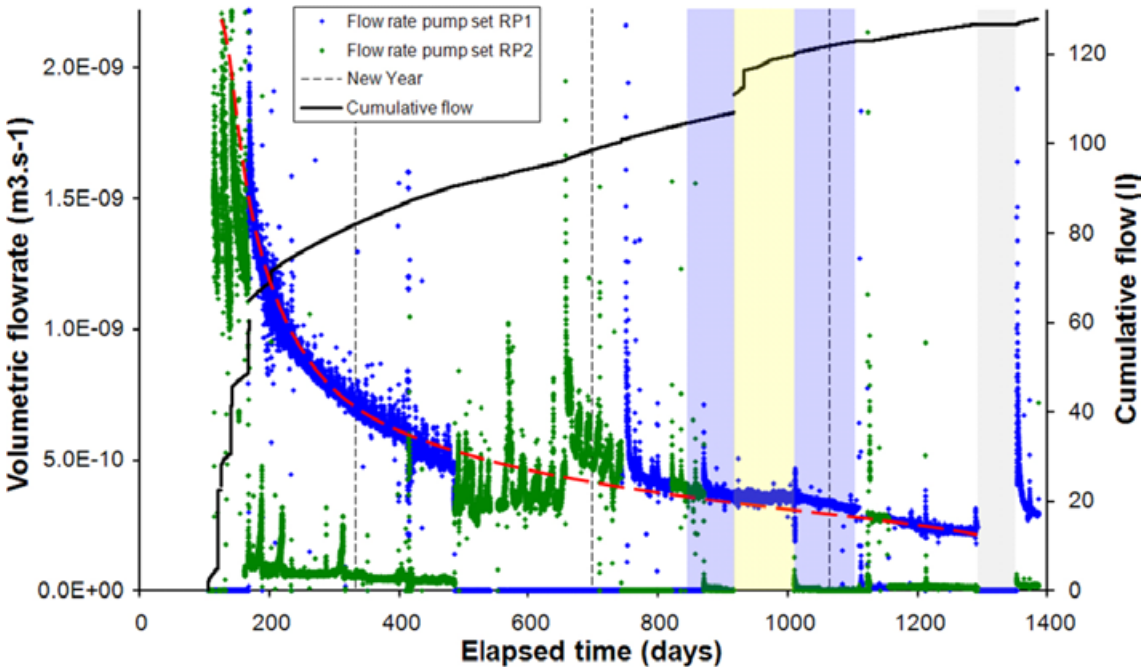

Figure 7-18. *Volumetric flow rate into the artificial hydration systems. The data show a general decrease in volumetric flow rate into the buffer with time, as shown by the red dashed line.*

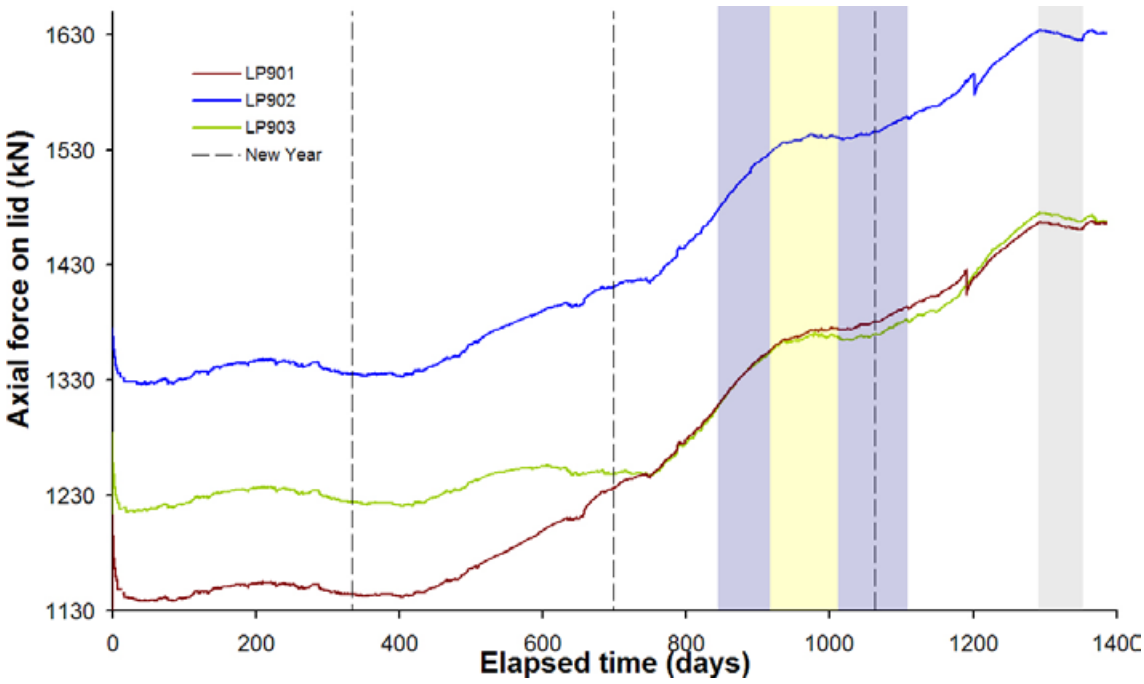

Figure 7-19. *Axial force acting on steel lid measured by 3 load cells attached to separate rock anchors.*

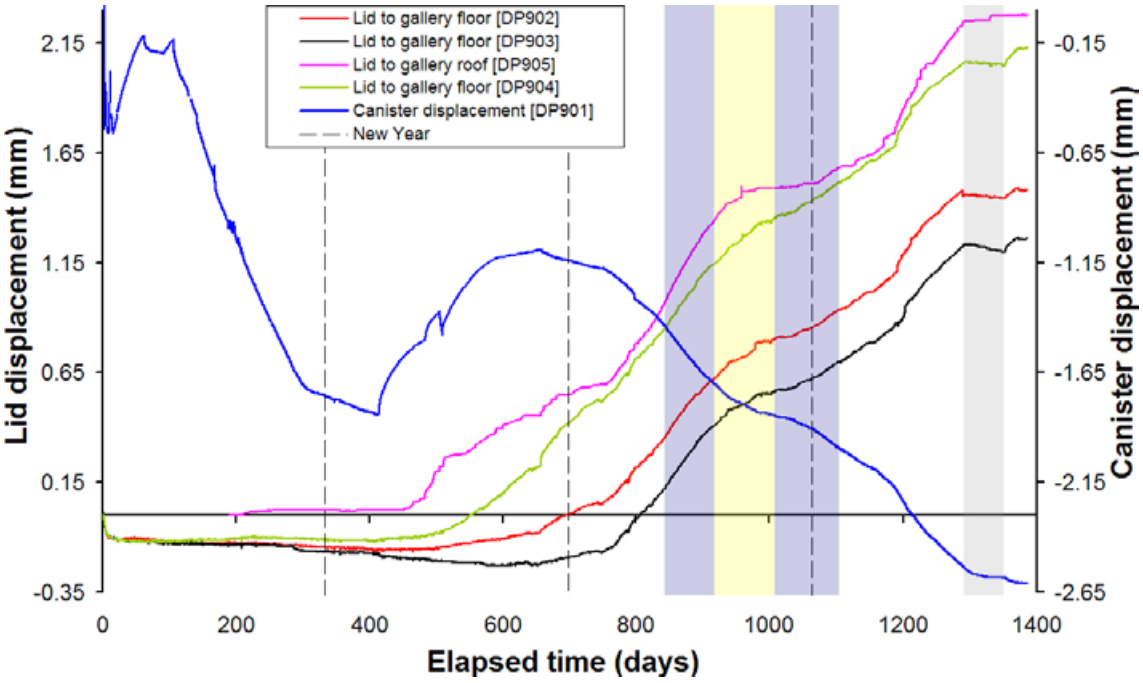

Figure 7-20. *Linear displacement of the steel lid and copper canister. Movements of the lid are measured relative to both the gallery floor and ceiling. Movements of the canister are measured relative to the steel lid.*

The position of the canister (Figure 7-21) can be determined by correcting for the relative positions of the gallery floor (DP902–DP904), gallery roof (DP905) and monel pipe position (DP901). During the first 400 days of the experiment the canister can be seen to have dropped in relative position. Over the next 400 days it then recovered to a position approximately 0.7 mm below where it began at day 1. Over the period day 800 to day 1,385 the relative position has slighting increased, but is fairly static. Seasonal variation is seen in the position relative to DP901 but not relative to DP904; which may relate to the thermal compliance of system components.

Figure 7-20 clearly shows that from approximately day 440 displacement of the lid has propagated upwards in a linear manner. The removal of this linear trend is shown in Figure 7-22 which reveals a similar underlying cyclicity as observed in previous sections. It can also be seen that as HRL temperature increases there is an acceleration of lid displacement rate. However, it is interesting to note that this correlation is not perfect and at times there is an offset between displacement and temperature at times.

Seasonal cyclicity is also seen in the stick-slip behaviour. Figure 7-23 shows the change in lid position for DP905, filtered to only show movements above 0.002 mm, which occur during stick-slip behaviour. The main conclusion from this data is that stick-slip occurs predominantly during the period of minimum canister temperature and increasing HRL temperature. The cause of the stick slip is uncertain, but could be linked to the thermal characteristics of the various system components and their interaction.

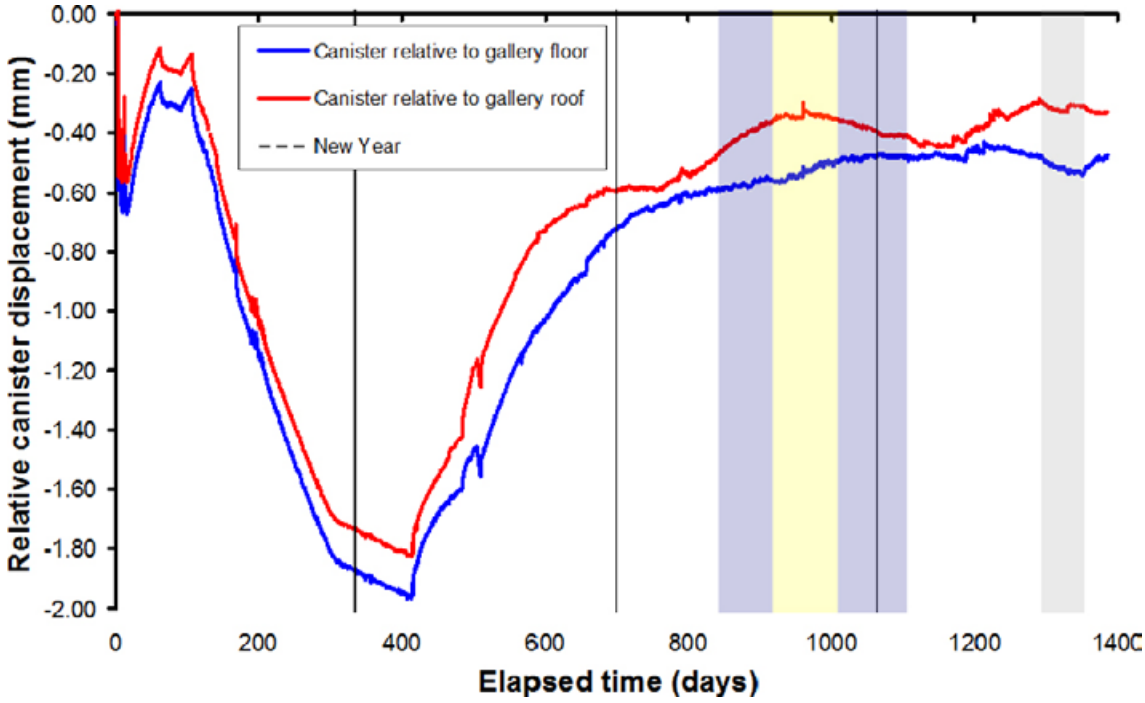

Figure 7-21. *Relative position of the canister with respect to the gallery floor and roof. After day 800 the position of the canister has been relatively static, despite the large variations seen in position (Figure 7-20).*

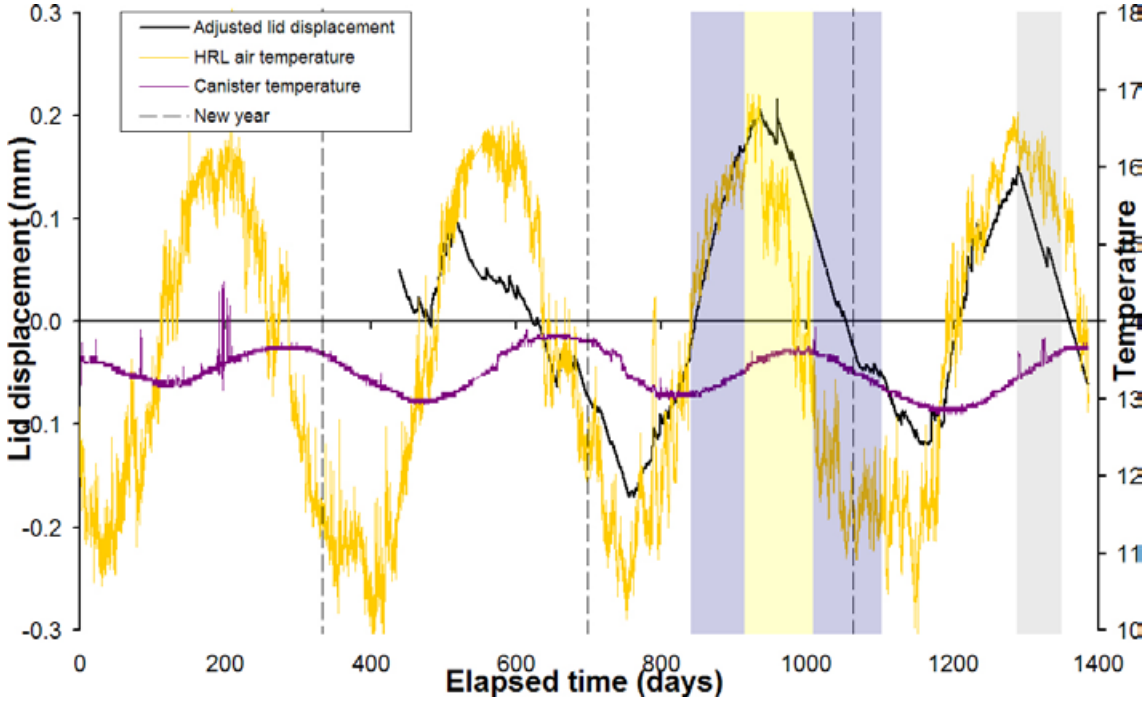

Figure 7-22. *Adjusted lid to gallery roof displacement data from DP905 plotted against temperature. The removal of the linear trend seen in DP905 in Figure 7-20 from day 400 onwards demonstrates that the seasonal variation is primarily related to HRL temperature.*

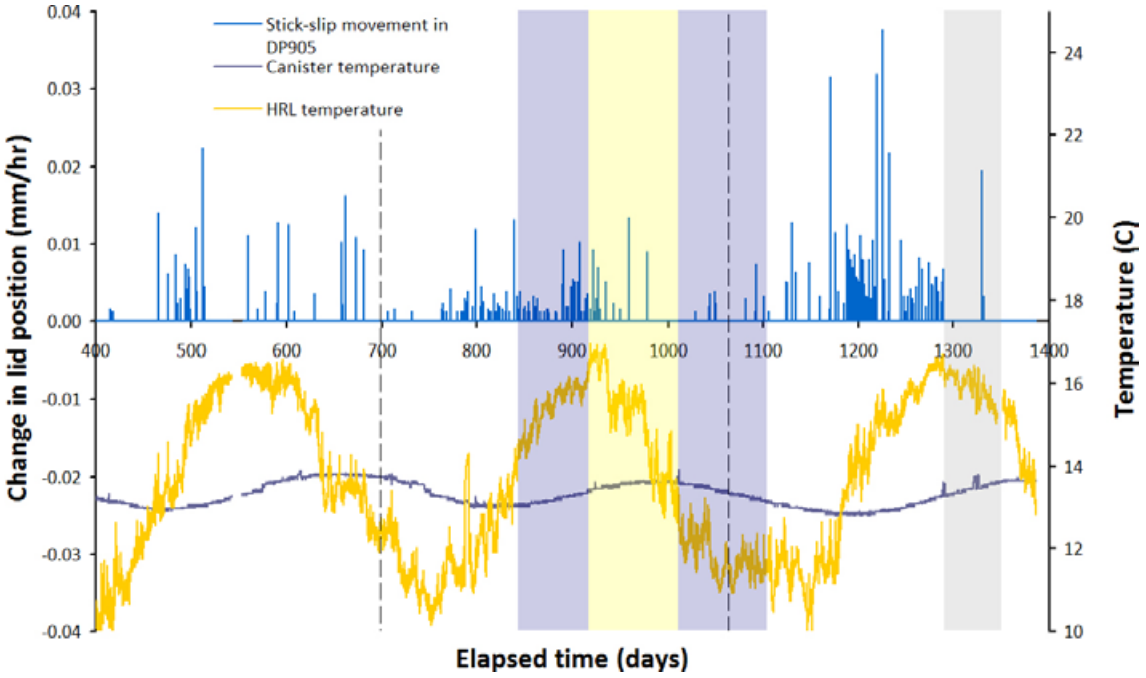

Figure 7-23. *Stick-slip movement of DP905 plotted against temperature. Individual stick-slip events can be seen to occur most frequently when HRL temperature is increasing.*

7.7 Comment on seasonal stress variation

Clear seasonal variation has been observed in many of the instruments recorded within Lasgit. The largest variation is seen in the HRL temperature. This measurement closely correlates with the variation seen in axial force on the lid, the position of the lid and the stick-slip behaviour. This suggests that all the variation seen in the lid (once the underlying trends have been removed) is associated with influence from the HRL and is not associated with movement from below the concrete plug.

Seasonal variation has also been observed in pore pressure within the bentonite (UB), pore pressure at the wall rock (UR), radial stress (PR) and the radial & axial stresses (PC). All of these appear to correlate with the canister temperature, which itself lags the HRL temperature by 90 days. With most of these types of instruments there is also some variation in the oscillation, many showing variation in lag with depth down the deposition hole. This suggests that the variation may be associated with either the thermal expansion of the copper canister or the thermal expansivity/contractancy of the bentonite, both of which may affect the observed hydromechanical behaviour of the system. As more data become available with increasing time, it will be easier to determine the interplay each parameter has on one another.

8 Summary

This report covers four distinct stages of the Lasgit experiment: 1) characterisation of the Lasgit deposition hole and construction of the experimental setup; 2) artificial hydration from day 106 to day 843[8]; 3) hydraulic and gas testing from day 843 to day 1,110; and 4) continued artificial hydration up to day 1,385.

Hydration Stage 1 (day 106–day 849)

The deposition hole was closed on the 1st February 2005 signifying the start of the hydration phase. Groundwater inflow through a number of highly-conductive discrete fractures quickly resulted in elevated porewater pressures throughout large sections of the borehole. This lead to the formation of conductive channels (piping), the extrusion of bentonite from the deposition hole and the discharge of groundwater to the gallery floor. This problem was addressed by drilling two pressure relief holes in the surrounding rock mass to lower the porewater pressure in the vicinity of the deposition hole.

Artificial hydration began on the 18th May 2005 after 106 days of testing. In general, from this time onwards, the pressures in all of the canister filters and hydration mats (excluding the FCT and FR901) were used to hydrate the clay. Initial attempts to raise porewater pressure in the artificial hydration arrays occasionally resulted in the formation of preferential pathways, even at relatively modest excess water pressures, resulting in localized increases in porewater pressure and total stress. These pressure dependent features were not focused in one location within the bentonite but occurred at multiple sites at different times in the test history. These pathways were relatively short lived, closing when water pressure was reduced. Packers were installed into the pressure relief holes on 23rd March 2006 and sections in them closed over the period to 5th July 2006. These operations caused clear effects throughout the deposition hole in both the measured porewater pressures and, to a lesser extent, the total stresses. However, there was no repeat of the formation of piping through discrete channels so, on 20th November 2006, pressures to the artificial hydration filters on the canister were increased to 2,350 kPa.

Hydraulic and gas injection tests Stage 1 (day 843–day 1,110)

A preliminary set of baseline hydraulic measurements were started on the 25th May 2007 (day 843) with the isolation of the lower canister filters FL901 to FL904 while artificial hydration continued through all other canister filters and filter mats. After a period of 27 days a constant head test was initiated on filter FL903, raising its pressure to 4.3 MPa for 28 days and then reducing it to 560 kPa for a further 19 days. Preliminary modelling of the initial hydraulic test has been carried out using a 2D axisymmetric variably saturated finite element porewater flow model. The initial saturation conditions for the hydraulic test cannot be determined *a-priori*, so it was necessary to try to model the whole hydration stage in order to set these initial conditions. Using this approach, fits were obtained to the initial pressure decay data for the four filters that were isolated using values for hydraulic conductivity ranging from 9×10^{-14} to 1.6×10^{-13} m.s^{-1} and specific storage values ranging from 5.5×10^{-5} to 4.4×10^{-4} m^{-1}. The constant pressure test on filter FL903 was modelled with a hydraulic conductivity of 7.5×10^{-14} m.s^{-1} and a specific storage of 2.5×10^{-5} m^{-1}. The design specifications of the KBS-3V concept states that hydraulic conductivity should not exceed 10^{-12} m.s^{-1} (SKB TR-09-22) and /Harrington and Horseman 2003/ report the hydraulic conductivity of MX-80 as between 3.9×10^{-15} and 9.28×10^{-14} m.s^{-1}.

Gas injection to FL903 was then begun on day 917 with an initial volume of gas being compressed at a steady rate for 13 days, a period of 22 days with gas pressure held constant and then a further period of 22 days during which pressures were raised again. Compression of the gas was then halted and the pressure monitored as it decayed for a further 4 weeks. Analysis of the data suggest that gas starts to flow into the buffer at a pressure of about 775 kPa, which is much lower than the expected gas entry pressure for intact bentonite. It therefore seems likely that gas is flowing between the bentonite and the canister and possibly between bentonite blocks. When initial gas pressurisation stopped and the pressure was held constant at around 1.85 MPa, flow into the clay suddenly reduced, indicating that propagation of the gas pathway(s) practically ceases when the pressure stopped increasing.

[8] Initial artificial hydration is only summarised in this report. For a more complete description of this stage of experimentation please refer to /Harrington et al. 2007/.

Upon restarting gas injection, the observed pressure begins to deviate from the predicted value, indicating pathway propagation continues at the onset of testing. Gas flux into the clay gradually increases as the pressure in the system rises. At a gas pressure marginally greater than the local total stress measured on the rock wall (but a little smaller than the radial and axial stresses measured on and near the canister surface respectively which are between 1,049 and 2,149 mm from the gas injection point), flux into the clay rapidly increases. Gas pressure continues to rise reaching a peak pressure of 5.66 MPa, which is marginally greater than the axial stress measured at PB902. This is followed by a small spontaneous negative transient leading to a quasi steady state. The post peak gas flux exhibits dynamic behaviour (over and undershooting flux into the system) suggestive of unstable gas pathways, which are linked to a strong couple between pore pressure and gas flow as indicated by changes in porewater pressure during and after gas breakthrough. This general behaviour is reminiscent of the responses observed in laboratory scale tests reported by /Horseman et al. 1999, Harrington and Horseman 2003/.

Following the cessation of pumping, the injection flux through the bentonite declines rapidly at first but then enters an extended period of very small flows. This is reflected in the pressure response which drops rapidly initially but then decays very slowly towards an asymptotic capillary threshold pressure, which is estimated to be about 4,900 kPa, equating to the average radial stress (PC902 and PC903) measured on the canister surface.

Following peak gas pressure a well pronounced increase in radial stress occurs around the entire base of the deposition hole, with the highest increase noted in the vertical plane below the point of injection. This indicates the gas preferentially moved downwards, probably along the interface between the canister and buffer. It is notable that the radial stress immediately adjacent to FL903 actually decreases during this time.

Porewater pressure data from the deposition hole wall exhibit similar behaviour to that of radial stress, though initial results suggest that the pulse in porewater pressure dissipates at a faster rate than that of the radial stress.

Analysis of the porewater pressure sensors located within the buffer show no obvious sensitivity to the injection of gas. In contrast, axial stress sensors located beneath and above the canister appear to register the passage of gas. Indeed, the slow and then rapid increase in PB902 immediately following the peak gas pressure is strongly indicative of the time dependent propagation of gas pathways.

A small inflection in the rate of increase in axial stress at the base of the canister occurs shortly after the peak in gas pressure. Such a reduction in stress can only be caused by the removal of load, suggesting some form of displacement has occurred as a result of gas injection.

While it is difficult to make definitive statements regarding the exact direction and number of gas flow paths, it seems highly probably that the gas moved generally downwards away from the injection filter and then along the interface between blocks C1 and R1 and/or R1 and R2. This is logical as there is a clear axial stress gradient running from high to low from the top of the deposition hole to the lowest stress sensor. Under most conditions gas flow would propagate along such a stress vector.

The observed general coupling between gas, stress and porewater pressure at the repository scale is extremely important and can be readily explained through concepts of pathway dilatancy. These observations are qualitatively similar to those reported by /Horseman et al. 2004/.

Hydration Stage 2 (day 1,110–day 1,385)

The second stage of artificial hydration began on day 1,110. This was interrupted by the failure of the Spiralair KS1/T compressor on day 1,289, which caused all air actuated valves to close and effectively shut-off the down-hole filter mats from the laboratory, preventing continued artificial hydration of the clay. Whilst this situation was not ideal, it allowed the pressure decay in all filters to be observed, giving an unexpected observation of the state of hydration of the bentonite buffer.

During this time, considerable decreases in pressure were observed with one of the smallest filters, the 5 mm radius FL902, recording a drop in pressure of over 85% from 2,235 kPa to 380 kPa. The pressure at the two circular filter mats reduced from approximately 2,500 kPa to 1,500 kPa. Filter mat FR902 dropped very rapidly from 2,500 kPa to an eventual asymptote of almost 400 kPa; this is a drop of almost 84% and is equal to the pore pressure at the corresponding depth in the pressure relief holes. Filter mat FR901 shows no influence of the compressor failure as it is isolated from artificial

hydration. It should be noted that pressure drops will be affected by local variations in saturation of the clay, which may help to explain anomalously large drops in pressure for certain filters.

Data from the canister filters during the compressor failure event were also interpreted using the same 2D finite element model. Good model fits were achieved for most of the filters, which suggests that the transient behaviour can be captured in terms of a single hydraulic transport coefficient and a single hydraulic storage coefficient. The upper filters generally indicate higher values for permeability and specific storage than elsewhere in the system, ranging from 9×10^{-21} m^2 to 50×10^{-21} m^2. The parameter values obtained for filters FL901 and FL904 (8×10^{-21} m^2 and 13.5×10^{-21} m^2 respectively) are quite similar to those from the hydraulic test earlier, indicating that little change has occurred since this time.

Monitored porewater pressures within the bentonite have significantly increased during the test, but remain relatively low ranging from 250 kPa to 685 kPa. This is in contrast to the water pressure measured at the face of the deposition hole which ranges from 1,025 kPa to 2,555 kPa. However, three sensors in the clay show a slow decrease in pressure initiated at approximately day 1,240, a time before the compressor failed.

Suction has decreased throughout the experiment confirming the ongoing hydration of the clay, though the rate of hydration appears to be slowing. Greatest progress has been made near to the large filter mats above the canister, whilst the least progress has occurred just below the canister. While a number of psychrometers appear to be levelling (e.g. WB906), close inspection of the data reveals a continuous downward trend, indicating that most of the clay remains in a state of suction.

Pore pressure at the rock wall greatly increased in response to the commissioning of the packers. Since this time, pore pressure has slowly decayed, ranging between 1,025 kPa and 2,555 kPa. During 2008 four pressure "break-throughs" were observed in three of the sensors. The events in UR907 and UR910 resulted in similar total pressures, both of which were significantly higher than the pressure imposed by the artificial hydration system. The third event, which also occurred in UR910, caused a less pronounced change, resulting in a small progressive increase in pressure over a ten day period. This was followed by pressure decay similar in manner to UR907. The final event occurred in UR903 on day 1,368 when a pressure drop of approximately 100 kPa occurred. Close examination of all available data shows that these four events are real and not symptomatic of sensor failure.

The presence of mapped or extrapolated fractures close to the three pore pressure sensors that displayed break-through (UR903, UR907, and UR910) suggest these fractures play a significant role in the observed behaviour. Mechanistically, it is hard to conceive of an event within the deposition hole that could result in the generation of porewater pressures that are significantly in excess of those imposed through the artificial hydration system. It seems more probable that events outside of the Lasgit deposition hole are in some way responsible for the behaviour seen. While a direct correlation to external events such as blasting cannot be made, it is reassuring to note that the measurement system within the deposition hole is sufficiently accurate to register these events, which bodes well for future testing.

The total pressure sensors mounted on the rock wall show a slow increase in total stress during the experiment to range between 1,890 kPa and 5,850 kPa. The spatial and temporal evolution in radial stress measured at the rock wall shows no significant variation in radial stress during 2008. The spatial distribution of effective stress remains fairly constant with only small variations noted, primarily caused by the spontaneous increases in porewater pressure. Effective stress generally changes around the circumference of the depositional hole and does not exhibit any significant correlation to depth.

Axial stress monitored within the clay has also increased steadily to range from 4,770 kPa to 6,480 kPa. The data clearly shows a non-uniform distribution of axial stress across the major axis of the emplacement hole. The effect of the compressor failure is complex with two sensors having no change, whilst all other sensors exhibit either an absolute decrease in total stress or a reduction in the rate of stress increase. The most prominent stress drop occurred at the interface between the bentonite buffer and the concrete plug (PB927), with a near 350 kPa reduction from 6,565 kPa to 6,215 kPa. However, sensors PB928 and PB929 show very small pressure drops suggesting that stress at the top of the bentonite has become very heterogeneous, but this may be due to the foot-print of FB904. Axial stress was quick to recover after artificial hydration was re-started at day 1,351. By the end of 2008, most of the stress sensors had reached a plateau, albeit at a magnitude below that in the corresponding sensors at the time of the compressor failure.

It is apparent from the intensity plots that high radial stresses are concentrated along part of the deposition hole wall at about 300º and that stress varies mainly with angular position rather than with

depth. The magnitude of the net force reached a well-defined plateau by about the time that packers were installed into the pressure relief holes. During the installation of the packers there were significant changes in net stress which, there afterwards, increases more rapidly. This has now levelled off once again, but there is no sign, as yet, of it reducing, as would be expected in a homogenous system approaching an equilibrium state. The locus plot shows a fairly erratic path during the first 200 days of hydration which then settles to an almost linear path between day 200 and day 400. The packer installation caused a further period of erratic change in the net pressure locus, but thereafter, the path returns to the previous gradient observed from day 200 to day 400. It is interesting to note that the rate of movement has greatly slowed during the last 800 days but there is clearly no indication of a return to the origin as one would expect for a true equilibrium condition.

Stress measurements on the canister surface indicate that radial and axial stress varies between 5,055 kPa and 5,385 kPa, which is comparable with the average value of radial stress monitored on the rock face. The increase in radial stresses has mirrored one another, while axial stress has increased at a much greater rate, such that it now represents the intermediate principal stress acting on the canister.

The axial force acting on the steel lid is now greater than the initial pre-stressing value applied during the installation phase and ranges between 1,465 kPa and 1,630 kPa. The initial reduction in the axial force following closure of the deposition hole can be explained by a time dependent relaxation of forces due to compression of the bentonite blocks and the engineering void space when the hole was first sealed. The slight reduction in force during the period from day 200 to day 400 can be explained by convex deformation of the steel lid in response to the uneven distribution in axial stress. Since the installation and closure of packers into the pressure relief holes there has been a marked rise in the axial force acting on the lid. There is also strong evidence in later data for the stick slip movement of the conical concrete plug.

Displacement sensors mounted on the steel lid indicated a fairly uniform drop in lid height relative to the gallery floor during the early part of the test history, mirroring the relaxation in the initial pre-stressing applied to the lid. During the early stages of hydration the canister moved away from the lid due to preferential swelling of the clay near the large filter mats located above the canister. Following closure of the packers in both pressure relief holes, pore water pressures in the base of the deposition hole increased and the canister changed direction of movement and returned to a position similar (~0.5 mm) to that at the start of the test.

Complete test history (day 1–day 1,385)

Clear seasonal variation has been observed in many of the instruments recorded within Lasgit when data are viewed over the entire 1,385 day (3.7 year) history. The largest variation is seen in the HRL temperature, with variation between 10 and 16°C. The canister shows similar variation, but with a 90 day lag from the HRL temperature and a range of only ±0.5°C from 13.3°C.

The temperature within the HRL closely correlates with the variation seen in axial force on the lid, the position of the lid and the stick-slip behaviour. This correlation is not perfect and an offset between displacement and temperature can on occasion be observed.

Other observations of seasonal variation appear to more closely correlate with the canister temperature, including pore pressure within the bentonite (UB), pore pressure at the wall rock (UR), radial stress (PR) and the radial & axial stresses (PC). With most of these instruments there is also some variation in the oscillation, many showing variation in lag with depth down the deposition hole.

As well as seasonal variation, it has been seen that pore pressure within Lasgit and the HRL around the 420 m level has displayed a long term gradual decay. The underlying cause for this behaviour remains unclear.

The early part of 2008 saw considerable blasting activity within the Hard Rock Laboratory at a depth of 450 m. It is worth noting that while a number of minor events in the data have been noted, few if any can be directly attributed to blasting. Therefore blasting has not had a detrimental effect on the Lasgit experiment.

Lasgit has yielded high quality data relating to the hydration of the bentonite and the evolution in hydrogeological properties adjacent to the deposition hole. The initial hydraulic and gas injection tests confirm the correct working of all control and data acquisition systems. Lasgit has been in successful operation for in excess of 1,385 days. The decreasing rate of change in sensor outputs demonstrates that significant progress in the hydration of the bentonite has been made.

9 References

Bäck R, 2003. Djupförvarsteknik: Large scale gas injection test: Lid report. SKB TD-04-07, Svensk Kärnbränslehantering AB.

Donohew A T, Horseman S T, Harrington J F, 2000. Gas entry into unconfined clay pastes between the liquid and plastic limits. Chapter 18. In: Environmental Mineralogy – Microbial Interactions, Anthropogenic Influences, Contaminated Land and Waste Management (eds J D Cotter-Howells, L S Campbell, E Valsami-Jones, M Batchelder), Mineralogical Society, London, Special Publication No. 9, 369–394.

Hardenby C, Lundin J, 2003. Geological mapping of the assembly hall and deposition hole. SKB IPR-03-28, Svensk Kärnbränslehantering AB.

Hardenby C, 2004. The LASGIT hole DA3147G01 Hydrogeology. SKB IPR-04-52, Svensk Kärnbränslehantering AB.

Harrington J F, Horseman S T, 1999. Gas transport properties of clays and mudrocks. In: Muds And Mudstones: Physical And Fluid Flow Properties (eds A C Aplin, A J Fleet, J H S Macquaker). Geological Society of London, Special Publication No. 158, 107–124.

Harrington J F, Horseman S T, 2003. Gas migration in KBS-3 buffer bentonite: Sensitivity of test parameters to experimental boundary conditions. SKB TR-03-02, Svensk Kärnbränslehantering AB.

Harrington J F, Birchall D J, Noy D J, Cuss R J, 2007. Large scale gas injection test (Lasgit) performed at the Äspö Hard Rock Laboratory: Summary report 2007. *British Geological Survey Commissioned Report*, CR/07/211. 87 pp.

Horseman S T, Harrington J F, Sellin P, 1997. Gas Migration In Mx80 Buffer Bentonite. In: Proc. Scientific Basis For Nuclear Waste Management XX, Boston, 2–6 Dec. 1996 (eds W J Gray, I R Triay), MRS Symposia Proceedings, Vol. 465, Materials Research Society, Warrendale, Pennsylvania, 1003–1010.

Horseman S T, Harrington J F, Sellin P, 1999. Gas migration in clay barriers. Engineering Geology, Vol. 54, 139–149.

Horseman S T, Harrington J F, Sellin P, 2004. Water and gas flow in Mx80 bentonite buffer clay. In: Symposium on the Scientific Basis for Nuclear Waste Management XXVII (Kalmar), Materials Research Society, Vol. 807. 715–720.

Hume H B, 1999. Gas breakthrough in compacted Avonlea bentonite. MSc thesis, Department of Soil Science, University of Manitoba, Winnipeg, Canada.

Johannesson L-E, 2003. Djupförvarsteknik: Large scale gas injection test: Manufacturing of buffer for the large scale gas injection test SKB TD-04-01, Svensk Kärnbränslehantering AB.

Nowak T, Köster H, Flentje R, Sanchez-Herrero S, Lege C, 2007. Hydraulic tests with surface packer system. SKB IPR-07-14, Svensk Kärnbränslehantering AB.

Pusch R, Ranhagen L, Nilsson K, 1985. Gas migration through Mx-80 bentonite. Nagra Technical Report NTB 85-36, Wettingen, Switzerland.

Pusch R, Hökmark H, Börgesson L, 1987. Outline of models of water and gas flow through smectite clay buffers. SKB TR 87-10, Svensk Kärnbränslehantering AB.

SKB, 2009. Design premises for a KBS-3V repository based on results from the safety assessment SR-Can and some subsequent analyses. SKB TR-09-22, Svensk Kärnbränslehantering AB.

Tanai K, Kanno T, Gallé C, 1997. Experimental study of gas permeabilities and breakthrough pressures in clays. In: Scientific Basis For Nuclear Waste Management XX, Boston (eds W J Gray, I R Triay), MRS Symposia Proceeding Vol. 465, Materials Research Society, Warrendale, Pennsylvania, 1003–1010.

Appendix

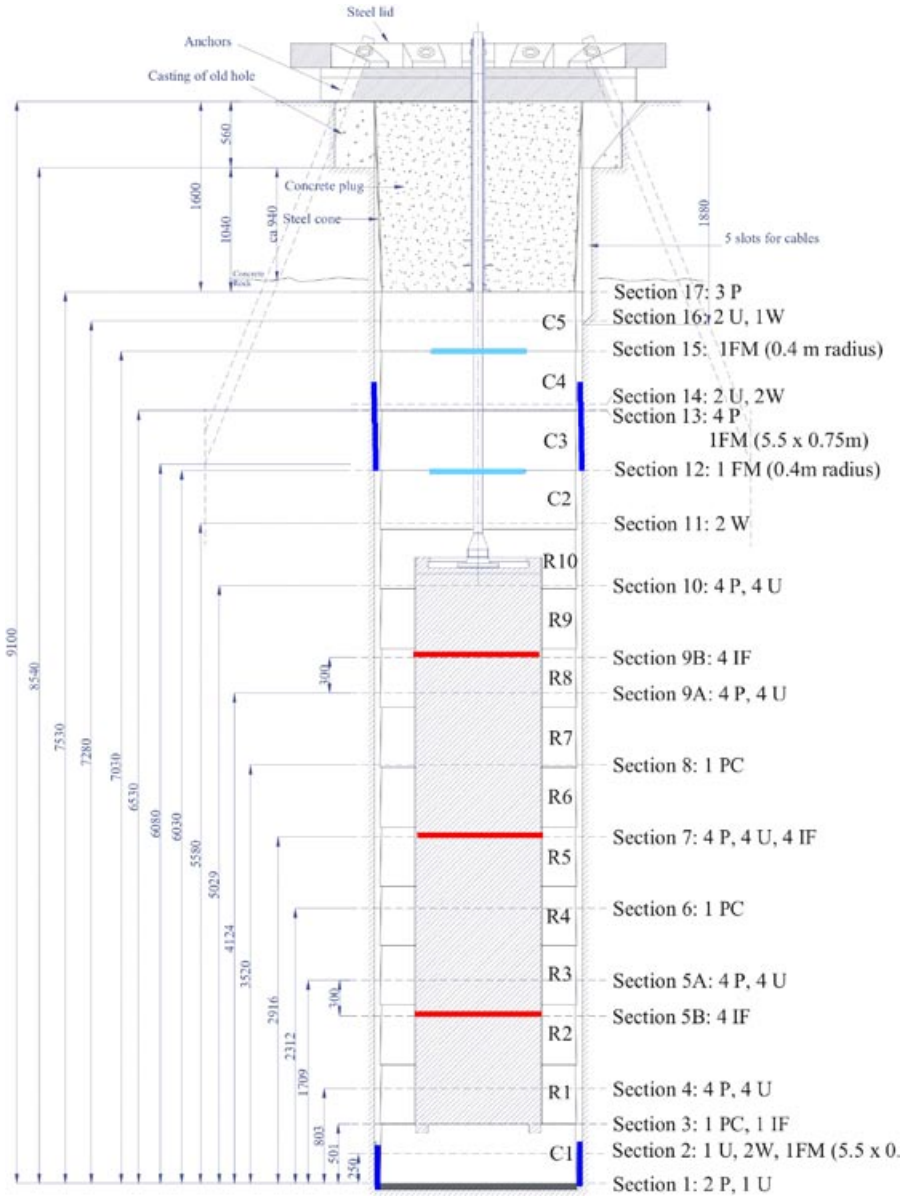

	Filters	Pore pressure in bentonite UB	Stress in bentonite PB	Pore pressure on rock wall UR	Stress on rock wall PR	Stress on canister PC	Relative humidity WB
Section 17			PB927 PB928 PB929				
Section 16		UB925 UB926					WB907
Section 15	FM904						
Section 14		UB923 UB924					WB905 WB906
Section 13	FM902		PB923 PB924 PB925 PB926				
Section 12	FM903						
Section 11							WB903 WB904
Section 10				UR919 UR920 UR921 UR922	PR919 PR920 PR921 PR922		
Section 9	UFA1 UFA2 UFA3 UFA4			UR915 UR916 UR917 UR918	PR915 PR916 PR917 PR918		
Section 8						PC903	
Section 7	MPFA1 MPFA2 MPFA3 MPFA4			UR911 UR912 UR913 UR914	PR911 PR912 PR913 PR914		
Section 6						PC902	
Section 5	LFA1 LFA2 LFA3 LFA4			UR907 UR908 UR909 UR910	PR907 PR908 PR909 PR910		
Section 4				UR903 UR904 UR905 UR906	PR903 PR904 PR905 PR906		
Section 3							
Section 2	FM901	UB902				PC901	WB901 WB902
Section 1		UB901	PB901 PB902				

ISSN 1404-0344
CM Gruppen AB, Bromma, 2010